THYROID HORMONE-INFORMED PATTERNING AND REMEMBERED POSITIONAL IDENTITY DIRECT ZEBRAFISH FIN RAY MORPHOLOGY

Melody Anastasia Sabrina Autumn

A dissertation
submitted to the Faculty of
the department of Biology
in partial fulfillment
of the requirements for the degree of
Doctor of Philosophy

Boston College
Morrissey College of Arts and Sciences
Graduate School

November 2024

THYROID HORMONE-INFORMED PATTERNING AND REMEMBERED POSITIONAL IDENTITY DIRECT ZEBRAFISH FIN RAY MORPHOLOGY

Melody Anastasia Sabrina Autumn

Advisor: Sarah K. McMenamin, Ph.D.

Resolving the mechanisms that orchestrate patterning in complex tissues – particularly how positional identity is instantiated, remembered, and directed – is imperative to understanding the morphogenesis of appendages. The zebrafish (*Danio rerio*) caudal fin skeleton is a powerful model to investigate these questions, as its precisely patterned bony fin rays are restored through regeneration. My aims in this thesis were to investigate the role of endocrine metabolic regulator thyroid hormone (TH) signaling during fin ray morphogenesis and how spatial identity is retained and redeployed during regeneration. I began my work by resolving TH signaling effects on the fin skeleton. Through nuclear receptor Thrab, TH acutely induces distal features in both development and regeneration (Chapter 2). To better understand how distal features are remembered, I established novel microsurgery techniques that would discriminate autonomous versus environmental components of ray patterning. While the rate of regeneration does appear to retain positional memory, I found ray patterning is instead informed by extrinsic cues (Chapter 3). During my investigation of TH activity in Chapter 2, I noted robust TH signaling in peripheral rays. Repurposing the microsurgeries developed in Chapter 3, I discovered this TH signaling is an inherent feature of peripheral rays, and this activity regulates local Notch pathway signaling (Chapter 4). My research has revealed many

mechanisms—both dependent and independent of TH—that regulate fin ray patterning and how this positional identity is retained and redeployed during regeneration.

TABLE OF CONTENTS

LIST OF FIGURES

TABLE OF ABBREVIATIONS

DMSO	dimethylsulfoxide
dpf	days post fertilization
dist-to-prox	regenerating distal-to-proximal transplanted ray
dpa	days post amputation
HyperTH	hyperthyroid
HypoTH	hypothyroid
MTZ	metronidazole
prox-to-prox	regenerating proximal-to-proximal transplanted ray
SL	standard length
TH	thyroid hormone

ACKNOWLEDGMENTS

So many people made this egregiously long document possible; bound-up all fancy like this it will make –at the very best– one informative dissertation, or – at the very least– a sturdy kitchen step stool.

I couldn't have chosen a better Advisor, and I'm immensely grateful for the 6 years we've shared.

It takes a village to raise a fish. Thank you to the whole McMenamin Lab for your collaboration and support.

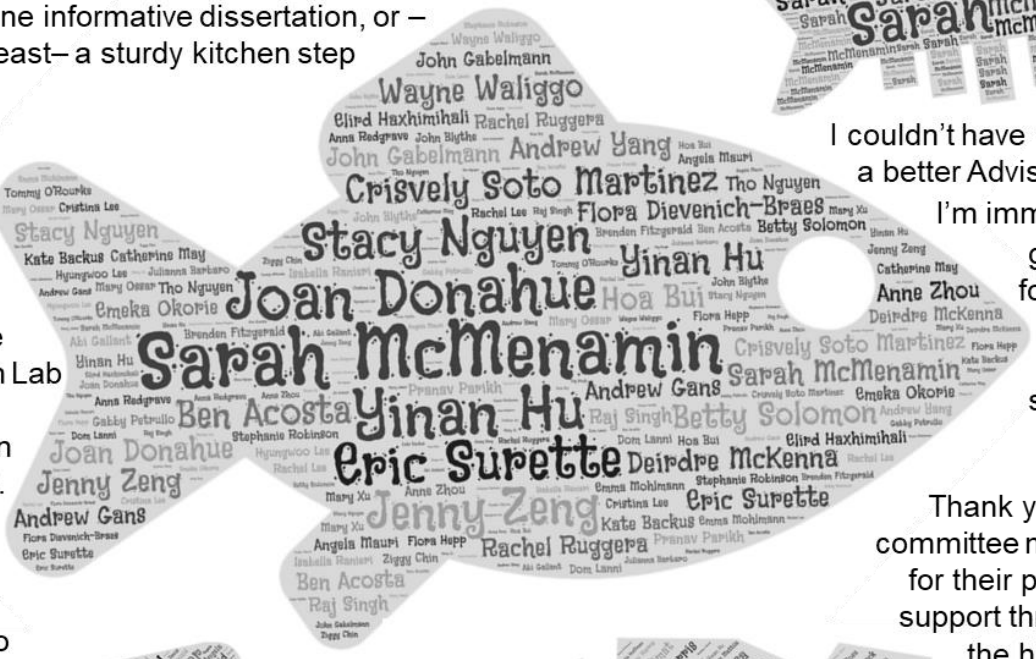

Thank you to my committee members for their persistent support throughout the highs and lows of my projects.

Thank you to my family for the lifelong hijinks and fun.

Thank you to my best friend for support from Year 1.

Thank you to my scientific mentors that paved the way for my grad school admission.

CHAPTER 1

Introduction: Positional identity, transplantation, and zebrafish skeletal patterning in development and regeneration

Some of the material in this chapter was adapted from:

Autumn, M., Zeng, J., Ranieri, I., McMenamin, S. Methods in Molecular Biology: Experimentally manipulating the thyroid hormone axis in zebrafish. Springer Nature. (accepted, 2025)

1.1 PATTERNING AND POSITIONAL IDENTITY

Tissues must develop into specific patterns to create functional morphologies. Developmental processes orchestrate the morphogenesis of tissue patterning to yield precise structures. As dysregulation of these can cause major morphological changes including congenital abnormalities, it is critical to resolve the mechanisms that generate proper tissue patterning. Studies of embryogenesis show developmental signaling pathways (including Sonic hedgehog and Notch, Kong et al., 2015) can presage shapes of organs and entire body plans (reviewed in Wolpert, 2011). Additionally, endocrine signaling is also imperative for tissue growth and development (reviewed in Gicquel & Le Bouc, 2006). All these cues are regulated spatially and temporally, the range, intensity, and perdurance of these signals are precisely deployed. Positional identity—intrinsic patterning information that can dictate final location and cell type—can be sufficient to coordinate the morphogenesis of different tissues to generate a complex structure. Many species can regenerate lost or damaged tissue, reactivating developmental signaling pathways in a novel context; accurately redeploying remembered positional identity and coordinating regenerative morphogenesis is essential for the regrowth of complex tissue patterns (reviewed in Goldman & Poss, 2020; Londono et al., 2018). Uncovering the processes that establish, retain, and execute morphogenesis is critical to understanding the emergence of patterning, and transplantation procedures have been a critical method for investigating these mechanisms.

1.2 100+ YEARS OF TRANSPLANTATION

For over a century, transplantation—grafting tissue into a non-native environment—has been used to interrogate how tissues can influence or be affected by novel biological environments, and the memory and fidelity of positional identity (Nabrit, 1929; Solini et al., 2017). From dorsal fin grafts in mummichog fishes (Kallman &

Gordon, 1957) to head transplants in axolotl (de Both, 1968), scientists showed complex structures could be successfully integrated into a novel environment. Primordium transplantations in embryos revealed grafted tissue could develop independent structures, as seen by chicken chimeras sporting quail wings (Kinutani et al., 1986; Kinutani et. al., 1985), or even direct morphogenesis of the host, as seen in *Xenopus* tadpole body axis duplications (reviewed in De Robertis, 2009). In regeneration-competent species (i.e. planaria (Rojo-Laguna et al., 2019), axolotls (Echeverri & Tanaka, 2005; Stocum, 1984), and zebrafish (Murciano et al., 2002; Shibata et al., 2018)), transplantation followed by regeneration of a graft in a non-native environment has been a powerful method for assaying the redeployment of remembered positional identity. If transplanted tissue can activate native signaling pathways to restore original morphology despite the novel environment, positional identity must remembered.

1.3 THE ZEBRAFISH CAUDAL FIN AS A MODEL

Zebrafish (*Danio rerio*) are a powerful model for biomedical research and they parallel mammalian endocrinology, allowing efficient investigation into hormonal regulation of development, growth, behavior, and metabolism (Ghaddar & Diotel, 2022; Löhr & Hammerschmidt, 2011; Porazzi et al., 2009). While zebrafish regenerate many tissues, the regenerating caudal fin specifically is an outstanding model to investigate interactions of developmental signaling pathways that guide skeletal patterning (as reviewed in Harris et al., 2021; Pfefferli & Jaźwińska, 2015; Poss et al., 2003; Sehring & Weidinger, 2020; Wehner & Weidinger, 2015). This organ has two mirrored lobes, each comprised of nine bony rays whose lengths shorten along the peripheral-central axis (Fig 1.1A). Rays are built with individual bone segments which taper and shorten progressively along the proximodistal axis (Fig 1.1A): proximal segments are long and thick, distal segments are short and thin (Fig 1.1B). These morphologies are robustly

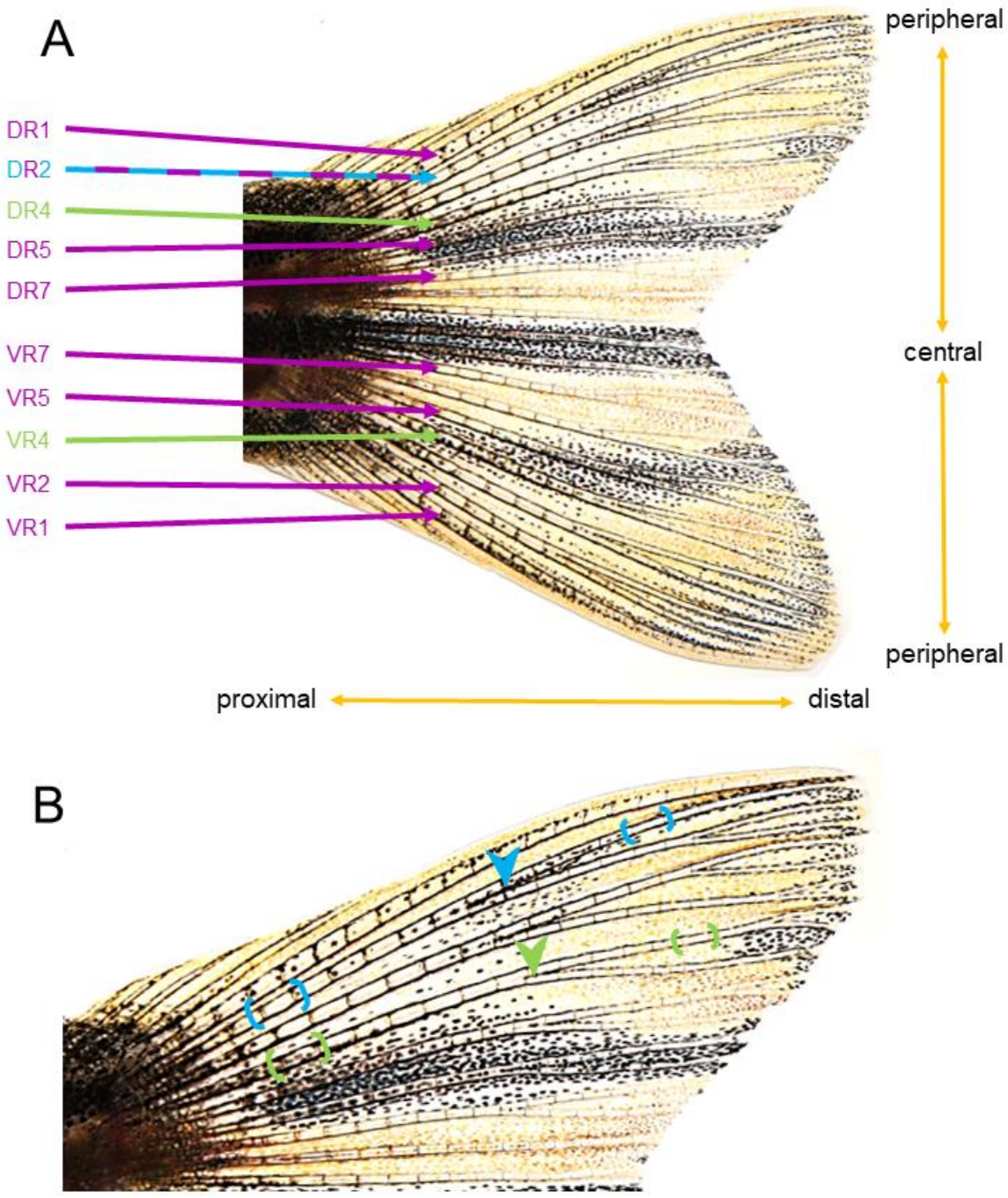

regenerated despite repeated injury (Autumn et al., 2024; Azevedo et al., 2011).

Figure 1.1 Zebrafish caudal fin morphology. (A) Intact caudal fin. Blue & magenta arrow, dorsal ray 2 (DR2): investigated in Chapter 2. Green arrows, DR4 and ventral ray 4 (VR4): investigated in Chapter 3. Blue & magenta arrow and magenta arrows, DR1, DR2, DR5, DR7, VR1, VR2, VR5, VR7: investigated in Chapter 4. (B) Dorsal lobe of intact caudal fin. Arrowheads, primary bifurcations. Brackets, individual ray segments of proximal and distal regions.

1.4 DEVELOPMENT OF THE CAUDAL FIN

Within the first two weeks of larval development, all eighteen skeletal rays show robust mineralization (Desvignes et al., 2022), with *even-skipped homeobox 1* (*evx1*; protein critical for segment development) positive cells instigating the formation of fibrous joints (Borday et al., 2001). Each ray has domain of Sonic hedgehog ligand (*shha*) expression at its distal end, and Shh activity extends along the ray (Braunstein et al., 2021). Between the second and third months of development, this *shha* domain will split, presaging the formation of a bifurcation (one ray branching into two daughter rays) (Harper et al., 2023). Zebrafish are indeterminate growers, extending ray length by adding segments to the distal end of the ray. Older segments also increase in thickness, with continued mineralization (Borday et al., 2001). Additional bifurcations will be added by this outgrowth, and we see secondary, tertiary, and even quaternary branches form.

1.5 EPIMORPHOIC REGNERATION OF THE CAUDAL FIN

Epimorphic regeneration occurs in three distinct phases: wound epithelium formation, blastema proliferation, and fin outgrowth. Upon amputation, epithelial cells rapidly migrate to the injury, assembling into a multilayer structure over the course of 24 hours (Ferretti et al., 1995). This wound epithelium will persist to the completion of regeneration, with the innermost basal layer functioning as a critical regenerative signaling center (Armstrong et al., 2017; Chablais et al., 2010; Wang et al., 2019).

Over the course of two days, cells adjacent to the amputation plane dedifferentiate, aggregate to the injury, and then proliferate into a mass of lineage-restricted cells (Knopf et al., 2011; Tu & Johnson, 2011; Wehner et al., 2014). Though grossly indistinguishable, the blastema arranges itself into discrete, organized units at the distal end of each ray (Wehner et al., 2014). Roughly classified into two domains, the

distal blastema minimally proliferates, instead functioning as a signaling center (Nechiporuk et. al., 2002; Wehner et. al., 2015). In contrast, the proximal blastema quickly proliferates to provide the cellular material needed by the third phase of regeneration: fin outgrowth.

By 3 days post amputation (dpa) outgrowth begins, a miniscule fringe of blastemal tissue maintained at the distal fin periphery (Fig 1.2A). New growth is added to the distal tip of the regenerate as developmental pathways reactivate (Fig 1.2B) to simultaneously create the complex arrangement of bone, blood vessels, and epithelium (Thorimbert et al., 2015). Depending on the location of amputation, regenerative outgrowth will proceed for up to three weeks to replace the entire caudal fin (Wehner et al., 2014).

1.6 REGENERATION OF CAUDAL FIN RAYS

By 2 dpa, epithelial and mesenchymal cells work together to build actinotrichia, collagenous fibrils that support and direct osteoblast activity (Durán et al., 2011; Duran et al., 2015; König et al., 2018; Sehring et al., 2022). Pre-osteoblasts migrate along the fibrils, forming a distinguishable gradient of osteoblast redifferentiation: distal proliferating pre-osteoblasts to proximal re-differentiated osteoblasts actively synthesizing new bone (Lalonde & Akimenko, 2018). This mineral deposition displaces actinotrichia into the medial mesenchyme, where the fibrils are degraded (König et al., 2018). Through this mechanism dermal bone elegantly rebuilds—without cartilage template—the specific morphology of each ray, including segment pattern and bifurcation placement (Fig 1.2).

1.7 CAUDAL FIN RAY PATTERNING

Each of the nine rays that comprise one lobe has a unique length, segmentation patterning, and bifurcation placement. Segments, individual bone segments linked by

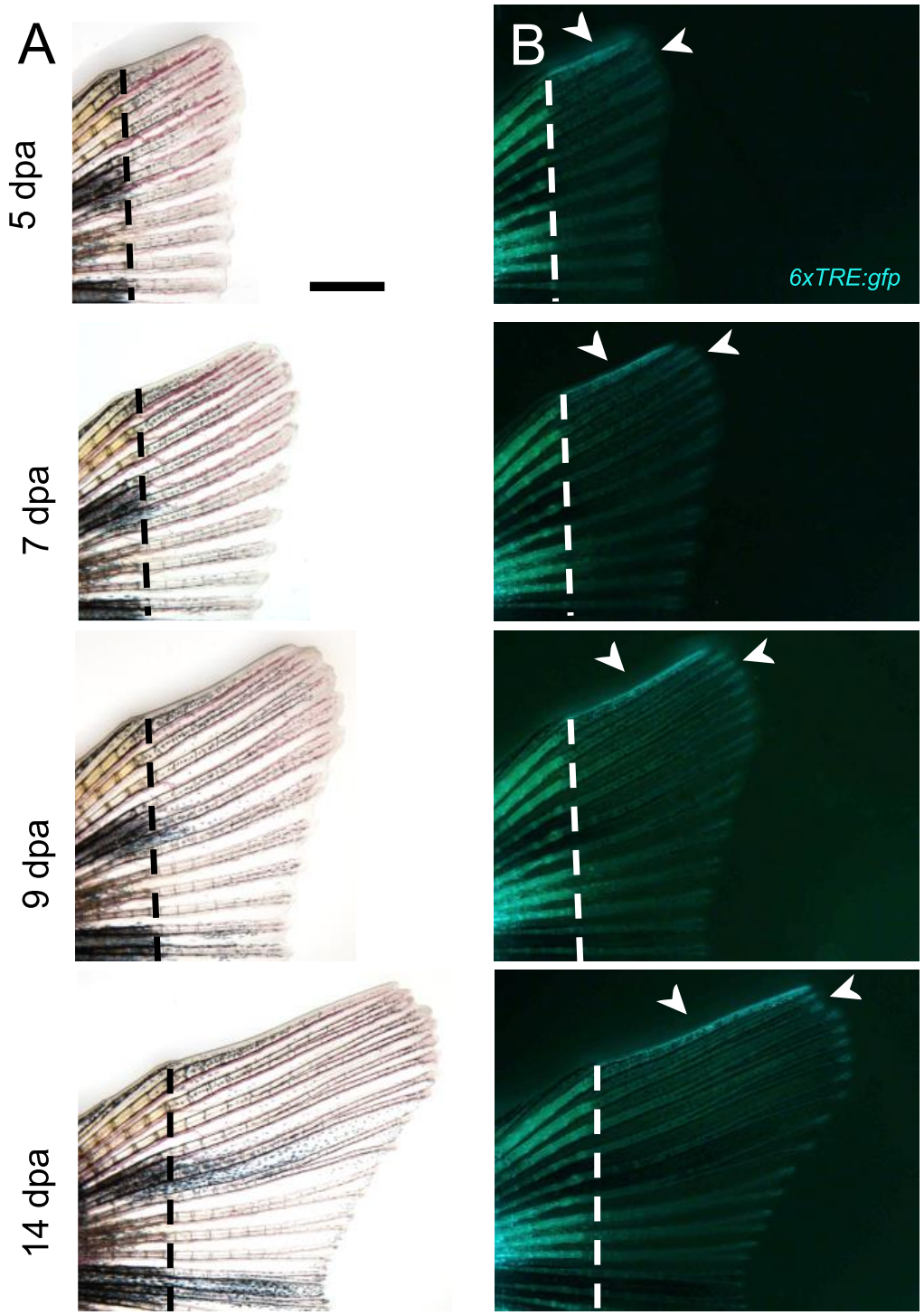

Figure 1.2 Regenerating fin tissue has active thyroid hormone signaling. (A-B) Zebrafish caudal fin lobes regenerating at various points after blastema formation has occurred and

regrowth has been initiated. (B) *6xTRE-bglob1:eGFP* reports TH activity. Arrowheads, TH activity. Dashed line, amputation plane. Scale bar, 1 mm.

fibrous joints, permit flexibility of the ray; various bioelectric mutants and drug (calcineurin, valproic acid) treatments increase or decrease segment length (Bhattacharya et al., 2020; Daane et al., 2018; Perathoner et al., 2014; Silic et al., 2020; Sims et al., 2009) or segment number (Goldsmith et al., 2003; Lee et al., 2020). Bifurcations commonly form at the ~12th segment away from the body, although thyroid hormone (TH) can shift this placement (Harper et al., 2023). The process of bifurcation morphogenesis relies on Sonic hedgehog-dependent cell interactions (Armstrong et al., 2017; Braunstein et al., 2021) and relative activities of osteoblasts and osteoclasts (Cardeira-Da-Silva et al., 2022).

While ventral rays match the lengths of their corresponding dorsal rays (i.e. ventral ray 2 versus dorsal ray 2), larger segments comprise these rays, as well as bifurcations occur at a more distal location (Autumn et al., 2024). Ray patterning is influenced by environmental cues (Autumn et al., 2024; Dagenais et al., 2021; Murciano et al., 2002, 2007), although local signaling within the mesenchyme can extend or reduce ray length regardless to the surrounding fin tissue (Daane et al., 2018, 2021; Perathoner et al., 2014; Stewart et al., 2021; Yi et al., 2021).

1.8 THYROID HORMONE SIGNALING IN ZEBRAFISH

Thyroid hormone (TH) is a globally circulating endocrine factor crucial for the development and function of organ systems across diverse vertebrate species (as reviewed in Van Der Spek et al., 2017; Zwahlen et al., 2024), including in fishes (Campinho, 2019; Laudet, 2011; McMenamin & Parichy, 2013). Endocrine systems in zebrafish (*Danio rerio*) have numerous similarities with mammalian systems and can allow efficient investigation into hormonal regulation of development, growth, behavior,

and metabolism (Autumn et al., 2025; Ghaddar & Diotel, 2022; Löhr & Hammerschmidt, 2011; Porazzi et al., 2009).

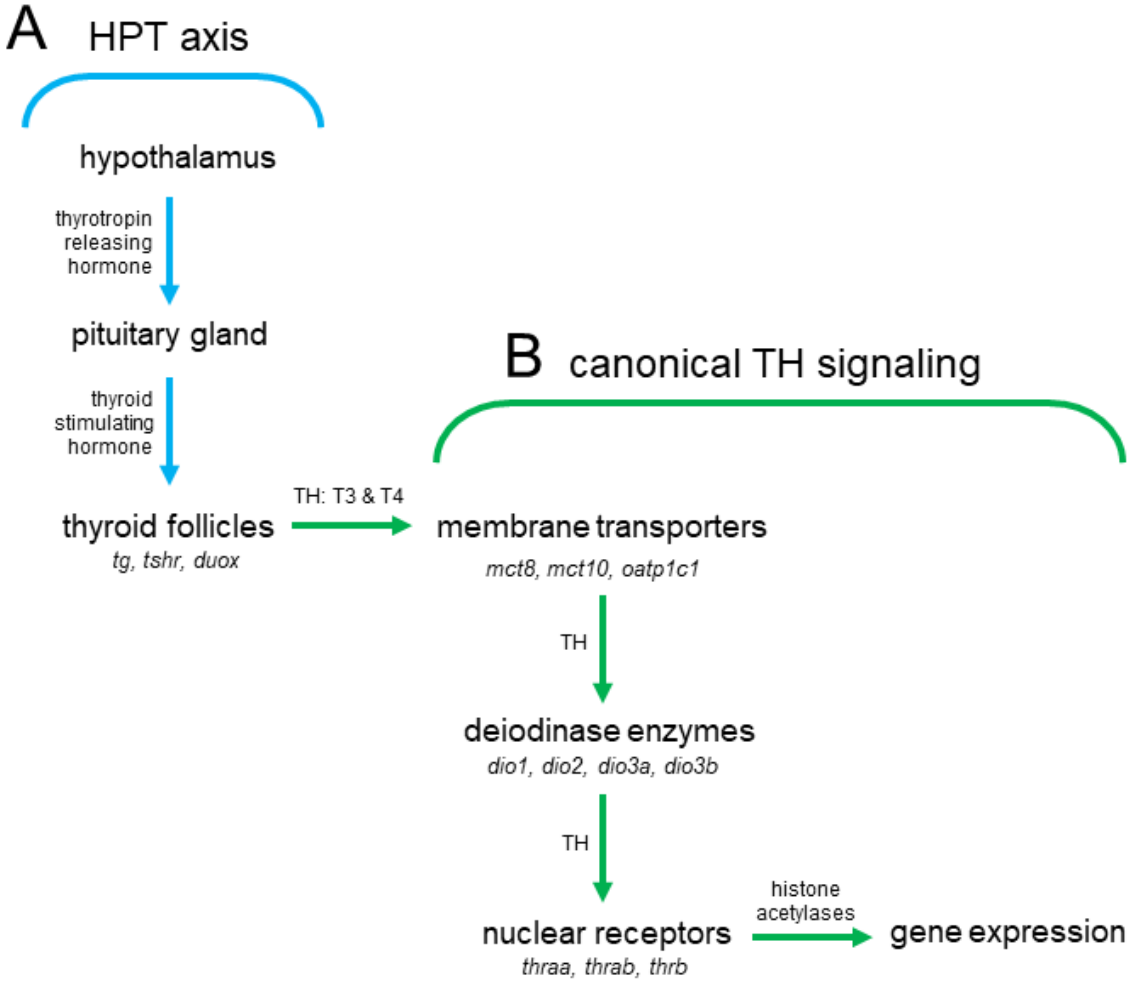

Figure 1.3 Canonical thyroid hormone signaling pathway in zebrafish. (A) TH synthesis is induced via the HPT axis. (B) Canonical TH signaling is mediated by nuclear receptors that bind to histone acetylases to induce target gene expression.

The axis of TH production is well characterized: the hypothalamus produces thyrotropin releasing hormone, triggering the pituitary gland to secrete thyroid stimulating hormone (TSH) (Fig 1.3A) (Mullur et al., 2014). TSH interacts with receptors on the thyroid follicular cells to induce the TH production cascade (Porazzi et al., 2009; Zwahlen et al., 2024). Once TH is released from the thyroid follicles into the circulatory system, canonical signaling is facilitated by locally-produced, function-specific

combinations of TH membrane transporters, deiodinases (Dios), and TH nuclear receptors (THRs), work together to modulate intracellular TH availability, bioactivity, and transcriptional effectivity (Fig 1.3B).

TH must be actively transported into peripheral cells by membrane transporters, which regulate the amount intracellular TH. Zebrafish have three characterized TH transporters (Muzzio et al., 2014; Vatine et al., 2012), each expressed in different tissues (Zada et al., 2016). As thyroid follicles secrete TH predominately as T4; the bioactivity of this prohormone is enhanced or reduced by deiodinase enzymes, of which zebrafish have at four (Heijlen et al., 2014; Thisse et al., 2003; Walpita et al., 2007), that can remove iodine atoms from the molecule(Orozco & Valverde-R, 2005). Zebrafish have several THR paralogues (Darras et al., 2011; Takayama et al., 2008) that interact with TH responsive elements in the genome. In the absence of TH, THRs associate with histone deacetylases to prevent target gene transcription (Bertrand et al., 2007; Sinha & Yen, 2000). When TH binds to and thus alters the conformation of THRs, they now can interact histone acetylases to permit gene expression (Bertrand et al., 2007; Li et al., 1999).

1.9 RESEARCH TOPICS

At the beginning of my research journey, proximal and distal zebrafish caudal fin tissues had many established differences. Proximal ray segments are longer and thicker than distally positioned ones and primary/secondary bifurcations are exclusive to the distal half of rays. These features would be properly regenerated, however proximal and distal amputation planes would initiate different rates of regrowth (Lee et al., 2005). Most notably, proximal and distal tissues collected from intact fins showed distinct transcriptomes and proteomes (Rabinowitz et al., 2017). Unlike other regenerative models that had known definitive factors regulating the proximodistal axis (Echeverri & Tanaka, 2005), no analogous factors had been discovered in zebrafish. A serendipitous

observation of hypothyroid zebrafish right before I started my research showed that TH may be responsible for distal feature formation. TH was well established as a factor in skeletal development and maintenance in other systems (Duncan Bassett & Williams, 2016), so I first investigated if TH was the driving factor of proximodistal axis polarization in development and regeneration.

Starting my second project, we now understood that proximodistal identity was progressively conferred by TH in distal tissues. Precocious distal patterning was minimal even in an excessively hyperthyroid environment, indicating that distal tissues may be particularly receptive to TH's distalizing action (Harper et al., 2023). Work with peripheral-to-central ray transplants revealed that individual rays could retain aspects of their original identity despite regrowing in a novel environment (Shibata et al., 2018). Varying regeneration speed indicated inherent difference between proximal and distal tissues (Lee et al., 2005), however distal-to-proximal blastema transplant experiments did not support that proximodistal information was retained (Shibata et al., 2018). As it was still undetermined how proximodistal information was remembered and redeployed, I asked if proximodistal morphology was inherent to the tissue or if it was progressively induced during outgrowth.

For my final project, I returned to investigate one of my initial findings from my first research question: peripheral ray (DR1, VR1) specific TH activity (see Fig1.2B). In central rays (all rays except DR1 and VR1, Fig 1.1A), hyperthyroid conditions yield additional bifurcations and TH is sufficient to rescue branching in hypothyroid fins (Harper et al., 2023). Despite markedly increased TH activity in development and regeneration, peripheral rays never bifurcate. Domains of *aristaless* 4 (*alx4,* pectoral ray identity factor) expression precede the formation of peripheral rays and then are maintained throughout adulthood but little is known about its purpose (Desvignes et al.,

2022). As peripheral rays had never been intensely studied, I wanted to interrogate the specific signals that characterize these skeletal elements.

In summation, my dissertation work began with the question of thyroid hormone's role during fin ray regeneration, and this inquiry led me to all three of my research chapters. First, I defined the role of TH in distalizing the appendicular fin skeleton (Chapter 2). I continued to probe the proximodistal axis, pioneering microsurgeries to disentangle autonomous components of fin ray identity (Chapter 3). Finally, using the data on TH acquired in Chapter 2 and the procedures developed in Chapter 3, I investigated a novel function of TH as a peripheral ray organizer (Chapter 4).

CHAPTER 2

Thyroid hormone regulates proximodistal patterning in fin rays

The material in this chapter was adapted from:

Harper (Autumn), M. & Hu, Y., Donahue, J., Acosta, B., Dievenich Braes, F., Nguyen, S., Zeng, J., Barbaro, J., Lee, H., Bui, H., McMenamin, S. Proceedings of the National Academy of Sciences. (2023). Thyroid hormone regulates proximodistal patterning in fin rays.

2.1 INTRODUCTION

2.1.1 How are appendages shaped?

How organisms generate complex shapes is a central question in Biology. To produce a robust phenotype, cells in a developing organ must interpret positional information and execute growth and pattern morphogenesis in a regionally appropriate and highly coordinated manner (Wolpert, 1969). Along an extending axis, even subtle shifts in patterning processes relative to outgrowth can profoundly alter the ultimate shape, e.g. by altering the number of somites along the anteroposterior axis (Gomez & Pourquie, 2009).

Appendages such as limbs show specific proximodistal patterning, with different character states expressed at different locations along the axis. Such patterning shows incredible diversity between lineages, and relative shifts in proximodistal identity likely facilitated major evolutionary transitions (T. A. Stewart et al., 2020). Developing tissues create patterns through morphogenetic processes that may be cued by regional gradients of morphogens, bioelectric or mechanical signals, as reviewed in (Mateus et al., 2021; Tung & Levin, 2020). In addition to these local processes, global factors such as hormones can coordinate morphogenesis in disparate tissues (Hu et al., 2019; S. McMenamin et al., 2022; S. K. McMenamin et al., 2013); such systemic signals could theoretically be leveraged to establish or reinforce patterns during outgrowth of an axis.

2.1.2 Zebrafish caudal fin rays are a model for proximodistal patterning.

Zebrafish fins are a premier model for studying growth and regeneration, and can serve as informative models of proximodistal patterning. Fin length mutants have allowed great progress towards understanding the mechanisms that regulate growth of rays (Harris et al., 2021; Perathoner et al., 2014; S. Stewart et al., 2021). In contrast, the signals underlying proximodistal patterning of the rays have remained largely elusive.

Although more subtle than the polarity of tetrapod limbs, individual fin rays show distinct patterning along the axis: ray segments taper and shorten distally, and periodically bifurcate into branches (see Fig 2.1*A*). Ray segments are added distally during fin outgrowth, in a manner resembling somitogenesis (Marí-Beffa & Murciano, 2010). Likewise, bifurcations are added terminally during development or regeneration, with most rays eventually forming one or more branches (e.g. see Supp Fig 2.1).

Changes in proximodistal patterning are important in evolutionary transformations and adaptations. Notably, the fin-to-limb transition involved major changes in patterning and proportion along the proximodistal axis (T. A. Stewart et al., 2020; Tanaka, 2018; Woltering et al., 2020). Among teleosts, fin ray patterning varies considerably between species, from uniformly thick rays with no bifurcations (e.g. syngnathids, sculpins), to tapering rays with multiple bifurcations along each ray (guppies, killifish). These differences in proximodistal morphology contribute to the functional and biomechanical properties of the appendages.

The local mechanisms governing aspects of certain proximodistal features have been elucidated. Formation of bifurcations requires precise Shh signaling as well as coordinated and opposing activities of osteoblasts and osteoclasts (Armstrong et al., 2017; Braunstein et al., 2021; Cardeira-Da-Silva et al., 2022; Zhang et al., 2012). Nonetheless, it remains unknown what positional identity cues direct bifurcation machinery to be deployed at correct locations along growing rays. Furthermore, while certain mechanisms governing overall segment length have been discovered (Schulte et al., 2011; Sims et al., 2009), pathways regulating the progressive distal shortening of

segments remain entirely unknown (although they can be modeled computationally) (Rolland-Lagan et al., 2012).

2.1.3 Thyroid hormone coordinates vertebrate development.

Thyroid hormone (TH) is an essential regulator of cellular metabolism and homeostasis, This endocrine factor coordinates post-embryonic developmental processes in diverse vertebrates, including zebrafish (Hu et al., 2019; Keer et al., 2019; S. K. McMenamin et al., 2014, 2017; S. K. McMenamin & Parichy, 2013; Saunders et al., 2019). In zebrafish reared under hypothyroid (HypoTH) or hyperthyroid (HyperTH) conditions, we observed changes in the fin skeleton consistent with coordinated shifts along the proximodistal axis. We hypothesized that TH regulates aspects of proximodistal patterning, and that these processes operate independently from size-instructive signals controlling fin ray length.

2.2 RESULTS

2.2.1 TH promotes distal features in developing fin rays.

We discovered that hallmarks of skeletal distalization are induced and coordinated by developmental TH titer (Fig 2.1). Transgenic ablation of the thyroid follicles during larval development results in permanently HypoTH fish (S. K. McMenamin et al., 2014); fins of adults reared under these HypoTH conditions showed markedly proximalized fin rays (Fig. 2.1*B*; Supp Fig 2.1*B*). Conversely, a congenitally HyperTH mutant (S. K. McMenamin et al., 2014) showed moderate distalization (Fig 2.1*C*). Bifurcations are the most discrete indicators of proximodistal patterning, and in caudal fins of WT adult fish, the majority of internal rays form at least one bifurcation (peripheral rays never bifurcate). In the absence of TH (HypoTH conditions), far fewer

bifurcations formed (Fig 2.1*D*). To examine the patterning along the length the axis, we focused on the 2nd dorsal ray. We found that bifurcations that did form in a HypoTH context were positioned considerably farther from the body, suggesting proximalization of the axis (Fig 2.1*E*). The shifted position of the bifurcation was also reflected in the number of ray segments proximal to the bifurcation (Supp Fig 2.2*B*) as well as the proportion of the total ray length at the bifurcation (Supp Fig 2.2*C*). A mutant with reduced TH production (Chopra et al., 2019) also showed fewer bifurcations that were shifted farther from the body (Supp Fig 2.3). Despite the differing pattern of branching, HypoTH fish maintained overall similar rates of growth during development compared to WT, euthyroid siblings (Supp Fig 2.1*B-D*). Contrasting with the proximalized patterning of HypoTH fin rays, conditions of excess TH (HyperTH) caused bifurcations to develop somewhat closer to the body, suggesting distalization of the axis (Fig 2.1*C, I*; Supp Fig 2.2*G-I*). All of the paired and median fins showed corresponding shifts in the relative location of bifurcations (Supp Fig 2.4). WT control groups, sex did not appear to influence ray patterning (Supp Fig 2.5).

Fin rays are composed of segments that become progressively shorter and thinner along the axis. TH regulates the progressive shortening of rays: in the absence of the hormone, longer segments continued to be built farther from the body (Fig 2.1*F-G*; Supp Fig 2.2*E-F*). In contrast, HyperTH conditions caused segments to shorten precociously along the axis (Fig 2.1*K*; Supp Fig 2.2*K*) resulting in slightly shorter distal segments (Fig 2.1*J*). Rays from HypoTH fish also showed proximalized trends in bone density (Supp Fig 2.6); the dense distal segments in the HypoTH context are particularly striking since HypoTH conditions tend to decrease overall mineralization and bone density in other skeletal elements(Keer et al., 2019).

We asked if treatment with TH during development could rescue proximodistal patterning in HypoTH fish. Early treatments (5-30 or 30-60 days post fertilization, dpf) did

not change patterning. However, treating HypoTH fish with exogenous TH during juvenile development (60-90 dpf) was sufficient rescue the formation of bifurcations (Supp Fig 2.7). In a WT background, continuous treatment with exogenous TH during development did not significantly alter bifurcations (Supp Fig 2.8).

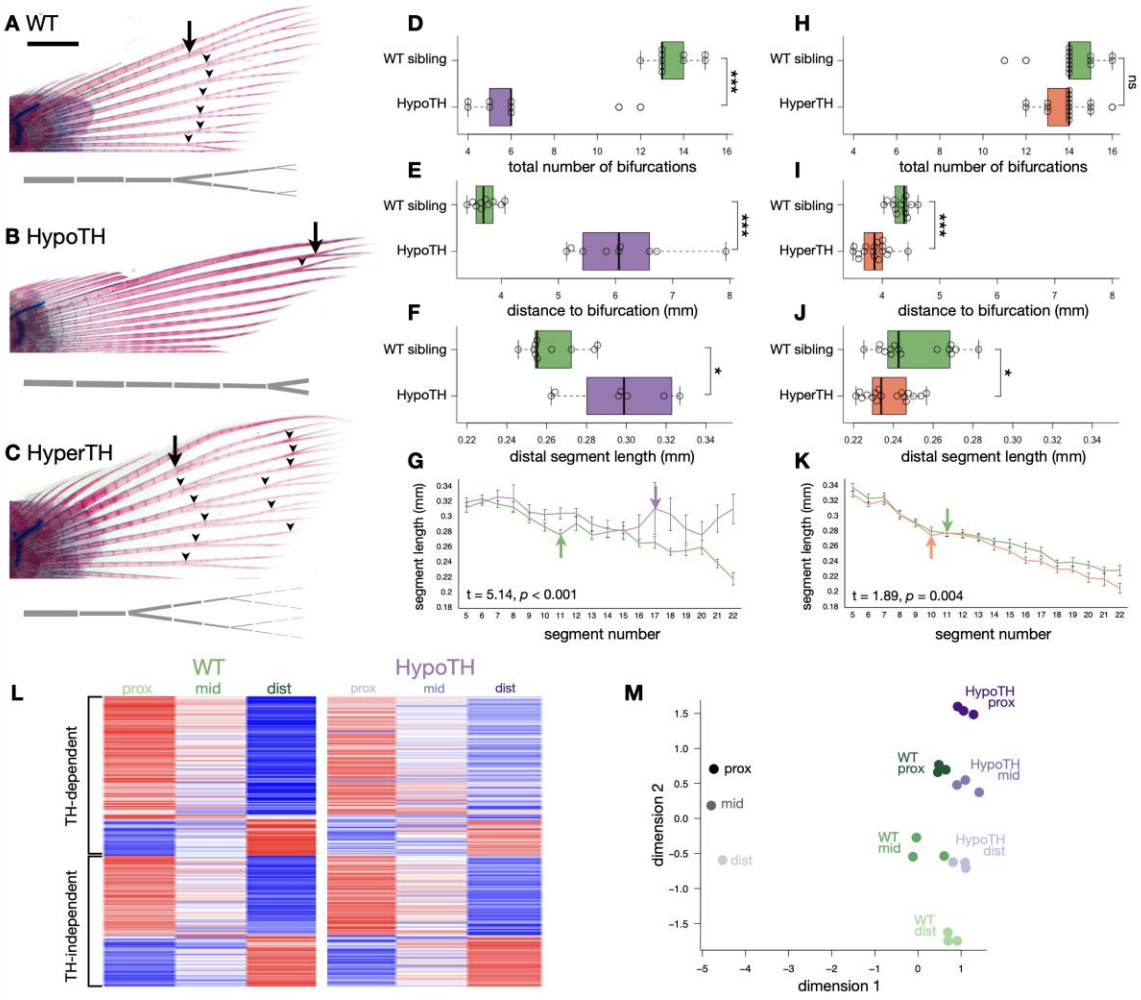

Figure 2.1 Thyroid hormone induces distal morphology in fin rays. (*A-C*) Cleared and stained dorsal lobes of caudal fins from zebrafish reared under different TH profiles. Black arrows indicate location of the primary bifurcation on the 2nd dorsal ray; arrowheads indicate all other bifurcations. Conceptual cartoons below each image show proximodistal patterning of a single ray. Scale bar, 1mm. Boxplots show (*D, H*) total number of primary bifurcations on each fin, (*E, I*) the absolute distance from the base of the ray to the bifurcation on the 2nd dorsal ray, and (*F, J*) the average length of distal segments 16-18 on the 2nd dorsal ray. Significance determined by Welch two sample t-tests. (*G, K*) Plots showing the average length of each segment on the 2nd dorsal ray, starting from the 5th segment. Error bars show standard error. Arrows indicate the average location of the primary bifurcation in each background. Significance reflects the interaction term in a linear mixed-effects model. (*L*) Heatmap of transcripts that are differentially expressed between proximal and distal regions of intact fins from WT (left). Right shows

expression of the same transcripts in a HypoTH background. The proximodistal difference is either lost in HypoTH (TH-dependent, top) or maintained in the HypoTH background (TH-independent, bottom). (*M*) Multidimensional scaling plot comparing gene expression profiles for different regions of the fin from WT and HypoTH fish; each data point represents a biological replicate. Also shown is a previously published reference dataset (greyscale; Rabinowitz et al., 2017). Note that dimension 2 captures proximodistality of all the datasets, and that HypoTH transcriptomes are overall shifted 'proximally' along this axis relative to WT controls.

2.2.2 TH induces distal expression patterns in developing fins.

If TH alters axis identity, we hypothesized that in addition to the proximalized aspects of patterning, HypoTH fins would show proximalized patterns of gene expression. Examining transcriptomes from three proximodistal regions of uninjured fins, we found 233 genes expressed differentially along the proximodistal axis in a control WT background (Fig 2.1*L*; Supp Fig 2.9*A*-*C*), showing strong correspondence with a previously published dataset (Rabinowitz et al., 2017). Of these proximally- or distally-enriched genes, the majority lost differential expression in a HypoTH context (128/233, 55%; Fig 2.1*L*; Supp Fig 2.9*B*). In particular, characteristically distal expression patterns were attenuated in distal regions of fins from HypoTH backgrounds (Fig 2.1*L*). Multidimensional scaling suggested that expression patterns were shifted proximally in a HypoTH context (Fig. 1*M*). Moreover, several transcripts known to characterize proximal or distal identities (Rabinowitz et al., 2017) showed proximalized patterns of expression in HypoTH conditions (Supp Fig 2.9*D*-*G*).

Consistent with previous analyses (Rabinowitz et al., 2017), we did not detect a signal of TH-related genes being expressed in a proximodistal gradient in WT, although we did find that *dio2* (deiodinase 2; converts circulating TH into a more bioactive form (Houbrechts et al., 2016)) was expressed more strongly in proximal regions of WT fins (Supp Fig 2.9*H*). RA mediates axis patterning in tetrapods, and many RA-pathway genes are expressed in a proximodistal gradient in uninjured WT fins (Rabinowitz et al., 2017; Yashiro et al., 2004). Many genes associated with RA metabolism show gradients along the proximodistal axis, and we asked if TH was required for this graded expression. Of

the six RA-associated transcripts expressed in a proximodistal differential, only one showed altered expression in a HypoTH context (Supp Fig 2.9*B,G*), suggesting that TH does not regulate distal identity by altering regional production of RA transcripts. Other genes associated with proximodistal identity in tetrapod limbs (e.g. *meis*, *pbx*, *hox*) did not show expression differences between proximal and distal regions in WT, and also did not show dependence on TH. The relative activities of osteoblasts and osteoclasts may mediate formation of bifurcations(Zhang et al., 2012). We asked whether markers for these two skeletogenic cell types might be relatively altered in a HypoTH context, but none were differentially expressed between TH conditions above the significance threshold (see Supp Fig 2.9*I-J*).

In all, these transcriptomic data suggest that TH is essential in establishing distal patterns of gene expression in mature, intact fins. We did not detect evidence that the hormone functions by regulating expression of a specific molecular pathway or cell type (Supp Fig 2.9).

2.2.3 Developmental TH regulates distal features in the context of altered fin length.

Fin length mutants show dramatic changes in the relative lengths of fins, but the overall patterning of the rays is comparable to that in WT (Harris et al., 2021)(Fig 2.2; Supp Fig 2.10). We predicted that altering TH in the context of a lengthened or shortened fin would alter ray patterning along the axis. Indeed, HypoTH conditions proximalized both *lof* and *sof* rays (Fig 2.2; Supp Fig 2.10), comparable to the proximalization seen in fins of non-mutant HypoTH. This apparent lack of genetic

interaction suggests TH regulation of proximodistal patterning operates independently from size-regulating pathways.

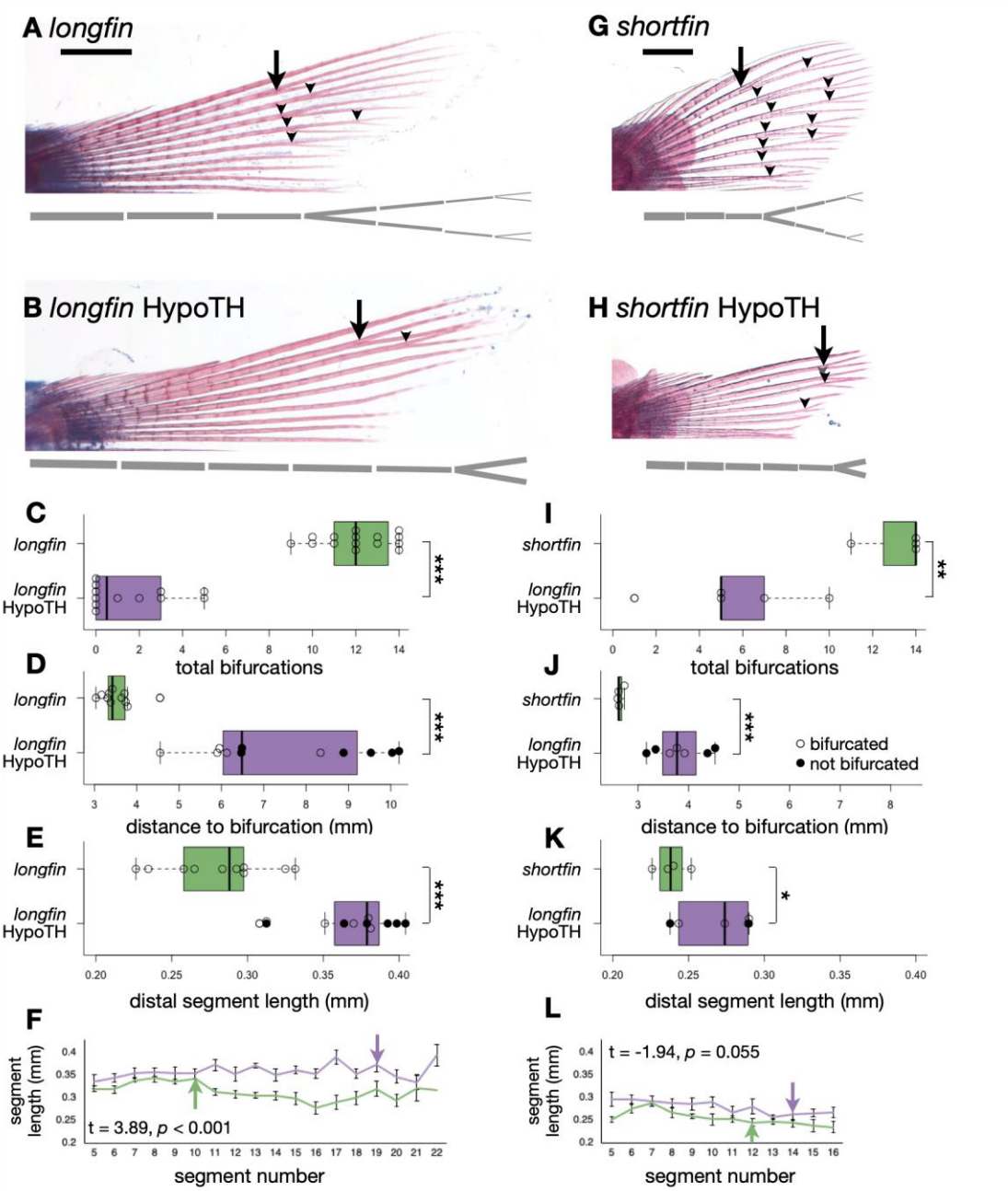

Figure 2.2 Thyroid hormone regulates patterning in *longfin* and *shortfin* backgrounds. Caudal fins of (*A-B*) *longfin* and (*G-H*) *shortfin* mutants that are either euthyroid (*A-G*) or HypoTH (*B-H*). Black arrows indicate location of the primary bifurcation on the 2nd dorsal ray, from which all quantifications were taken. Arrowheads indicate all other bifurcations. Cartoons below each fin show proximodistal patterning of a single ray. Scale bars, 1mm. Boxplots show (*C, I*) total number of primary bifurcations on each fin, (*D, J*) the absolute distance from the base of the ray to the

primary bifurcation (or the total length of the ray for non-bifurcating rays; filled datapoints), and (*E, K*) the average length of distal segments (*E*) 16-18 or (*K*) 14-16. In *D-E* and *J-K*, filled circles represent measurements from non-branching rays, empty circles represent measurements from branching rays. Significance determined by Welch two sample t-test. (*F, L*) Plots showing the average length of each segment, starting from the 5th segment. Error bars show standard error. Arrows indicate the average location of the primary bifurcation in each background. Significance reflects the interaction term in a linear mixed-effects model.

2.2.4 Unliganded Thrab inhibits distal identity.

Canonical TH signaling functions through dual-action nuclear TH receptors, which repress transcription when the hormonal ligand is absent, and promote expression when the hormone is present (Hörlein et al., 1995). We hypothesized that TH functions through one or more of the three zebrafish TH receptors—Thraa, Thrab and Thrb—to modulate fin ray patterning. Rays of euthyroid *thrab* mutants showed patterning comparable to that of WT siblings; in contrast, HypoTH *thrab* mutants showed a striking rescue relative to HypoTH non-mutants (Fig 2.3*A-F*; Supp Fig 2.11). While HypoTH non-mutant siblings (and HypoTH *thrab* +/- heterozygotes, see Supp Fig 2.11) rarely formed bifurcations, *thrab* knockout (-/-) permitted formation of bifurcations even in a HypoTH context (Fig 2.3*C*). We infer that unliganded Thrab actively represses distalization. Nonetheless, the absence of Thrab did not completely rescue a WT morphology in the HypoTH background (Fig 2.3*C-E*; Supp Fig 2.11), suggesting that Thrab-independent TH mechanisms also positively regulate distalization of the rays. Contrasting with the rescued patterning evident in HypoTH *thrab* mutants, HypoTH *thraa* and *thrb* mutants showed typical HypoTH phenotypes with no evidence of rescue (Supp Fig 2.12).

We found that *thrab* is expressed at the tips of rays during regeneration, including in both blastema and epidermis (Fig 2.3*G-H*), along with many other genes actively expressed at the growing edge. We asked whether regional differences in *thrab* expression along the proximodistal axis might mediate distalization by modulating regional responses to circulating TH. However, the level of *thrab* expression remained

comparable as different regions of the proximodistal axis regenerated (Fig 2.13*A*-*B*). Thus, although the receptor is expressed during regeneration, regional differences in Thrab expression along the axis do not correlate with different stages of proximodistal morphogenesis.

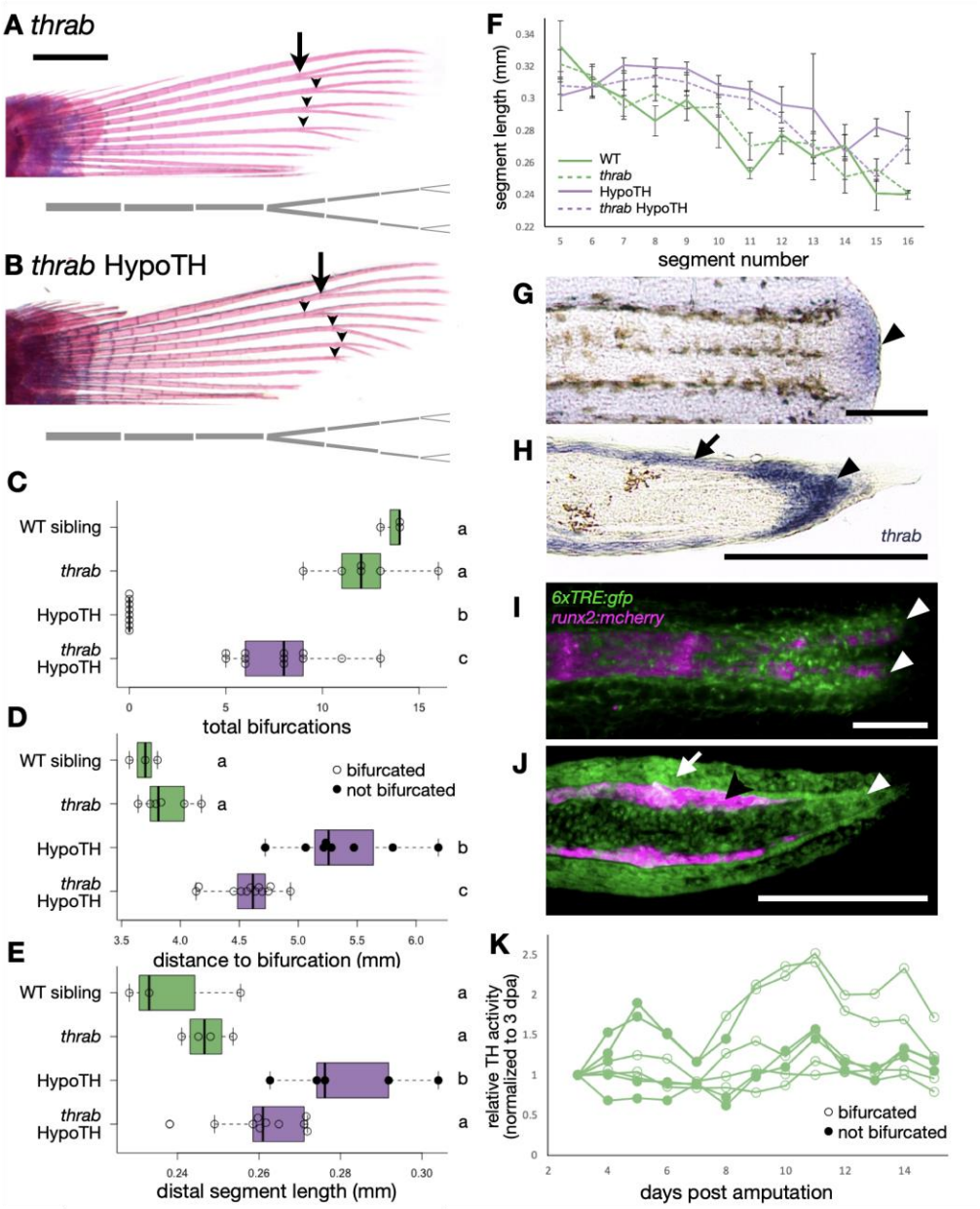

Figure 2.3 Unliganded Thrab inhibits distal patterning. Caudal fins of *thrab* -/- mutants reared under (*A*) euthyroid or (*B*) HypoTH conditions. Arrows indicate location of the primary bifurcation on the 2nd dorsal ray, from which all quantifications were taken. Arrowheads indicate all other bifurcations. Boxplots show (*C*) total number of primary bifurcations on each fin, (*D*) the absolute distance from the base of the ray to the primary bifurcation (or the total length of the ray for non-

bifurcating rays; filled datapoints), and (*E*) the average length of distal segments 15-17. Significance determined by an ANOVA followed by Tukey's HSD; significance indicated by letter groups, with statistically indistinguishable groups sharing the same letter. (*F*) Plot showing the average length of each segment, starting from the 5th segment. Error bars show standard error. Arrows indicate the average location of the primary bifurcation in each background. (*G-H*) *In situ* hybridizations showing *thrab* expression during regeneration in (*G*) a single ray of a whole-mount fin and (*H*) longitudinal section of a ray. In the section, *thrab* is detectable in the blastema (arrowhead) and epidermis (arrow). (*I*) *6xTRE-bglob1:eGFP* reports TH activity and *runx2:mCherry* identifies pre-osteoblasts as bifurcation forms in regenerating ray. Shown in (*J*) is a longitudinal section of a regenerating ray stained with secondary antibodies against the fluorophores. TH is active in the blastema (white arrowhead), epidermis (arrow) and presumptive osteoblasts (black arrowhead). (*K*) Graph showing relative TH activity (reported by *6xTRE:eGFP*) of 2nd dorsal ray quantified throughout regeneration. The fluorescence of each individual is normalized to fluorescence at 3 dpa. In *D-E* and *K*, filled circles represent measurements from rays before bifurcation; open circles identify rays after they have bifurcated. Scale bars for *A, B*, 1mm; Bars for *G*, *H*, *I*, *J*, 200μM.

2.2.5 TH is active at the leading edge of the fin.

We asked if *thrab* expression domains might correspond to regions of high TH activity. A TH activity reporter (Matsuda, 2018) showed TH is indeed active at the distal tips of both uninjured (Supp Fig 2.13*C*) and regenerating rays (Fig 2.3*I-J*, Supp Fig 2.13*E;* Supp Fig 2.14). TH activity was detectible in the presumptive blastema as well as in the epidermis (Fig 2.3*J*; Supp Fig 2.13*F*). TH also appeared to be active the pre-osteoblast lineage, and showed activity in regions where osteoblasts were present (Fig 2.3*J*; Supp Fig 2.13*F*). The TH activity reporter showed reduced activity in regenerating *thrab* mutants, suggesting that the hormone acts via Thrab during regeneration (Supp Fig 2.13*G-I*). We asked whether TH activity showed a gradient along the proximodistal axis or any shifts in activity coincident with bifurcation. However, TH activity showed no clear trends over the course of regeneration (Fig 2.*3K*; Supp Fig 2.14*A-C*).

2.2.6 TH is sufficient to distalize rays during outgrowth.

We tested if patterning could be rescued in fins from HypoTH fish during regeneration. Indeed, treating HypoTH fish with exogenous TH throughout 3 weeks of regeneration was sufficient to robustly rescue distalization (Fig 2.4*C*; Supp Fig. 2.15).

Positional information in the early blastema dictates regenerate length (Tornini et al., 2016; Wang et al., 2019), and we asked if our rescue of distal morphology was due to effects of TH on the early blastema. To test this, we treated HypoTH fish with TH for 24 hours during each of the first 3 dpa, but none of these treatments were sufficient to rescue distal patterning in regenerates (Supp Fig 2.16). This led us to hypothesize that TH is acutely required to create distal morphology, and we tested this possibility by delaying TH treatments until later stages of regenerative outgrowth. Even when the onset of treatment was delayed to 7 or 14 dpa, exogenous TH was still sufficient to rescue the formation of bifurcations (Fig 2.4*D-E*; Supp Fig 2.15). These data suggest that fin rays remain receptive to TH-induced distalization throughout the regenerative process.

2.2.7 Proximodistal patterning is not remembered, but is built in response to TH.

Our rescue experiments demonstrated that previously proximalized HypoTH patterning can be overridden during regeneration by treatment with TH. We next asked if normal distal patterning could be remembered and rebuilt during regeneration even in the absence of TH, and we tested this in two different ways. First, we treated WT fish with either of two TH-blocking drugs during regeneration; these indeed inhibited bifurcations from forming (Supp Fig 2.17). Second, we used HypoTH fish that had been rescued with TH during development (as in Supp Fig. 2.7), then regenerated the fins in the absence of TH. Despite developing with a WT-like pattern, regeneration in the absence of additional TH caused fins to revert to a proximalized HypoTH pattern (Supp Fig. 2.18). These experiments demonstrate that proximodistal patterning is not remembered by tissues, but is generated in direct response to TH during outgrowth.

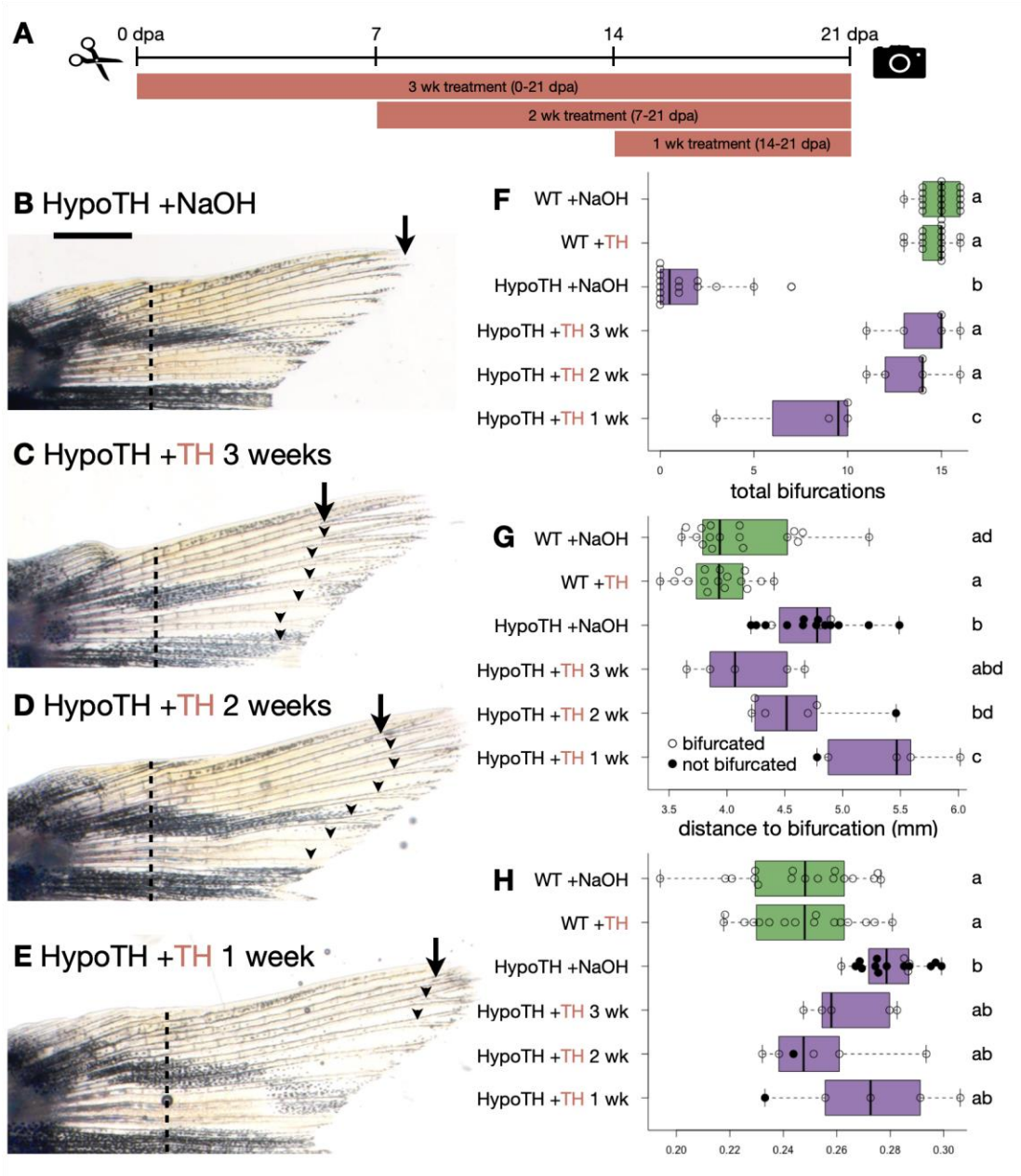

Figure 2.4 Exogenous thyroid hormone is sufficient to distalize hypothyroid fin rays during regeneration. (*A*) Experimental timeline for treatments. (*B-E*) Regenerated fins from a HypoTH background, treated with either (*B*) vehicle control or (*C-E*) 5nM T4 during different time periods of regeneration. Amputation planes indicated with dashed lines. Arrows indicate primary bifurcation of the 2nd dorsal ray (or total ray length when ray does not branch); arrowheads indicate all other bifurcations. Scale bar, 1mm. Boxplots show (*F*) total number of primary bifurcations on each fin, (*G*) the absolute distance from the base of the ray to the primary bifurcation (or the total ray length for non-bifurcating rays; filled datapoints), and (*H*) the average length of distal segments 15-17. Filled circles represent measurements from non-bifurcating rays, empty circles represent measurements from bifurcating rays. Significance determined by an ANOVA followed by Tukey's HSD; significance indicated by letter groups, with statistically indistinguishable groups sharing the same letter.

2.2.8 Proximalized patterning despite intact Shh/Smo machinery.

Since Shh signaling is essential for the establishment of bifurcations (Armstrong et al., 2017; Braunstein et al., 2021; Zhang et al., 2012), and since *thrab* and TH activity are detectible in the epidermis where Shh is active, we hypothesized that the hormone might be required for Shh activity. We found that HypoTH regenerates maintained *shha* expression, although the overall expression level was somewhat decreased relative to WT (Fig 2.5*A*-*C*). Notably, *shha* domains failed to distinctly separate in the absence of TH (Fig 2.5*B"*). This finding contrasts markedly with experimental treatments that can functionally inhibit or delay bifurcations, but nonetheless show clear separation of *shha* expression domains (Armstrong et al., 2017; Azevedo et al., 2011; Zhang et al., 2012).

We asked if TH was required for the integrity of downstream Shh machinery and the migration of Shh-responsive cells. As fins regenerate, Shh/Smo signaling is essential for establishing bifurcations(Armstrong et al., 2017; Braunstein et al., 2021), and as in (Armstrong et al., 2017) we used a photoconvertable *ptch2* reporter (Huang et al., 2012) to assess dynamic activity of the pathway. Even in a HypoTH context, new *ptch2* was continuously expressed during regeneration. Previously Shh/Smo responsive cells are shown to be displaced to the distal tips of growing rays in WT regenerates (Armstrong et al., 2017; Braunstein et al., 2021). This process was not dependent on TH, and previously *ptch2*-expressing cells showed displacement even in HypoTH (compare arrows, Fig 2.5*D*-*E*). In all, the Shh-dependent machinery underlying branch formation appears to be intact in regenerating fins of HypoTH fish; yet bifurcation processes are

not initiated at the appropriate locations.

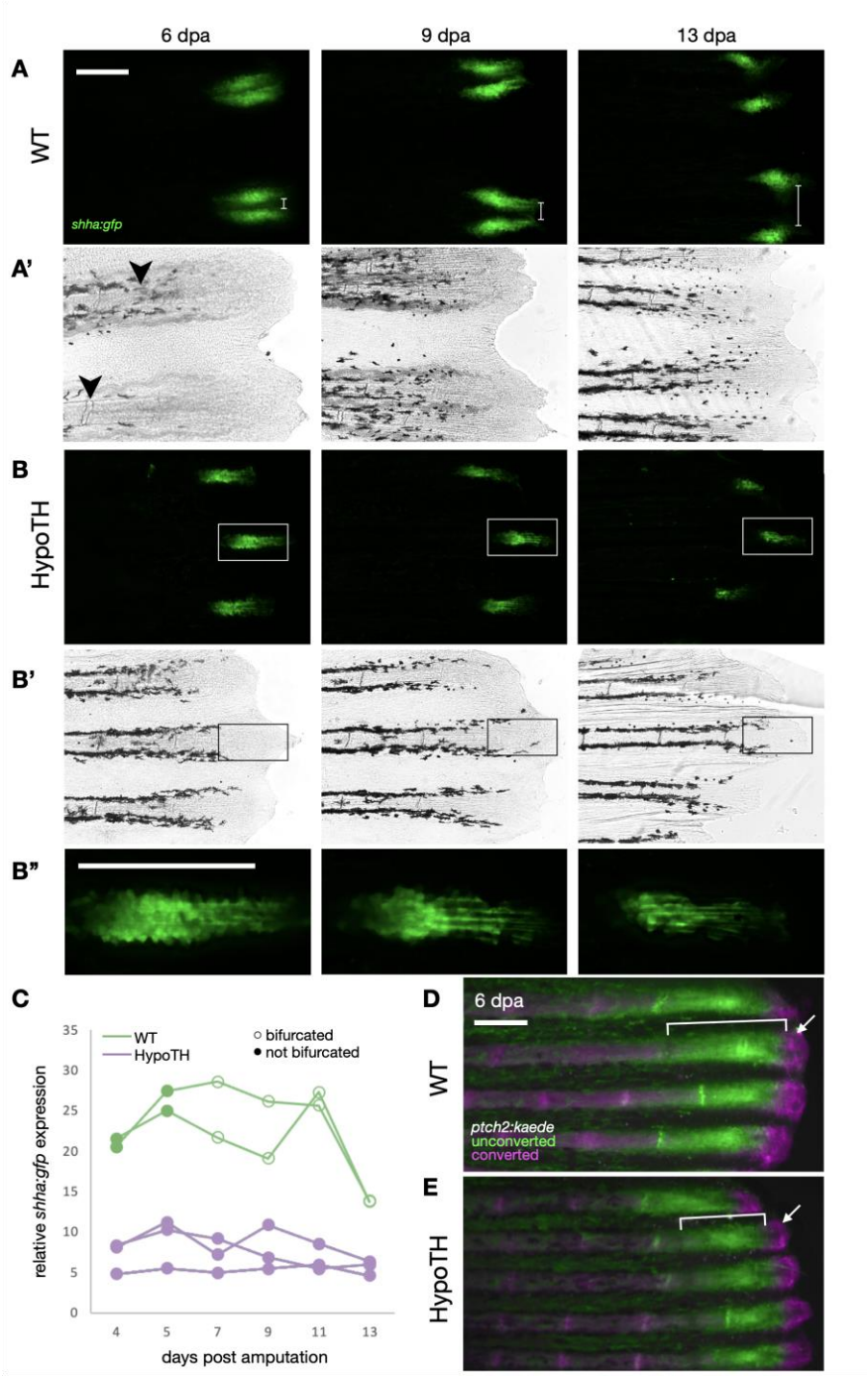

Figure 2.5 Thyroid hormone acts upstream of the Shh pathway to coordinate bifurcation with outgrowth. (*A-B*) Expression of transgene *-2.7shha:GFP* as bifurcations form in fins of WT (*A,* arrowheads) and HypoTH fish (B). A' and B' show brightfield images of the corresponding regions. Note failure of *shha* domains to separate in (*B"*) HypoTH, a magnification of the boxes in *B*. Representative images captured and processed to best show domains at each time point; brightness should not be compared between images. (*C*) Quantification of relative *shha:GFP*

expression in regenerating rays (2nd dorsal) from WT and HypoTH imaged under identical conditions. (*D-E*) Regenerating fins of fish transgenic for *BAC(ptch2:Kaede)* at 6 dpa in (*D*) WT and (*E*) HypoTH backgrounds. Entire fins were photoconverted at 5 dpa so that unconverted kaede (green) in brackets represents new expression produced in 24hr post photoconversion on the 2nd dorsal rays. Arrows indicate regions of old, converted kaede (magenta) displaced to the distal edges. Scale bars, 200 μM.

2.2.9 TH regulates ray patterning across teleost species.

We asked if a requirement for TH in ray patterning was limited to zebrafish. TH was required for distal patterning in a closely related *Danio* species(Mccluskey et al., n.d.): transgenic thyroid ablation in *Danio albolineatus* resulted in proximalized fin rays as it did in *D. rerio* (Fig 2.6*A-B*; Supp Fig 2.19*A-F*). Medaka (*Oryzias latipes*) are separated from zebrafish by ~200 million years of evolution (Chowdhury et al., 2022; Furutani-Seiki & Wittbrodt, 2004), and even in this distant relative, pharmacologically blocking TH inhibited bifurcation during regeneration (Fig 2.6*C-D*; Supp Fig 2.19*H-J*).

2.3 DISCUSSION

2.3.1 Summary of findings.

Collectively, our results demonstrate that TH is both necessary and sufficient to induce distal patterning of fin rays during developmental and regenerative outgrowth. Numerous indicators of proximodistal identity showed coordinated responses to developmental TH titer: the location of bifurcations, ray segment morphology, bone density, and expression patterns along the axis are all influenced by TH. The requirement for TH to build bifurcations in an appropriate proximodistal location is shared across all the fins of the zebrafish as well as across multiple teleost species.

Our findings suggest that the processes regulating size and processes regulating patterning are governed by distinct developmental modules that may be decoupled. Previous work established that growth of the rays is regulated by bioelectricity pathways

(Harris, 2021), and we have shown that even when fin length is disrupted, there remains a requirement for TH in patterning the rays (Fig 2.2; Supp Fig 2.10). In principle, modulating proximodistal patterning can produce a spectrum of different ray phenotypes like those found in nature, from non-branching, uniformly thick, proximalized rays (e.g. those of sculpin) to highly distalized, multi-branched rays (e.g. guppy). These types of modular changes to patterning could underlie evolutionary diversity across fins and other appendages. Patterning shifts in the fins could be mediated by changes in local or global TH metabolism, or could be entirely independent of TH, acting on downstream or parallel mechanisms that regulate axis patterning.

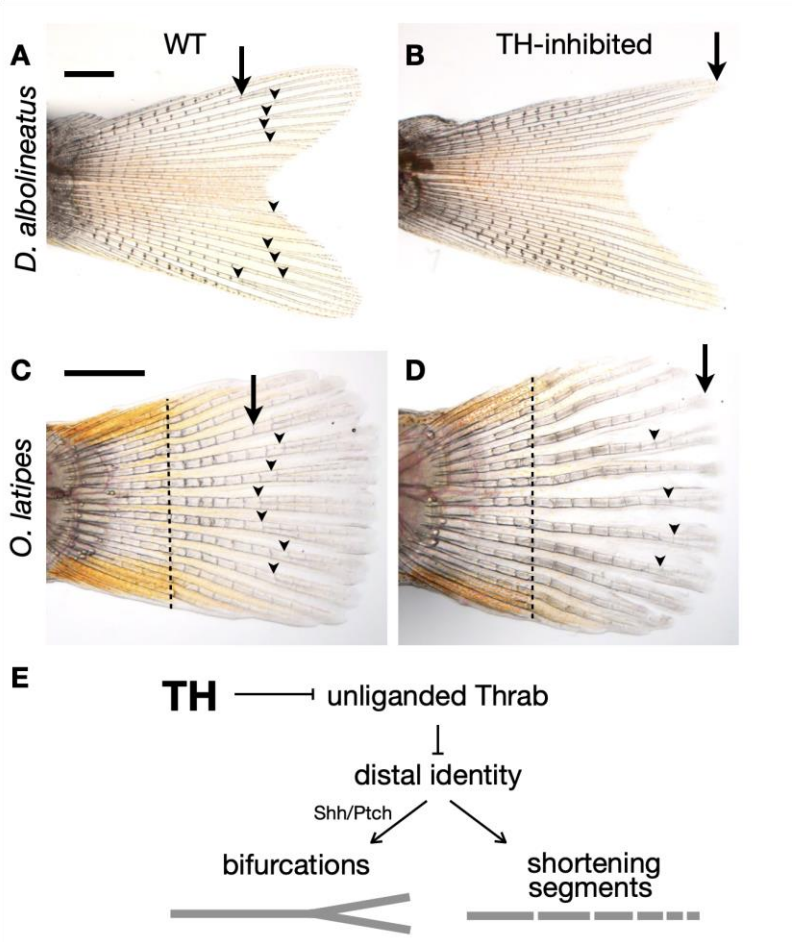

Figure 2.6 TH is required for bifurcation morphogenesis in other teleost species and a model for TH-induced distal identity. (*A-B*) *Danio albolineatus* that are either (*A*) WT or (*B*) trangenically thyroid-ablated. (*C-D*) *Oryzias latipes* (medaka) treated with a (*C*) vehicle control or (*D*) a TH-inhibiting cocktail throughout regeneration. Arrows indicate primary bifurcation of the 2nd

(A-B) or 3rd (C-D) dorsal ray or total ray length when ray does not branch. Arrowheads indicate all other bifurcations. Scale bars, 1mm (*E*) Model for progressive TH action across the proximodistal axis during fin outgrowth.

2.3.2 Segment morphology is sensitive to thyroid hormone.

In addition to the location of bifurcations, our study considers the morphology of ray segments as a readout of proximodistal patterning. Certain mutations cause fins to develop with overall shorter segments (Iovine et al., 2005; Nakagawa et al., 2022) or overall lengthened segments along the entire length of the ray (Harris et al., 2021; Lanni et al., 2019; Perathoner et al., 2014). In contrast, fins from HypoTH and HyperTH backgrounds showed proximal segments comparable in length to those of WT siblings, but which exhibited shifts in the slope of segment length decrease (Fig 2.1*G, K*; Supp Fig 2.2*E, K*), resulting in distal segments with lengths significantly different than those in WT siblings (Fig 2.1 *F, J*). In addition to the 'flattened' slope of segment length in fins of HypoTH, we note that there is increased variability in segment length (see Fig 2.1*G* and Supp Fig. 2.2*E*), which suggests a role for TH in stabilizing placement of the segment joints.

2.3.3 Thyroid hormone independent fin patterning.

Notably, not every distal feature is dependent on TH. Leucophores still form at the peripheral, distal edges of HypoTH fins (see Supp Fig 2.13*C-D*) and segment width tapering occurs regardless of TH titer (Supp Fig 2.2*F, L*). Despite enriched TH activity (see Supp Fig 2.13; Supp Fig 2.14), the peripheral-most rays were never observed to produce bifurcations, even under HyperTH conditions or when Thrab was absent. Peripheral rays maintain unique expression of several genes(Desvignes et al., 2022), highlighting the uniqueness of these rays in the fin and potentially suggesting additional roles for TH in ray identity beyond proximodistal patterning. In the absence of TH, some distal features are eventually produced—the longest rays of HypoTH fish produce

bifurcations and moderately shortened distal segments—but these processes are deployed in a delayed fashion and the ultimate fin structure is consequently highly proximalized. In the other extreme, there appears to be a limit to how distalized a fin can become by modulating TH levels: HyperTH conditions shift the proximodistal axis only slightly (Fig 2.1*H-K*). Indeed, HyperTH conditions did not change the total number of bifurcations in the fin (Fig 2.1*H*), presumably because the maximum number of fin rays bifurcate even in a WT background. Although the extent of HyperTH-induced distalization is limited, it appears to be dose-sensitive, as individuals heterozygous for the HyperTH mutation *opallus* typically showed intermediate phenotypes for aspects of proximodistal patterning (see Supp Fig 2.2*G-J*). In all, it is likely that other TH-independent pathways buffer the proximodistal morphology of the rays, limiting the severity of the phenotypes in Hypo- and HyperTH contexts.

2.3.4 Thyroid hormone action is acute.

The phenotype of a HypoTH fin can be rescued both during development (Supp Fig 2.7) and regeneration (Fig 2.4) by treatment with exogenous TH. Moreover, rays regenerating in a HypoTH context remain competent to produce distal features into late stages of outgrowth (Fig 2.4). Treatment with TH at early stages of development (Supp Fig 2.7) or during early periods of regeneration (Supp Fig 2.16) produces no effects on the fin patterning phenotype. Together, these findings suggest that the hormone acts on tissues acutely during outgrowth.

2.3.5 Sonic hedgehog signaling.

During regeneration, TH is active in the epidermis and promotes high Shh pathway activity. Shh-active basal epidermal cells are required for branching morphogenesis (Armstrong et al., 2017; Braunstein et al., 2021), and these cells still

exhibit distal displacement in HypoTH fins as in WT (Fig 2.5*D-G*), suggesting that these components of bifurcation machinery are not dependent on TH. Nonetheless, the hormone appears to be required for the two Shh domains to separate (Fig 2.5*A-C*).

Recent evidence suggests that bone resorption activity counteracts mineralization activity to produce branches (Cardeira-Da-Silva et al., 2022). Our RNAseq data did not suggest that TH affects expression levels of genes associated with the overall abundance of osteoblasts or osteoclasts in intact, uninjured fins (see Supp Fig 2.9*I-J*). However, these data from intact tissue may differ from expression during regeneration; osteoclast/osteoblast ratios may be altered after injury. Moreover, it is possible that TH might regulate relative activities of these cell populations along the proximodistal axis to regulate where bifurcations form along the growing axis. Indeed, pre-osteoblasts appear show TH activity during regeneration (Fig 2.3*J*), which may alter their relative activity.

2.3.6 There is no single distalizing factor.

Fins developed under HypoTH conditions showed proximalized gene expression profiles (Fig 2.1*L-M*), suggesting that proximodistal identity is legitimately shifted in a TH-disrupted context. Our data do not identify a single ‘smoking gun’ pathway or cell type through which TH likely acts to impart distalization. Instead, the hormone appears to progressively orchestrate numerous suites of genes along the axis, including pathways regulating skeletal morphogenesis, extracellular organization, as well as gas transport and adhesion (Supp Fig. 2.9*C*). We note, however, that the shifts in gene expression could be either causes or effects of the phenotypic distalization observed, and that expression patterns during outgrowth may differ from these profiles in the intact organ.

The repressive activities of unliganded Thrab and the permissive context of TH appear to work in conjunction to mete out progressively distal features during fin

outgrowth. Unliganded TH receptors serve to repress developmental processes in other contexts, inhibiting amphibian metamorphosis (Buchholz et al., 2003) and gating morphogenesis of zebrafish skin and pigment (Aman et al., 2021; Saunders et al., 2019). Removing the repressive unliganded receptor rescues patterning in a HypoTH background (Fig 2.3). HypoTH *thrab* mutant fin rays are still somewhat proximalized relative to those of WT and euthyroid mutant siblings, suggesting that TH-related mechanisms independent of Thrab also help to promote distalization. Furthermore, the euthyroid *thrab* mutants show patterning comparable to that of WT (despite showing less TH activity, see Supp Fig 2.13*G-I*), suggesting that Thrab is more active as an inhibitor than as an enhancer of distal morphology.

2.3.7 Distalization of the fin is progressive.

Unlike a limb, the fin grows indeterminately from the distalmost edge throughout adult life (Iovine & Johnson, 2000). TH is active at this growing edge, even in an uninjured adult fin (Supp Fig 2.13*C*), potentially reflecting the metabolic demands of continuous isometric growth. During regeneration, functional TH activity at the leading edge remains relatively constant as outgrowth progresses (Fig 2.3*K*), suggesting that the hormone does not function in the “source-sink” manner of certain limb identity pathways. Indeed, distalization appears to be a progressive process along the continuously growing axis of the fin. The proximodistal patterning of the rays is actively orchestrated by TH during outgrowth. During regeneration it is the continuous presence of TH—rather than memory of previous pattern—that dictates ray morphology along the axis. In parallel, active bioelectric signaling during outgrowth—rather than positional memory of size—determines fin length (Daane et al., 2018).

We propose a model in which TH relieves the repression of Thrab to deploy bifurcation morphogenesis in the correct proximodistal contexts by coordinating suites of

pathways that result in progressive distalization during outgrowth (Fig 2.6*E*). In all, modulating the TH pathway changes the ultimate proximodistality of the appendicular skeleton. Thus, the TH axis and its downstream targets are attractive candidates for fin ray diversification and changes to axis identity in other contexts. Our study demonstrates that ray patterning changes may be largely decoupled from size, providing insight into the regulatory logic underlying fin morphogenesis during development and regeneration.

2.4 MATERIALS AND METHODS

2.4.1 Fish lines.

HypoTH and their WT controls were both *Tg(tg:nVenus-v2a-nfnB)* (S. K. McMenamin et al., 2014). HyperTH zebrafish were *opallus*^{b1071}, which constitutively overproduce TH (S. K. McMenamin et al., 2014). The other transgenic strains used were: *Tg(6xTRE-bglob1:eGFP)* (Matsuda, 2018); *Tg(-2.7shha:GFP)* (Neumann & Nuesslein-Volhard, 2000); *TgBAC(ptch2:Kaede)* (Huang et al., 2012); and *Tg*(*runx2:mCherry)* (Shannon Fisher Lab, Boston University). The other mutant strains used were: *duox*^{sa9892} (Chopra et al., 2019); *longfin*^{dt2}/*kcnh2a* (Daane et al., 2021; S. Stewart et al., 2021; Van Eeden et al., 1996); *shortfin*^{dj7e2}/*cnx43* (Perathoner et al., 2014); *thrab*^{vp31rc1}, *thraa*^{vp33rc1}, and *thrb*^{vp34rc1}(Saunders et al., 2019). Other species used were pink pearl danios (*Danio albolineatus*) transgenic for *tg:nVenus-v2a-nfnB* (S. K. McMenamin et al., 2014) and commercially-obtained Japanese medaka (*Oryzias latipes*).

2.4.2 Fish rearing conditions.

All fish were reared at 28°C with a 14:10 light:dark cycle, and fed 2-3 times per day. All larval fish were fed with live marine rotifers and *Artemia*. Juvenile and adult fish

stocks that were not TH-modulated (e.g. the *6xTRE-bglob1:eGFP* line) were fed with Gemma Micro (Skretting, Stavanger, NOR) and Adult Zebrafish Diet (Zeigler, Gardners PA, USA). To minimize potential introduction of exogenous TH, HypoTH adults (below) and their WT controls were fed pure Spirulina flakes (Pentair, London, UK) and live *Artemia* instead of the enriched pellet diet.

2.4.3 Thyroid follicle ablations.

To generate HypoTH fish, we performed conditional transgenic ablations of the larval thyroid follicles. The thyroid ablation line *Tg(tg:nVenus-v2a-nfnB)* expresses a gene encoding bacterial nitroreductase specifically expressed in the TH-producing thyroid follicles (S. K. McMenamin et al., 2014). In the presence of the drug metronidazole, nitroreductase produces cytotoxic metabolites that specifically ablate cells (Curado et al., 2008). We incubated *tg:nVenus-v2a-nfnB* 4-5 dpf larvae overnight in 1% DMSO with 10 mM metronidazole (Thermo Scientific Chemicals, AAH6025814; for HypoTH), or with 1% DMSO alone (for euthyroid, WT controls) in 10% Hanks or fish water (S. K. McMenamin et al., 2014). Thyroid-ablated fish remain HypoTH throughout their lives (S. K. McMenamin et al., 2014).

2.4.4 Imaging.

Anesthetized (using MS-222, ~0.02% in system water) or cleared and stained (Walker & Kimmel, 2007) samples were imaged on an Olympus SZX16 stereoscope using an Olympus DP74 camera, or on an Olympus IX83 inverted microscope using a Hamamatsu ORCA Flash 4.0 camera. Images were processed in CellSense (Olympus, Tokyo JPN) or on FIJI and adjusted for contrast, brightness and color balance; corresponding adjustments were made for images of both control and experimental fish.

For paired images shown in figures, adult fish were size-matched as closely as possible and always within 2mm SL (Parichy et al., 2009).

2.4.5 Statistical analysis.

Analyses were performed in RStudio (build 372). Morphological data were typically analyzed with either Welch two sample t-test or ANOVA followed by Tukey's Honest Significant Differences (using a 95% family-wise confidence level). In graphs showing a single comparison, significance is indicated as follows: p <0.05, *; p <0.001, **; p <0.0001, ***. In graphs showing multiple comparisons, significance is indicated on graphs by letter groups, with statistically indistinguishable groups sharing the same letter (p-value threshold <0.05).

2.4.6 Photoconversions.

Sibling WT and HypoTH *TgBAC(ptch2:Kaede)* individuals were imaged at 5 dpa. Kaede was photoconverted by ~90s DAPI exposure at 4x on a Olympus IX83 inverted microscope. Images were acquired pre- and post-DAPI exposure to confirm complete photoconversion. Fins were reimaged 24hrs later (at 6 dpa) to assess new Kaede expression as in (Armstrong et al., 2017).

2.4.7 Fin amputation.

All regeneration experiments were performed on adult zebrafish 18-23 mm SL. Caudal fins were amputated from anesthetized fish under a stereoscope at the 4-5th ray segment using a razor blade.

2.4.8 Pharmacological treatments.

Stocks of T4 (L-thyroxine; Sigma, St. Louis MO, USA) were prepared in NaOH, then diluted into fish system water to 5 nM T4 with 194 nM NaOH or 10 nM with 388 nM NaOH; vehicle controls were prepared with a corresponding amount of NaOH in system water. Stocks of MPI cocktail (Salis et al., 2021) were prepared in DMSO, then diluted into system water to a final concentration of 1.0 mM methimazole, 0.10 mM potassium perchlorate, and 0.010 mM iopanoic acid with 0.05% DMSO; vehicle controls were 0.05% DMSO in system water. Thiourea was diluted to 0.1125% directly in system water. Water changes were performed at least every other day throughout the treatment period.

2.4.9 *In situ* hybridization.

For *In situ* hybridization fin tissues were collected at different stages during regeneration, fixed in 4% paraformaldehyde in PBS, then stored in methanol (Thisse & Thisse, 2007). Probes for *thrab* were prepared using the primers F: agtgcacgtcctaaagagcaaac and R: acgtcacacgtcctgatcctc. Riboprobes were fractionated to an average size of ~600nt. To ensure probe penetrance (Smith et al., 2008), a subset of specimens were embedded and cryosectioned, *in situ* hybridization was subsequently performed on sectioned tissues.

2.4.10 Immunohistochemistry.

Fin tissues was collected during regeneration, fixed in 4% paraformaldehyde in PBS, embedded in agarose/sucrose solution re-embedded in Tissue-Plus™ Optimal Cutting Temperature Compound (Fisher Healthcare, 23-730-571) and frozen. Blocks were cryosectioned into 16μM slices, dried overnight on slides, then immunostained with anti-GFP (Sigma Aldrich, Burlington MA, USA, SAB4301138) and anti-mCherry (Novus Biologicals, Minneapolis MN, USA, NBP2-25158) followed by secondary antibodies (Jackson ImmunoResearch, West Grove PA, USA, 711-545-152 and 703-585-155).

2.4.11 Fluorescence quantifications.

A size for a region of interest was determined for each experiment, such that the smallest domain in the image series would be captured by the region. Using ImageJ, the region of interest was placed over the terminal portion of the ray to capture the mean fluorescence intensity.

2.4.12 Fin ray morphology quantifications and comparisons.

A landmark-based approach was used to quantify fin ray morphology using the R package StereoMorph (Olsen & Westneat, 2015) . Landmarks were manually placed on segment joints (to measure segment length), both sides of the segment (segment width), and bifurcations for the 2nd dorsal ray (zebrafish and *D. albolineatus*) or 3rd dorsal ray (medaka). Fin ray morphology was calculated using the coordinates of these landmarks (See Fig. S2*A*). Measurements from occasionally misshapen or obviously damaged rays were excluded from analyses. In all analyses, we make statistical comparisons between clutch mates reared simultaneously, and present only a single ray from each individual. To obtain sibling controls for HyperTH and *thrab* mutants, full siblings from heterozygote crosses were individually genotyped and identified as +/+, +/- or -/-. Sibling controls for *thraa* mutants came from a homozygous mutant backcross; offspring were genotyped as +/- or -/-.

2.4.13 Parametric and non-parametric tests.

Parametric statistics were used to test for differences between groups and are shown in figures. For datasets that were not normally distributed (according to a Shapiro-Wilks test with a *p*-value threshold of 0.01), we additionally performed a Mann-Whitney U test or Kruskal-Wallis test (*p*-value threshold of 0.01) followed by a Dunn Test.

The parametric and non-parametric test outcomes were largely consistent throughout; all statistical results are shown in Dataset S1. Multiple preliminary analytical methods were applied to comparisons, and a subset are presented, detailed in the two following sections.

2.4.14 Quantifications of bifurcation location.

There are several ways to geometrically capture the location of the bifurcation point along the axis of the ray, each with certain shortcomings. We present two different methods for evaluating the location of the bifurcation in the context of the fin. In the primary figures, we present the absolute distance from the base of the ray to the bifurcation—or the total length of the ray in non-bifurcating rays. A shortcoming of this approach is that if a ray is short but does not bifurcate, it can appear statistically similar to a ray that branches at a similar length. For example, in Fig 4G, control HypoTH fish look statistically more similar to WT than HypoTH fish that were rescued late with TH. Additionally, in the SI figures, we present the location of the bifurcation as a proportion of the total ray length—which is captured as 1.0 in non-bifurcating rays. This allows the bifurcation (or lack thereof) to be taken in the context of the actual length of the ray, however this proportion data violates the assumptions of an ANOVA. Since in many experiments with overall shorter rays, none of the rays in HypoTH fins actually form bifurcations (and therefore all have a proportion of 1.0), normality is frequently violated.

2.4.15 Quantifications of segment lengths.

Distalmost segments were removed from assessments of segment length, since these did not represent fully formed ray segments. We assessed the progressive shortening of distal segments by multiple methods, presenting two of these for most experiments. First, we compared the average length of distal segments. Between

experiments, the sizes of the fins differed, therefore, within each experiment, we selected 3 consecutive segments as far distally as possible such that they could be captured from most fins. Second, we considered the overall trends in segment length decrease, plotting the length of every segment from the 5th to the penultimate segment. After preliminarily testing several models, we used linear mixed effects to evaluate interaction between experimental treatment and segment number.

2.4.16 Micro-computed tomography scans.

Samples were fixed and embedded in 1% agar and scanned on a SkyScan 1275 micro-CT system (Bruker, Billerica MA, USA) at a scanning resolution of 10.5 μm with an x-ray source at 40 kV and 250 mA. >2800 projection images were generated over 360° with a 0.1° rotation step and 6 averaging frames. Thresholding, ring artifact reduction, and beam hardening corrections were performed consistently across all scans during reconstruction using NRecon (Bruker). Reconstructed BMP slices were analyzed using Amira 6.5 (Thermo Fisher Scientific, Waltham MA, USA). Density heatmaps were generated with the volume rendering module and physics load transfer function. Density along the proximodistal axis of the 2nd dorsal ray was measured from greyscale density renderings using ImageJ v.1.49(1).

2.4.17 RNA sequencing.

Intact caudal fin tissue was sampled from adult siblings (>18 mm SL) reared under WT or HypoTH conditions. Each fish was first anesthetized and the entire fin was amputated using a razor blade. Proximal, middle and distal regions of the fin were collected and flash frozen. Three biological replicates each containing five fin regions were collected for each TH backgrounds. RNA was immediately extracted using Quick-

RNA Microprep kit R1050 (Zymo Research, Irvine CA, USA). Sample libraries were made with NEBNext Ultra II RNA Library Prep kit and sequenced on an Illumina Novaseq 6000 platform with 20M 150bp paired-end sequences per sample (Novogene, Beijing, China). Raw sequence reads were aligned to Zebrafish GRCz11 using STAR version 2.7.3(Robinson et al., 2010), gene counts were called using Ensembl GRCz11 gene annotation. Differential gene expression analyses were performed with Bioconductor package edgeR(Robinson et al., 2010). Genes were considered significantly expressed if they showed a $\log_2$ fold difference higher than 2 and a false discovery rate lower than 0.01. Genes were considered to be differentially expressed between proximal and distal regions if the log fold change difference the WT condition was higher than 2, and the false discovery rate was less than 0.01. Differentially expressed genes were determined to be TH-dependent if they showed proximal or distal enrichment in the WT condition, but not in HypoTH condition. Gene Ontology analysis was performed using clusterProfiler (Yu et al., 2012).

2.4.18 Quantitative PCR.

Regenerating fin tissue (~4 segments wide) was sampled on days 5, 7, 9 and 15 post amputation in adult WT zebrafish. Four samples were pooled as one biological replicate and a total of three biological replicates were collected at each time point. Sample was stored in RNAlater at -80°C. RNA was extracted with Quick-RNA Microprep kit (Zymo Research, Irvine, CA) cDNA was produced using the SuperScript IV First-Strand Synthesis System (Invitrogen, Carlsbad, CA), qPCR of *thrab* was performed on QuantStudio 3 (Applied Biosystems, Foster City CA, USA) cycler using primers F: tctgatgccatcttcgacttg; R: gtacatctcctggcacttctc. Data were analyzed with ThermoFisher Connect software (Thermo Fisher Scientific).

2.5 SUPPLEMENTAL DATA

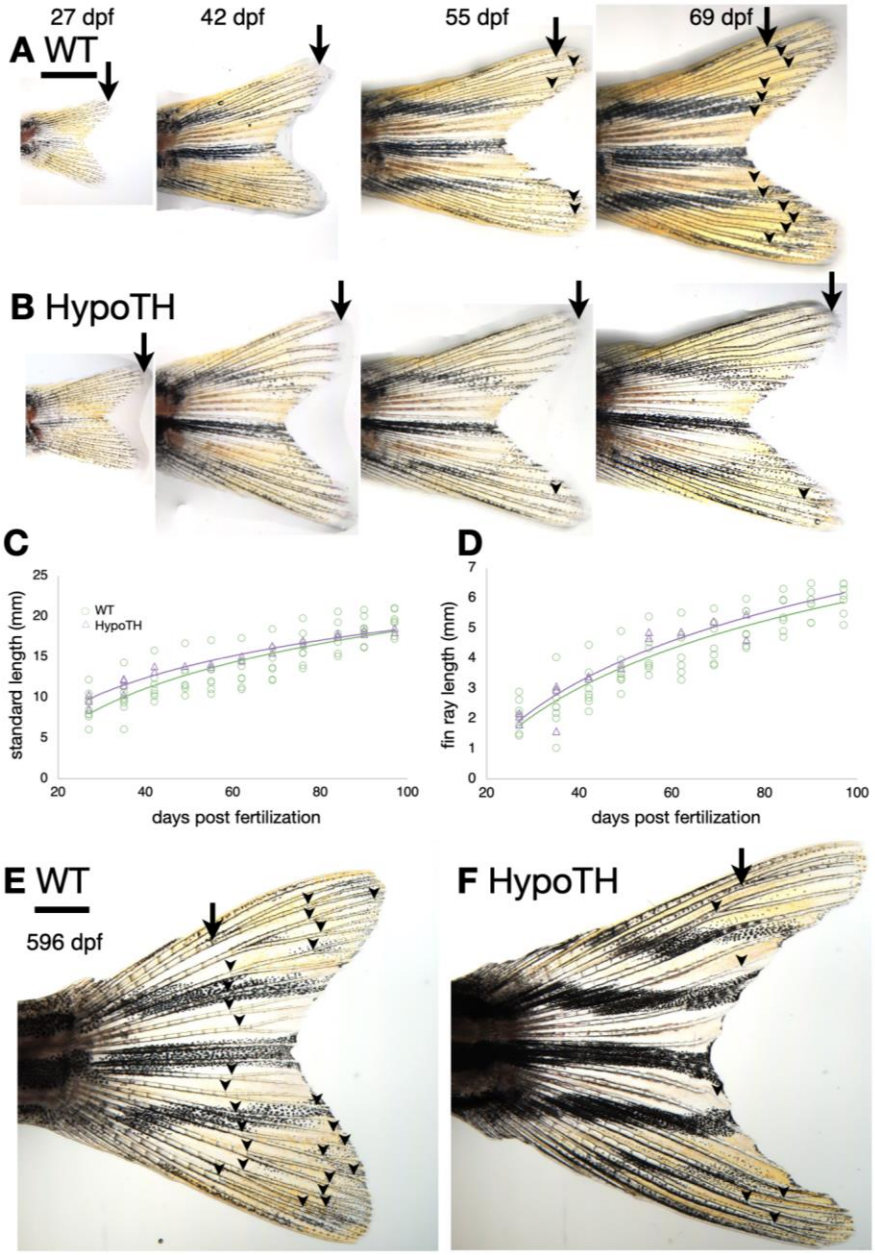

Supplemental Figure 2.1 Developmental hypothyroidism inhibits ray bifurcation but has little influence on growth rates. A clutch of (*A*) WT and (*B*) HypoTH fish was imaged weekly throughout development; fins shown at 27, 42, 55 and 69dpf. Graphs of (*C*) standard length and (*D*) total length of 2nd dorsal ray as a function of days post fertilization (dpf). Note that fins of HypoTH fish are extremely prone to damage when imaged repeatedly; after 76 dpf no undamaged 2nd dorsal rays could be measured from HypoTH backgrounds. Fins of 20-month-old fish showing (*E*) normal patterning in the WT and (*F*) proximalized patterning in the HypoTH context. Arrows indicate primary bifurcation of the 2nd dorsal ray or total ray length when ray does not branch; arrowheads indicate all other bifurcations. (Scale bars, 1 mm).

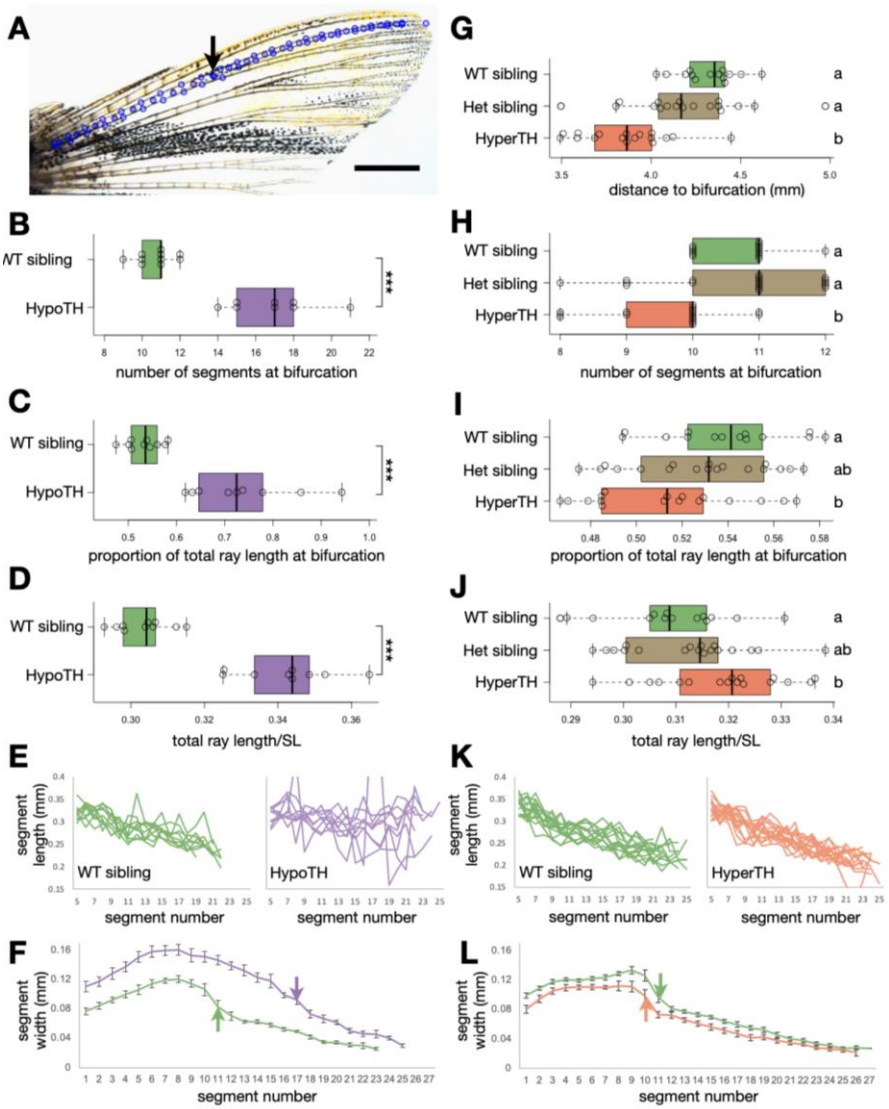

Supplemental Figure 2.2 Thyroid hormone regulates proximodistal morphology. (*A*) On the 2nd dorsal ray, individual landmarks (blue dots) were manually placed to capture bone morphology. Landmarks were placed on the joints between segments to measure segment length; two landmarks were placed across the middle of each segment to measure width, and one landmark was placed at the primary bifurcation node (indicated with arrow). The distance to the bifurcation on each ray was the sum of all segments (and the partial segment) proximal to the primary bifurcation. The total length of the ray was the sum of all complete segments in the ray. (Scale bar, 1 mm). Boxplots showing (*B*, *H*) the number of segments on the ray up to the bifurcation, (*C*, *I*) the proportion of the total ray length at the primary bifurcation, and (*D*, *J*) the total ray length divided by SL and (*G*) the absolute distance from the base of the ray to the bifurcation. Note that heterozygote data is added here alongside its sibling WT/HyperTH data shown in Fig. 1. Significance determined by a Welch two-sample *t* test or an ANOVA followed by Tukey's HSD. (*E, K*) Plots showing the average length of each segment, starting from the 5th segment. Note that for clarity, some of the extreme outliers are cut off in the graphs. (*F*, *L*) Plots show average segment width as a function of segment number. In *G-L* data are shown for a single clutch genotyped as WT (+/+), heterozygote (+/*opallus*), or HyperTH mutant homozygote (*opallus*/*opallus*).

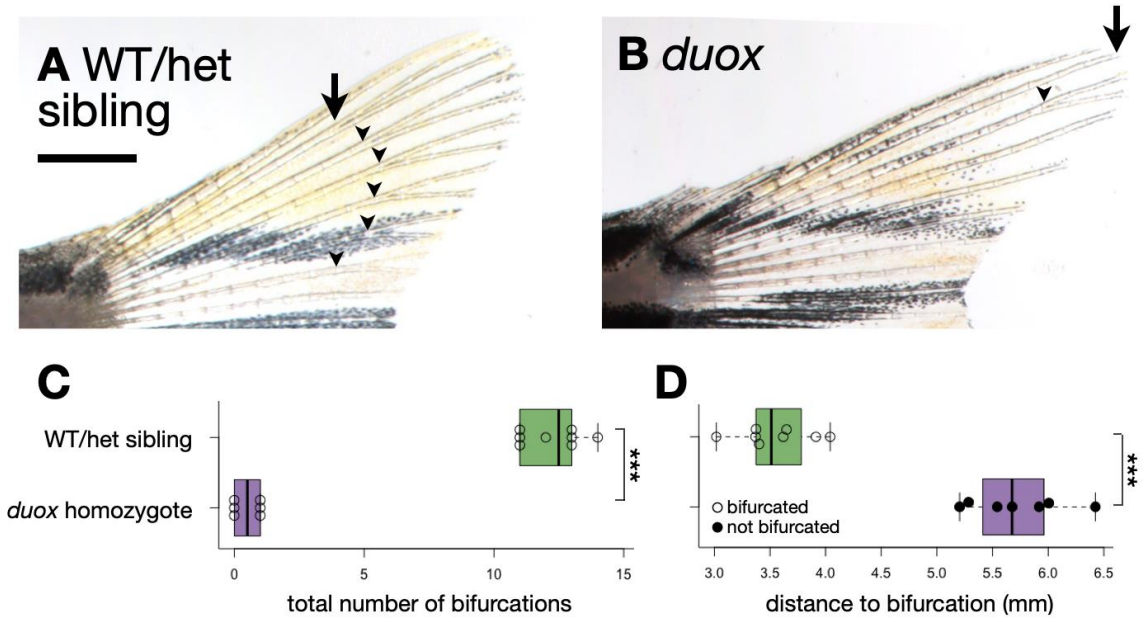

Supplemental Figure 2.3 Genetic hypothyroidism proximalizes fin rays. Developed fin from adults of a heterozygous intercross of congenitally hypothyroid mutant *nadph*^{duox} (Chopra et al. 2019) (*A*) Fin of either WT (+/+) or heterozygous sibling (*+/duox*) and (*B*) homozygous mutant (*duox/duox*). Arrows indicate primary bifurcation of the 2nd dorsal ray or total ray length when ray does not branch; arrowheads indicate all other bifurcations. (Scale bar, 1 mm). Boxplots showing (*C*) the total primary bifurcations of each fin, and (*D*) the absolute distance to bifurcation of the 2nd dorsal ray (or the total ray length for non-bifurcating rays). In *D*, filled circles represent measurements from non-bifurcating rays, empty circles represent measurements from bifurcating rays. Significance determined by a Welch two-sample t-test.

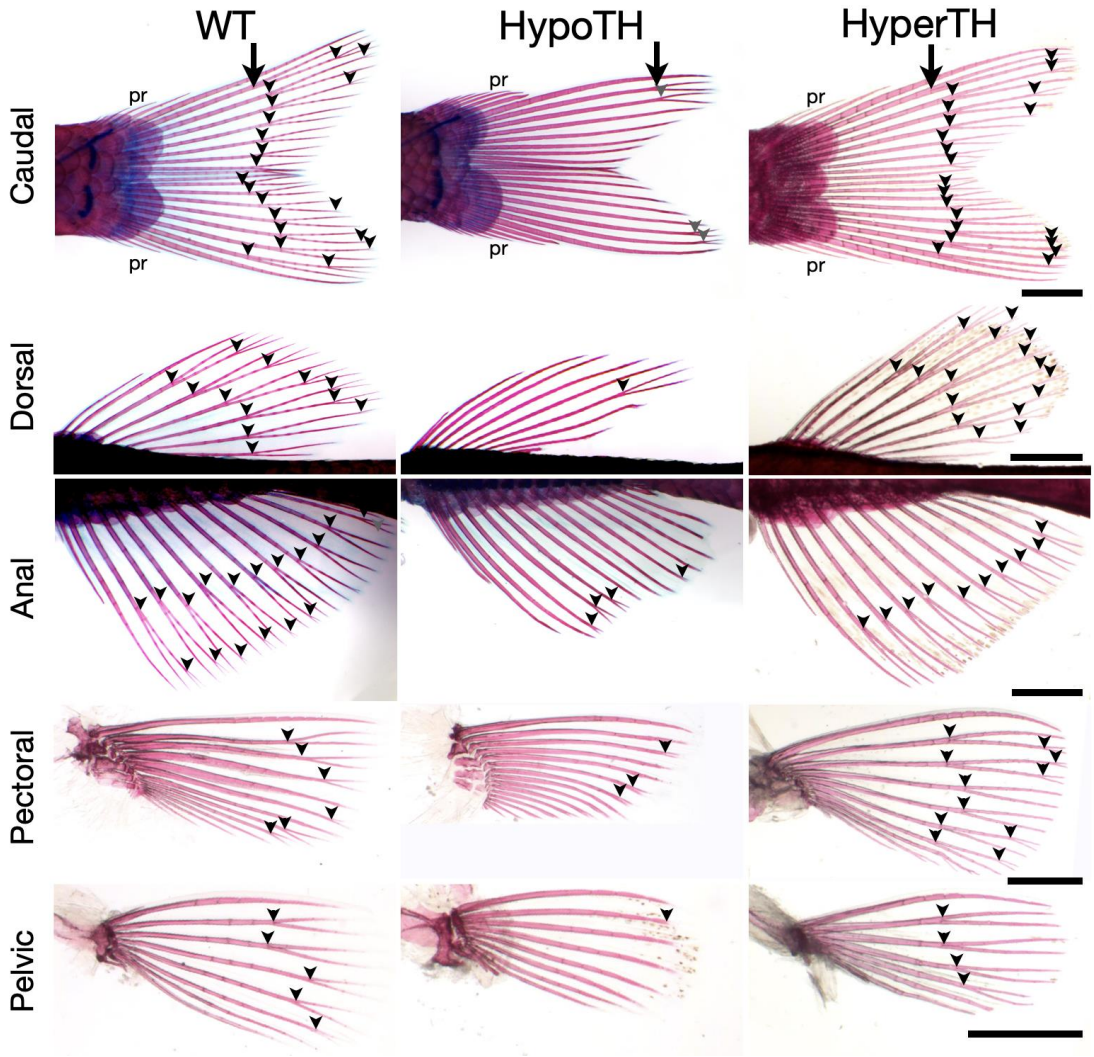

Supplemental Figure 2.4 Thyroid hormone is required for distal ray morphology in paired and medial fins. The three medial fins (caudal, dorsal, and anal) and two paired fins (pectoral and pelvic) of adult zebrafish reared under three TH profiles. Black arrows, location of the primary bifurcation on the 2nd dorsal caudal ray; grey arrowheads, all other bifurcations. pr, procurrent rays. Note that the number of procurrent rays scales inversely with developmental TH titer: procurrent rays in HypoTH fish are longer, wider, and more numerous; HyperTH fish have fewer, shorter procurrent rays. (Scale bars, 1 mm).

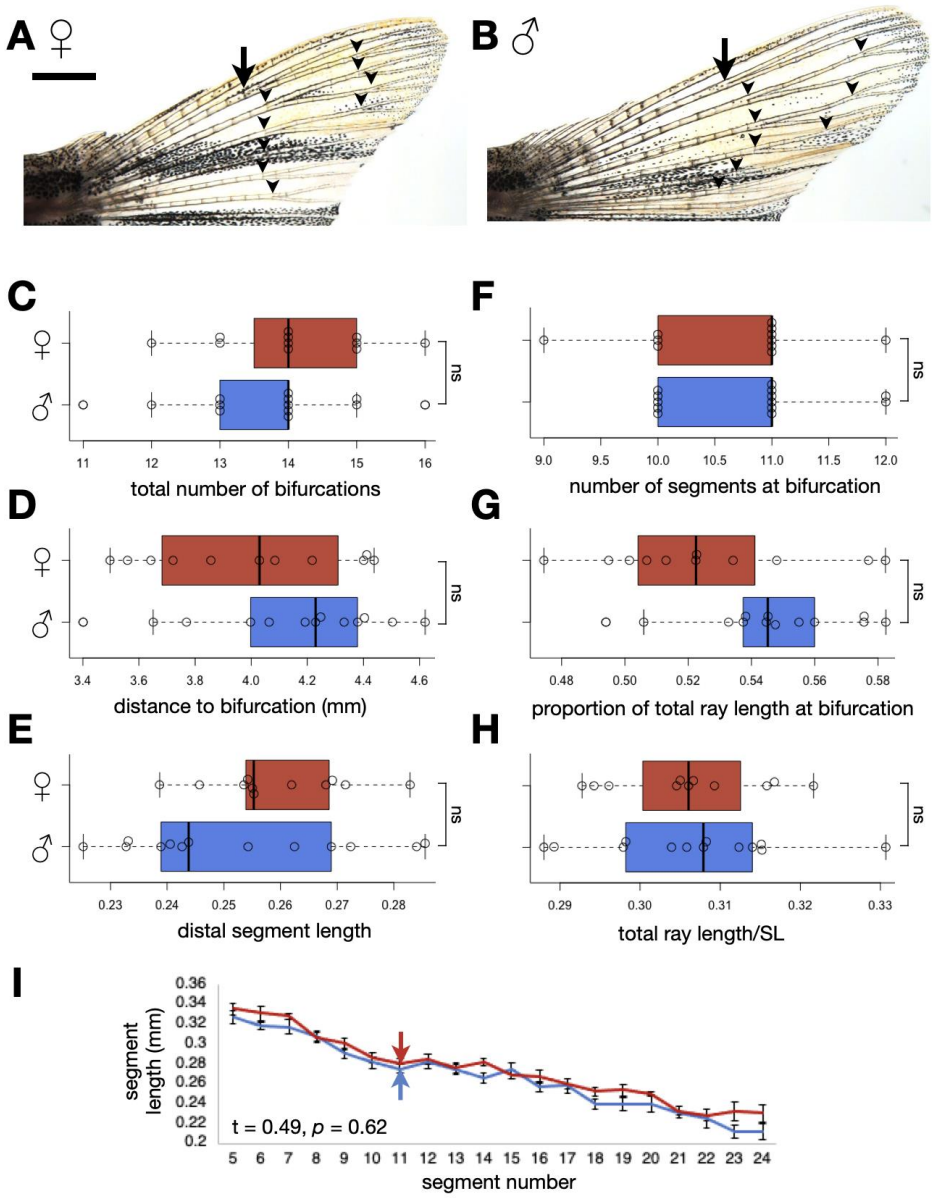

Supplemental Figure 2.5 Sex does not influence ray patterning. (*A-B*) Caudal fin from adult female (*A*) and male (*B*). Box plots showing (*C*) the total number of primary bifurcations of each fin, (*D*) the absolute distance of the ray up to the bifurcation, (*E*) the average length of distal segments 16-18, (*F*) the number of segments of the ray up to the bifurcation, (*G*) the proportion of total ray length at bifurcation, and (*H*) the ratio of total ray length to SL. (*I*) Plot showing the average length of each segment, starting from the 5th segment. Error bars indicate standard error; Red, female; blue, male. Arrows indicate the average location of the primary bifurcation in each background. None of comparisons show significant differences. Groups used to assess for effects of sex were the DMSO-treated transgenics (controls for HypoTH) and the individuals genotyped as WT that were siblings of the *opallus* mutant clutch; individuals were sexed visually in images. For distal segment length (shown in *E*), we note that when the control groups are analyzed separately, males have somewhat longer distal segments within DMSO-treated transgenic controls (t=-3.01, df=4.70, *p*=0.03), while females have somewhat longer distal segments within WT siblings of HyperTH (t=3.46, df=9.40, *p*=0.01). Significance determined by Welch two-sample *t* tests.

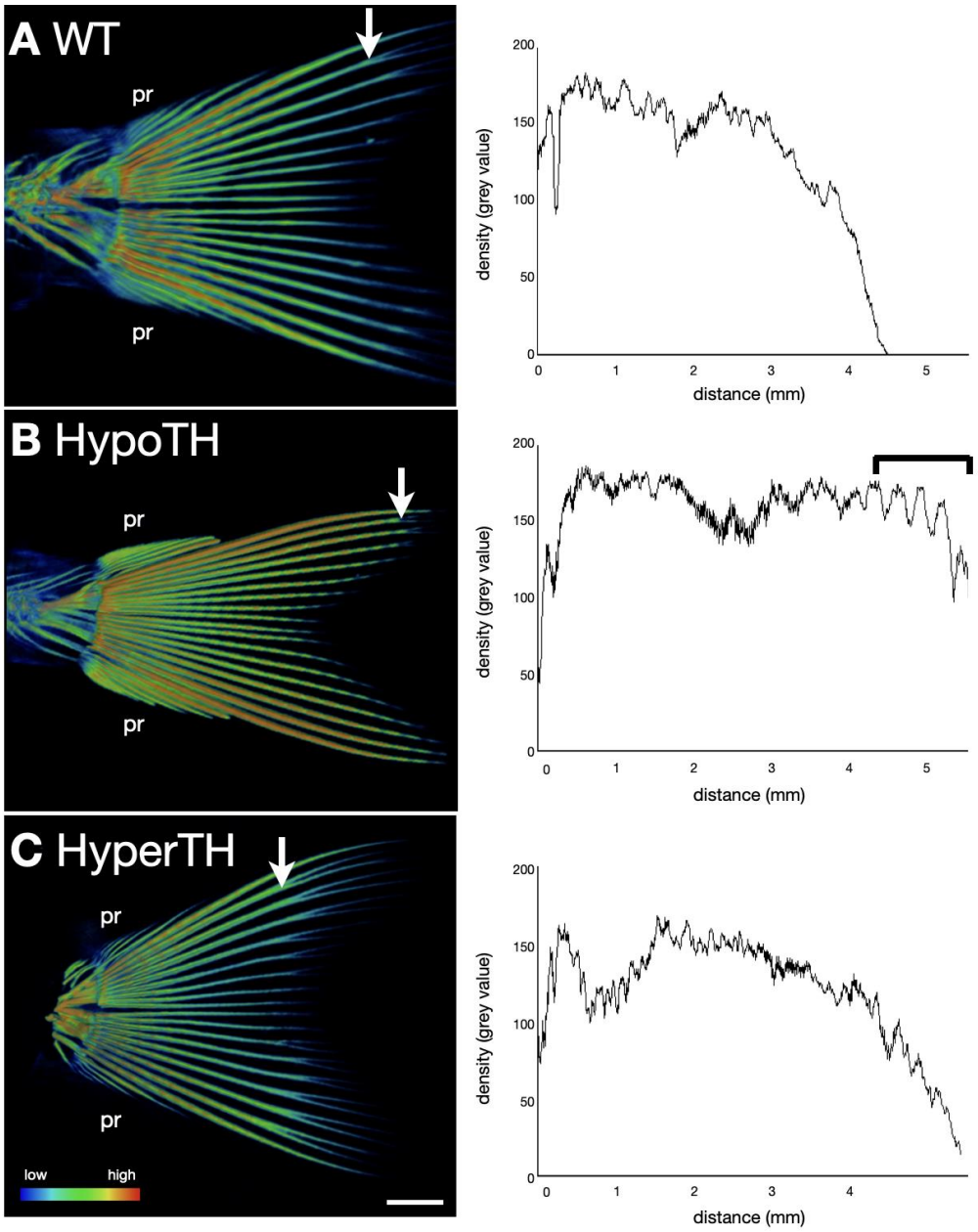

Supplemental Figure 2.6 Thyroid hormone regulates density of fin rays along the proximodistal axis. Left shows Micro-CT scans of fins from fish reared under different TH profiles. Scanning conditions and thresholds are identical, and each fish is 20 SL. Warmer colors show higher density tissue; cooler colors show less dense tissue. Procurrent rays indicated with "pr" in each scan; note that the density of procurrent ray density appears to scale inversely with TH. Arrows indicate primary bifurcations of the 2nd dorsal ray. Right graphs show density of the 2nd dorsal ray along the proximodistal axis. Note that the ray in a HypoTH background shows high density along the entire length of the ray and into distal regions, highlighted by bracket. (Scale bar, 1 mm).

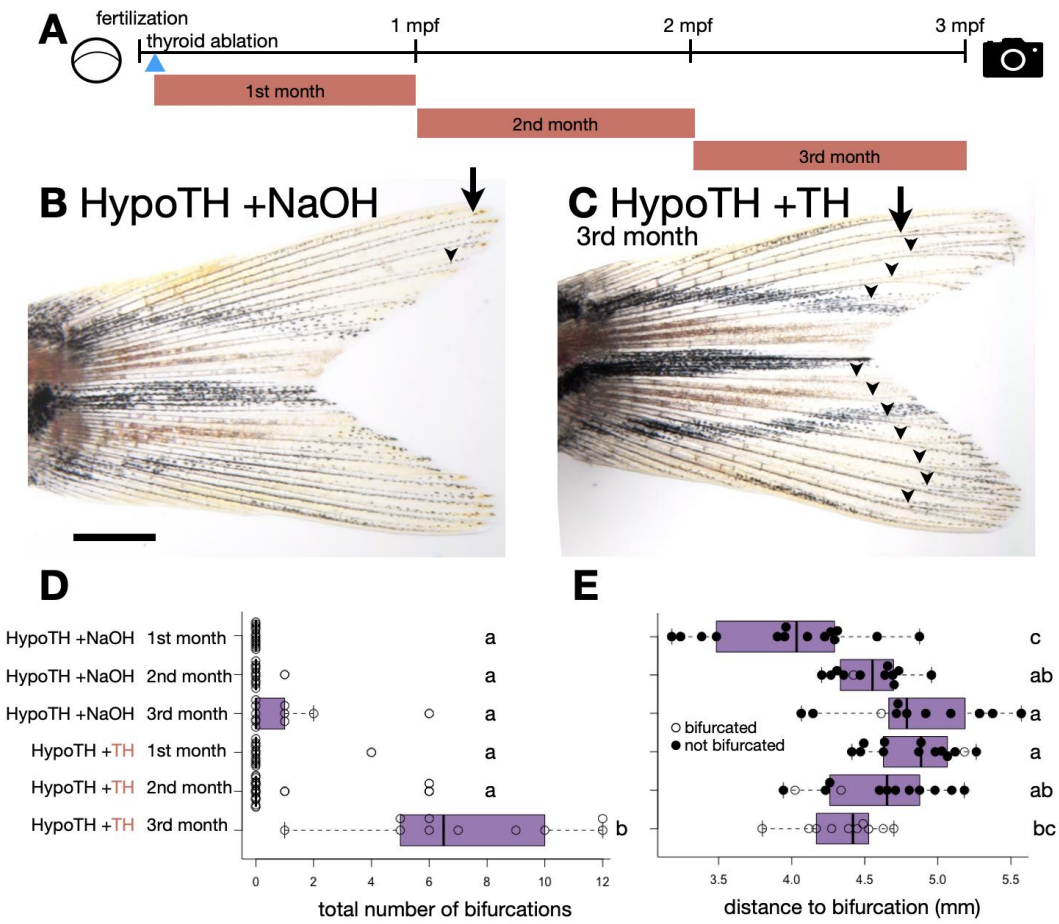

Supplemental Figure 2.7 Effects of developmental hypothyroidism can be rescued by exogenous thyroid hormone during the third month. (*A*) Experimental timeline: developed fins from a HypoTH background, treated 0-1, 1-2, or 2-3 months post fertilization with either (*B*) vehicle control or (*C*) 5nM T4. Arrows indicate primary bifurcations of the 2nd dorsal ray, arrowheads indicate all other primary bifurcations. (Scale bar, 1 mm). Boxplots show (*D*) the total primary bifurcations of each fin and (*E*) the absolute distance of the ray up to the bifurcation (or the total ray length for non-bifurcating rays). Filled circles represent measurements from non-bifurcating rays, empty circles represent measurements from bifurcating rays. Significance determined by an ANOVA followed by Tukey's HSD.

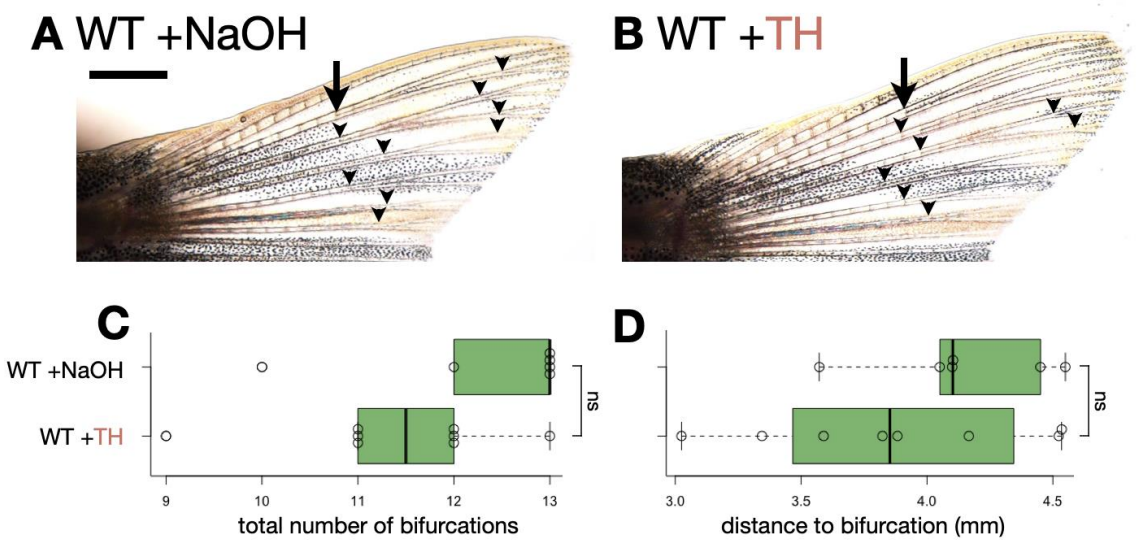

Supplemental Figure 2.8 Treatment with exogenous thyroid hormone is not sufficient to induce detectable supernumerary or precocious bifurcation in WT. WT fish were treated with (*A*) vehicle control or (*B*) 10nM T4 from a larval stage until adulthood. (Scale bar, 1 mm). Boxplots showing (*C*) the number of total primary bifurcations of each fin, and (*D*) the absolute distance of the ray up to the bifurcation. Significance determined by a Welch two-sample *t* test.

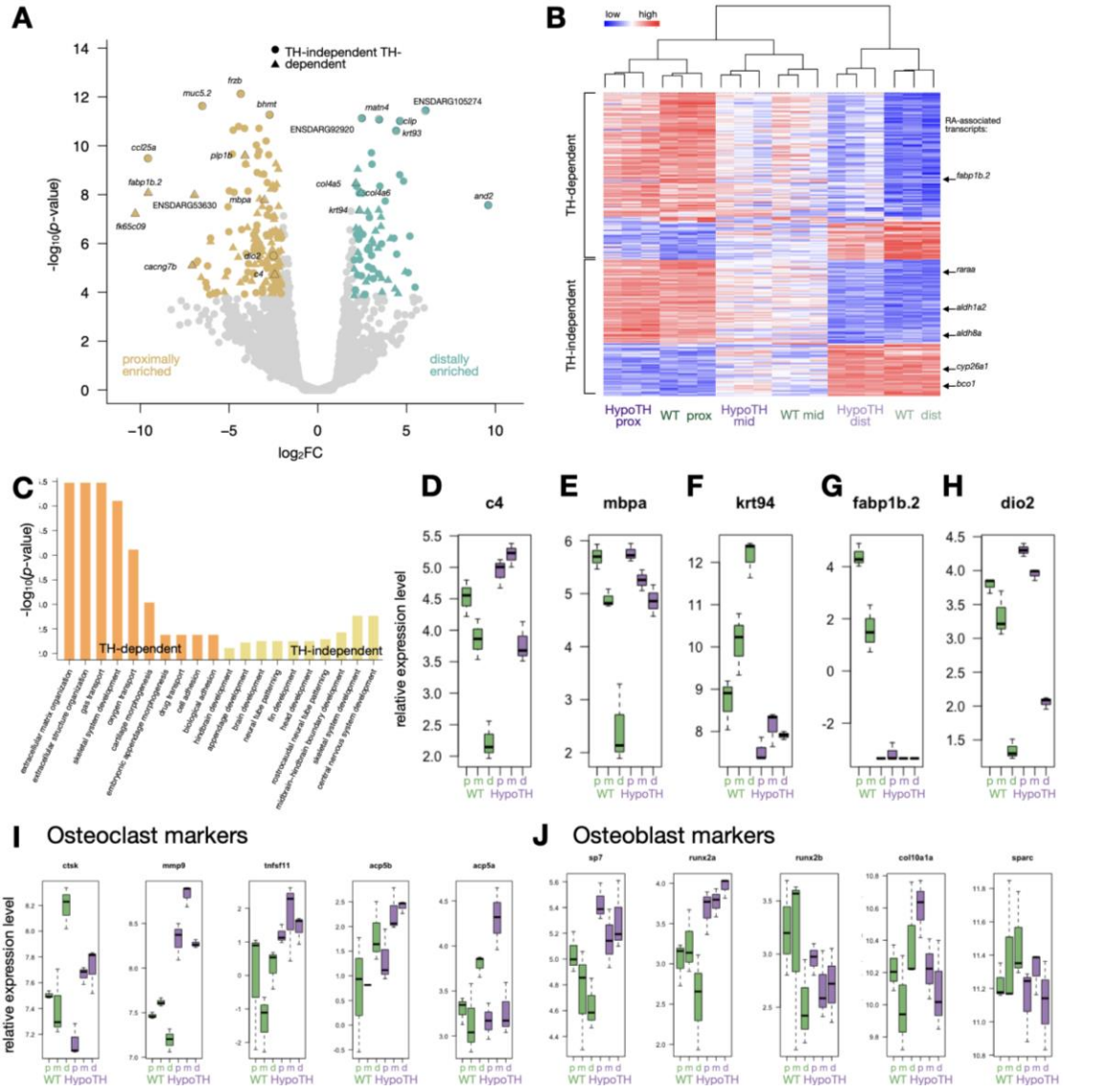

Supplemental Figure 2.9 Thyroid hormone promotes distal gene expression profiles. (*A*) Volcano plot showing genes differentially expressed between proximal (yellow) and distal (blue) regions of fins from WT zebrafish. Genes with proximodistal differential expression independent of TH are shown as circles; genes with proximodistal differential expression that is dependent on TH are shown as triangles. (*B*) Heat map of the 233 genes expressed in a proximodistal differential in WT fins. Dendrogram at the top represents hierarchical clustering of the samples. Relative high expression shown as red; relative low expression shown as blue. Arrows to the right of the heat map identify transcripts associated with the RA pathway. Note that *fapb1b.2*, associated with RA metabolism (Rabinowitz et al., 2017), is the only of these transcripts showing a proximodistal differential that is dependent on TH. (*C*) Gene Ontology terms for genes that show proximodistal expression differentials. Terms enriched in differentials that are dependent on TH shown in orange; terms enriched in differentials that are not dependent on the presence of TH are shown in yellow. (*D-J*) Boxplots comparing expression levels of select proximodistal-differentiated genes between WT and HypoTH fish. Each boxplot shows expression in the three regions of tissue (proximal, middle, and distal) from WT (green) and HypoTH (purple) backgrounds. (*D-G*) Each of these four genes was identified in (Rabinowitz et al., 2017) as proximally or distally enriched by both RNAseq and proteomic analysis. Note that while *c4*, *mbpa*

and *krt94* show proximalized expression patterns in fins of HypoTH fish, *fabp1b.2* expression is merely depressed at all proximodistal levels. (*H*) Boxplot showing the proximal enrichment of *dio2*, which encodes an enzyme that converts TH into its more active form; it is proximally enriched in a non-TH-dependent manner. Boxplots showing relative expression of markers of (*I*) osteoclasts and (*J*) osteoblasts. None of these genes rose above a significance threshold for being TH-dependent or expressed in a proximodistal gradient.

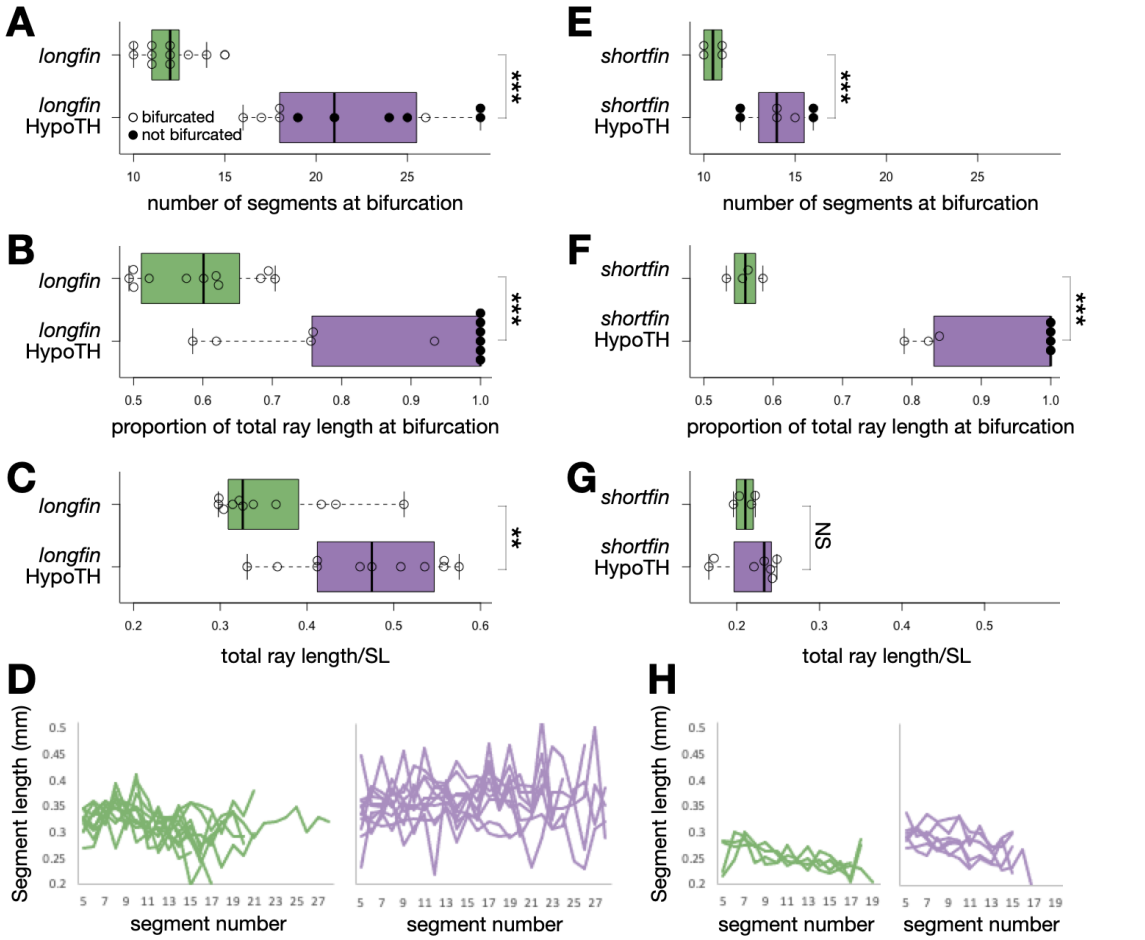

Supplemental Figure 2.10 Thyroid hormone distalizes fins in *shortfin* and *longfin* mutant backgrounds. Boxplots showing (*A, E*) number of segments to the bifurcation (or the total number of segments for non-bifurcating rays), (*B, F)* the proportion of total ray length at bifurcation, and (*C, G*) the total ray length divided by body length (SL). Plots (*D, H*) show individual segment lengths, starting at the 5th segment, for every 2nd dorsal ray in each condition. Filled circles represent measurements from non-bifurcating rays, empty circles represent measurements from bifurcating rays. Significance determined by a Welch two-sample *t* test.

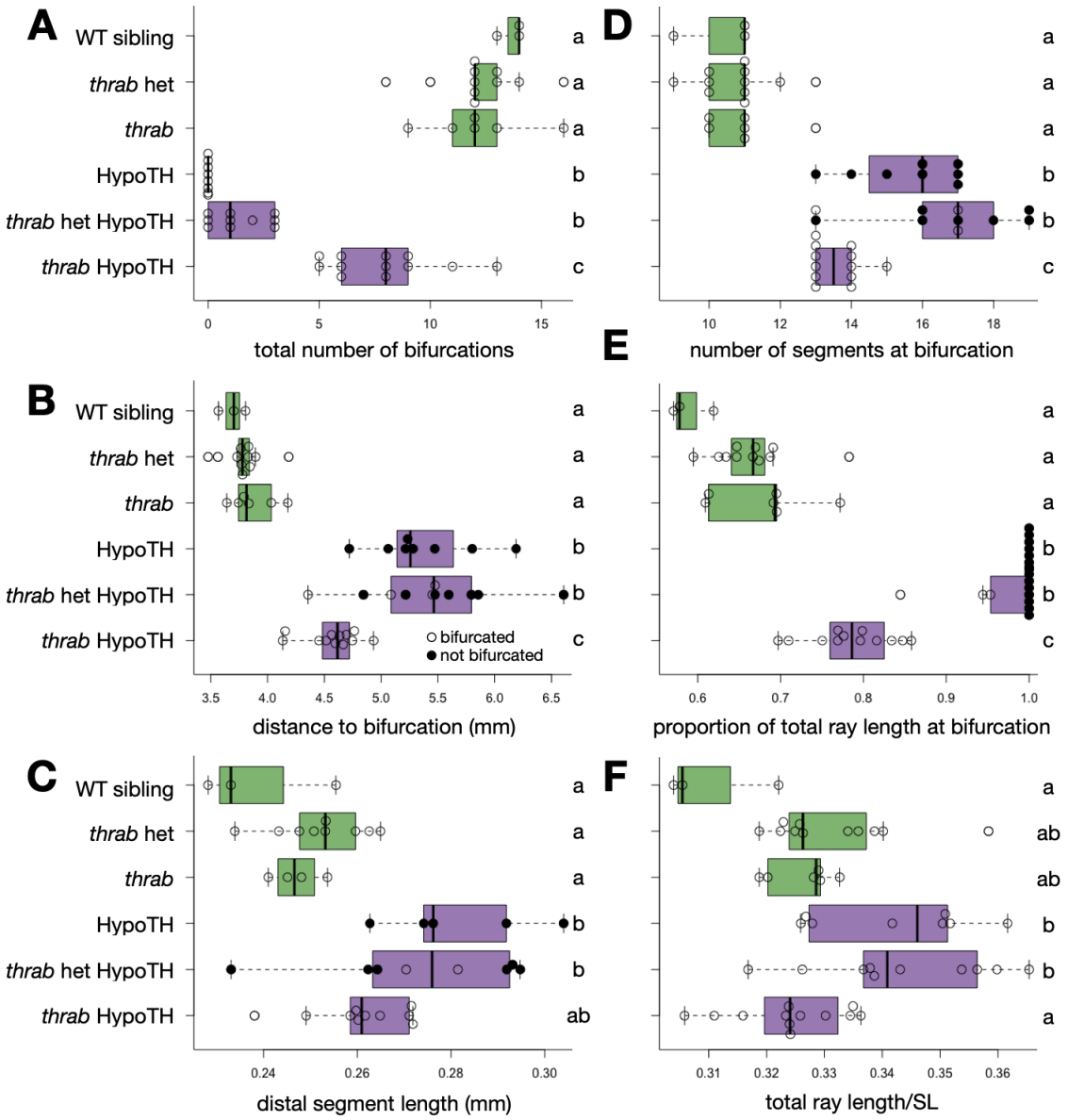

Supplemental Figure 2.11 Unliganded Thrab inhibits distal morphology. Boxplots showing (*A*) the total primary bifurcations of each fin, (*B*) the absolute distance of the ray up to the bifurcation (or the total ray length for non-bifurcating rays), (*C*) the average length of distal segments 15-17, (*D*) the number of segments of the ray up to the bifurcation (or the total number of segments for non-bifurcating rays), (*E*) the proportion of total ray length at bifurcation, and (*F*) the total ray length divided by body length (SL). Filled circles represent measurements from non-bifurcating rays, empty circles represent measurements from bifurcating rays. Significance determined by an ANOVA followed by Tukey's HSD.

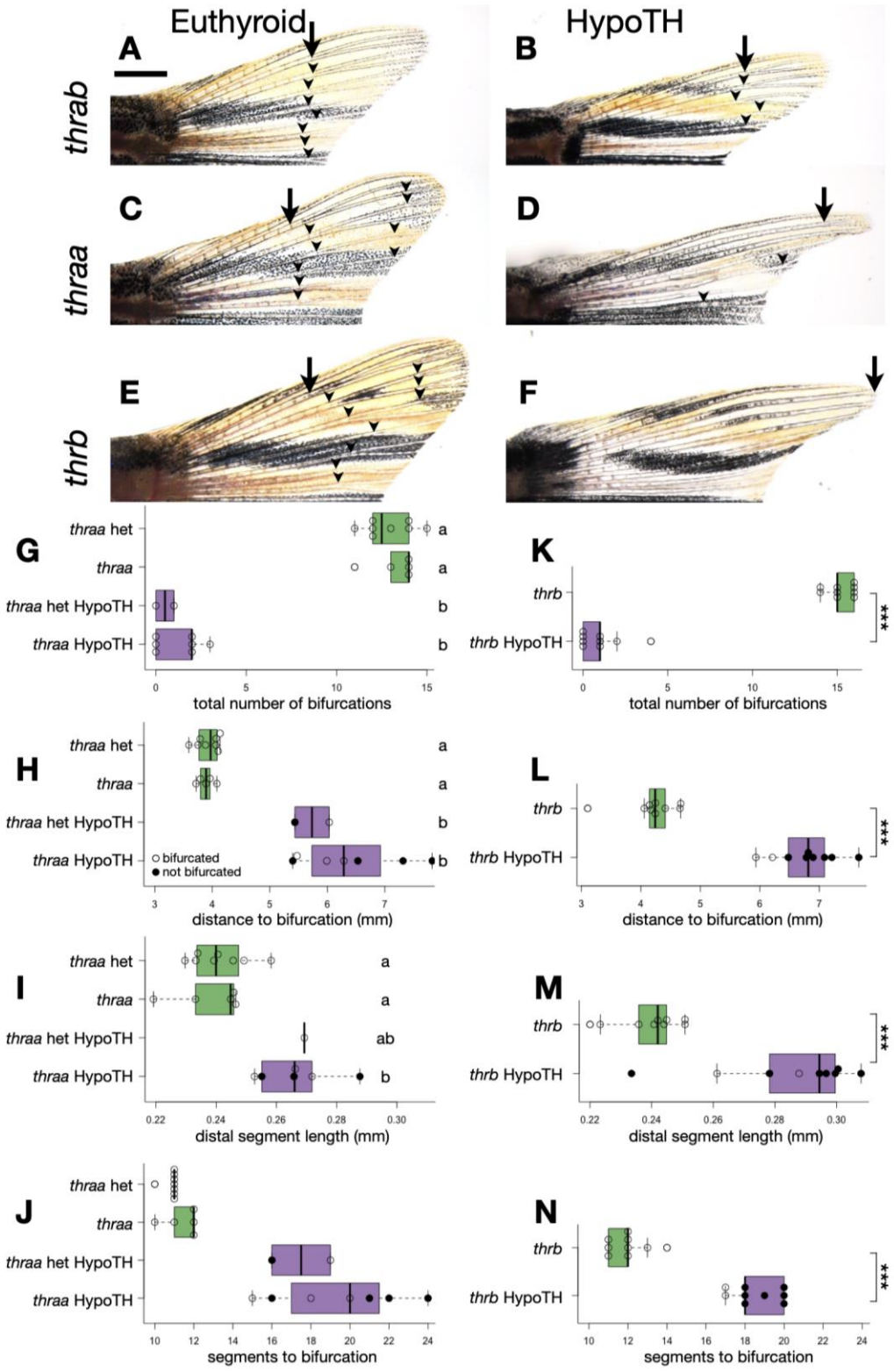

Supplemental Figure 2.12 Thraa and Thrb are not required for proximodistal patterning. Homozygous mutants for (*A, B*) *thrab*, (*C*, *D*), *thraa* or (*E, F*) *thrb* that were reared under either (*A, C, E*) normal euthyroid or (*B, D, F*) HypoTH conditions. (Scale bar, 1 mm). Arrows indicate primary bifurcations of the 2nd dorsal ray, arrowheads indicate all other primary bifurcations. Note

that *thraa* and *thrb* HypoTH mutants show proximalized patterning comparable to non-mutant HypoTH, contrasting the rescued phenotype of the *thrab* mutant (*B*). For (*G-J*) *thraa* and (*K-N*) *thrb* mutants and siblings, boxplots show (*G, K*) the total primary bifurcations of each fin, *(H, L)* the absolute distance of the ray up to the bifurcation (or total ray length for non-bifurcating rays), *(I, M)* the average length of distal segments 16-18 and (J, N) the number of segments proximal to the bifurcation (or the total number of segments for non-bifurcating rays). Filled circles, non-bifurcating rays; empty circles, bifurcated rays. Significance determined by a Welch two-sample *t* test or an ANOVA followed by Tukey's HSD.

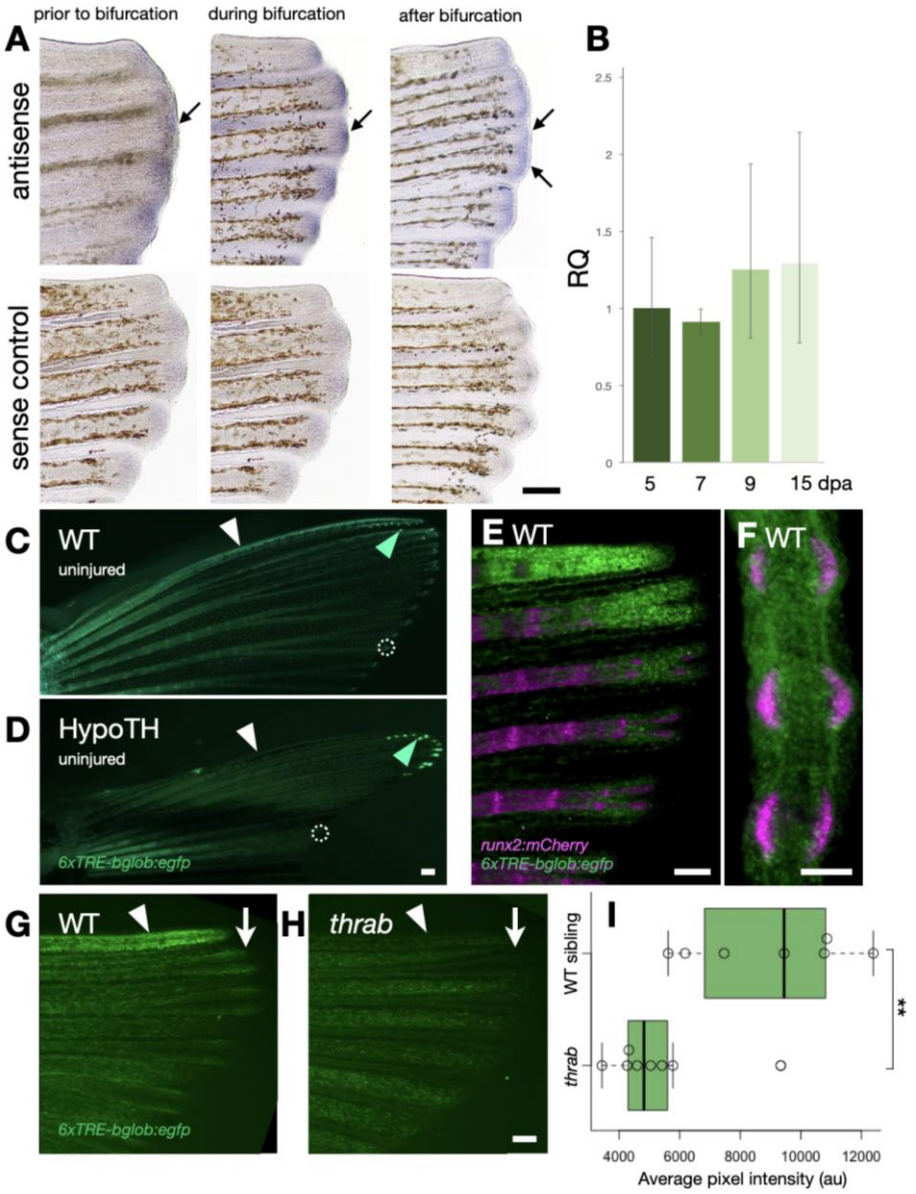

Supplemental Figure 2.13 *thrab* is expressed at the leading edge throughout fin regeneration. (*A*) *In situ* hybridization of fins at different stages of bifurcation morphogenesis. Top, *thrab* antisense probe; bottom, *thrab* sense control. Arrows show *thrab* expression at the leading edges of regenerating rays. (Scale bar, 200 uM). (*B*) Relative quantification of gene expression levels from the distal edge of regenerating fins at 5, 7, 9 and 15 dpa determined by

quantitative PCR. (*C-D*) TH activity as reported by *6xTRE-bglob:egfp* (Matsuda, 2018)expression in (*C*) an uninjured, WT fin and (*D*) absence of GFP in the fin of a HypoTH fish. Green arrowheads indicate leucophores at the tips of the peripheral rays, present in both WT and HypoTH. Note the presence of autofluorescence in the bones and leucophores in both WT and HypoTH backgrounds. In the WT, expression is high in the peripheral ray (arrowhead) and at the tips of the rays (dashed circle). (*E-F*) *6xTRE-bglob1:egfp* reports TH activity and *runx2:mCherry* identifies pre-osteoblasts in regenerating fins. (*E*) Whole-mount regenerating fins at 6dpa, and (*F*) fluorophores are stained with secondary antibodies in a transverse section at 4dpa. (*G-I*) Expression of *6xTRE-bglob:egfp* reporter in (*G*) WT sibling control expressed in peripheral ray (arrowhead) and ray tips (arrow) and (*H*) reduced expression in sibling *thrab -/-* mutant. (*I*) Graph showing TH activity of regenerating 2nd dorsal rays at 10dpa.

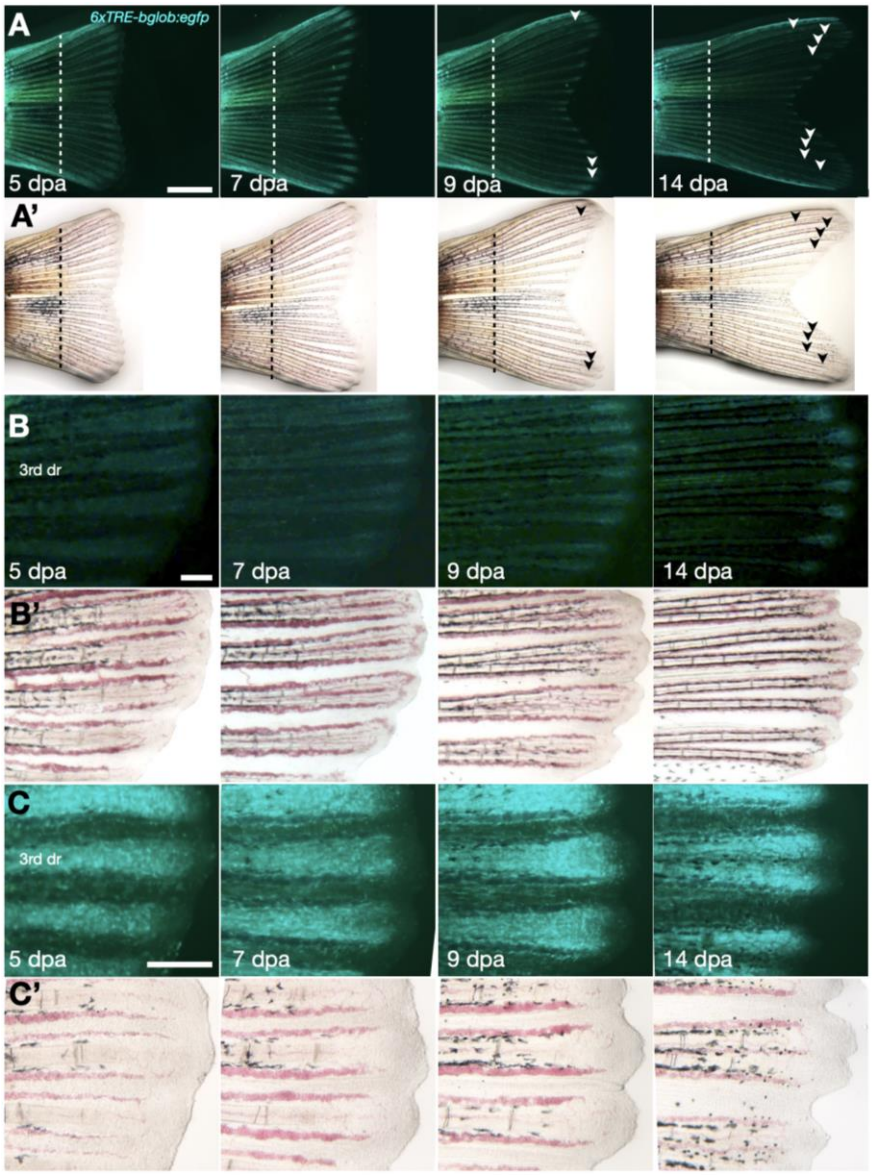

Supplemental Figure 2.14 Thyroid hormone is active at the tips of adult fin rays. (A-C) Three different WT transgenic regenerating fins at different magnifications. Paired images (A'-C')

show matched brightfield images of the regions. In *A*, dashed line shows amputation plane and arrowheads indicate bifurcation nodes as they appear. In *B-C*, the 3rd dorsal ray is labeled. In *C*, scale bars, 1 mm; in *B-C*, scale bars, 250 uM.

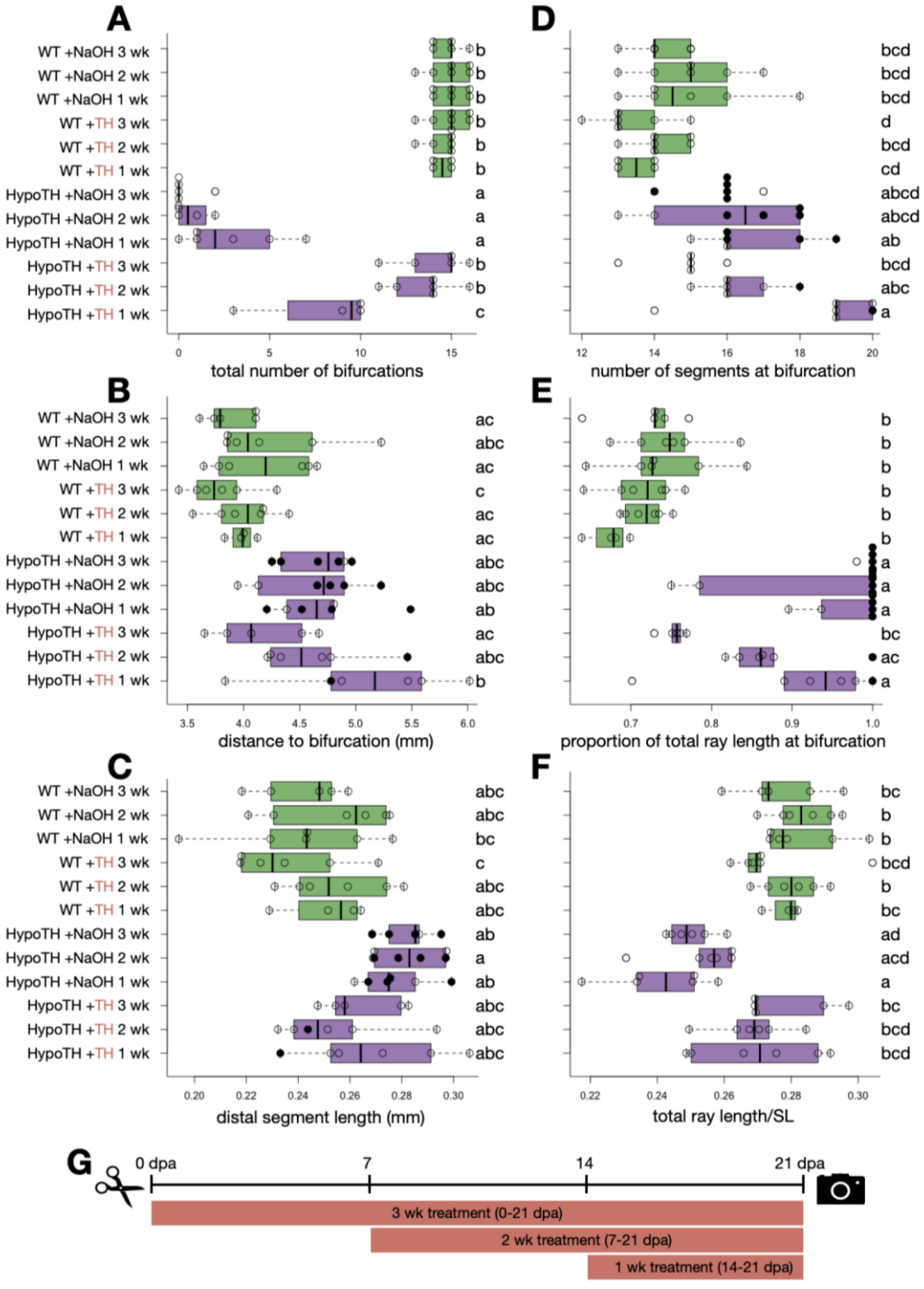

Supplemental Figure 2.15 Effects of hypothyroidism can be rescued during regeneration with exogenous thyroid hormone. WT or HypoTH fish were treated with 5nM T4 or vehicle for 7, 14 or 21 days, starting at 14, 7, or 1dpa, respectively. Boxplots showing (*A*) the total primary bifurcations of each fin, (*B*) the absolute distance of the ray up to the bifurcation (or the total ray

length for non-bifurcating rays), (*C*) the average length of distal segments 15-17, (*D*) the number of segments of the ray up to the bifurcation (or the total number of segments for non-bifurcating rays), (*E*) the proportion of total ray length at bifurcation, and (*F*) the total ray length divided by body length (SL). In B-E, filled circles represent measurements from non-bifurcating rays, empty circles represent measurements from bifurcating rays. Significance determined by an ANOVA followed by Tukey's HSD. (*G*) Experimental timeline for treatments.

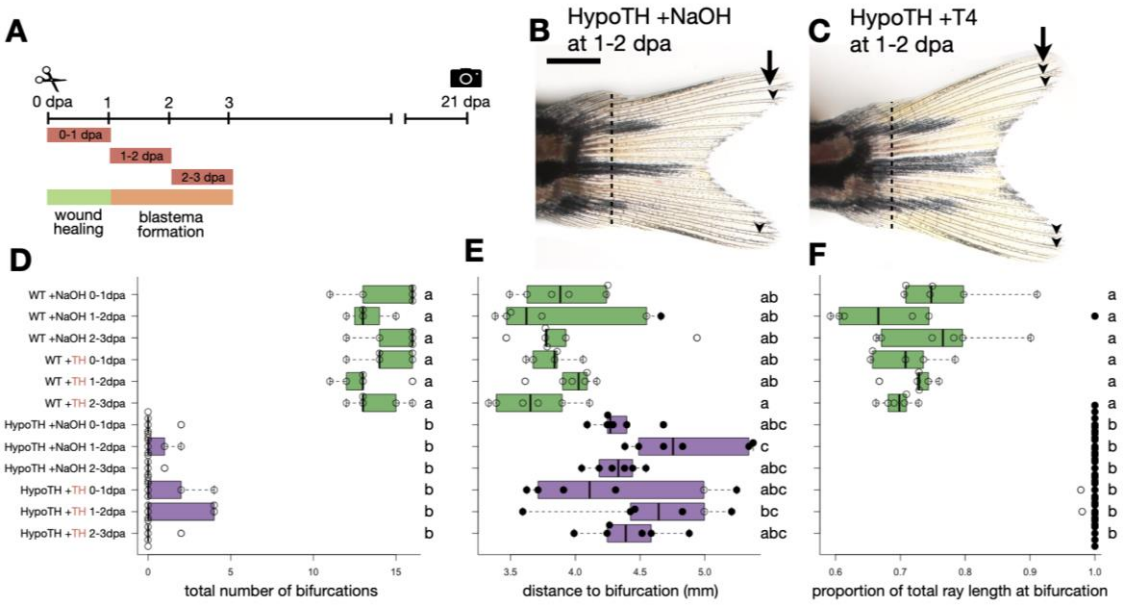

Supplemental Figure 2.16 Exogenous thyroid hormone treatment during blastema formation does not rescue distalization in the regenerated fin. (*A*) Experiment timeline: fish were treated with either 5nM T4 or NaOH vehicle for periods 0-1, 1-2 or 2-3dpa. HypoTH fish were treated with (*B*) vehicle or (*C*) 5nM T4 for 24 hours starting 1 day after amputation. Arrows indicate primary bifurcations of the 2nd dorsal ray, arrowheads indicate all other primary bifurcations. (Scale bar, 1 mm). Boxplots showing (*D*) the total primary bifurcations of each fin, (*E*) the absolute distance of the ray up to the bifurcation (or the total ray length for non-bifurcating rays), and (*F*) the proportion of total ray length at bifurcation. In *E-F*, Filled circles represent measurements from non-bifurcating rays, empty circles represent measurements from bifurcating rays. Significance determined by an ANOVA followed by Tukey's HSD.

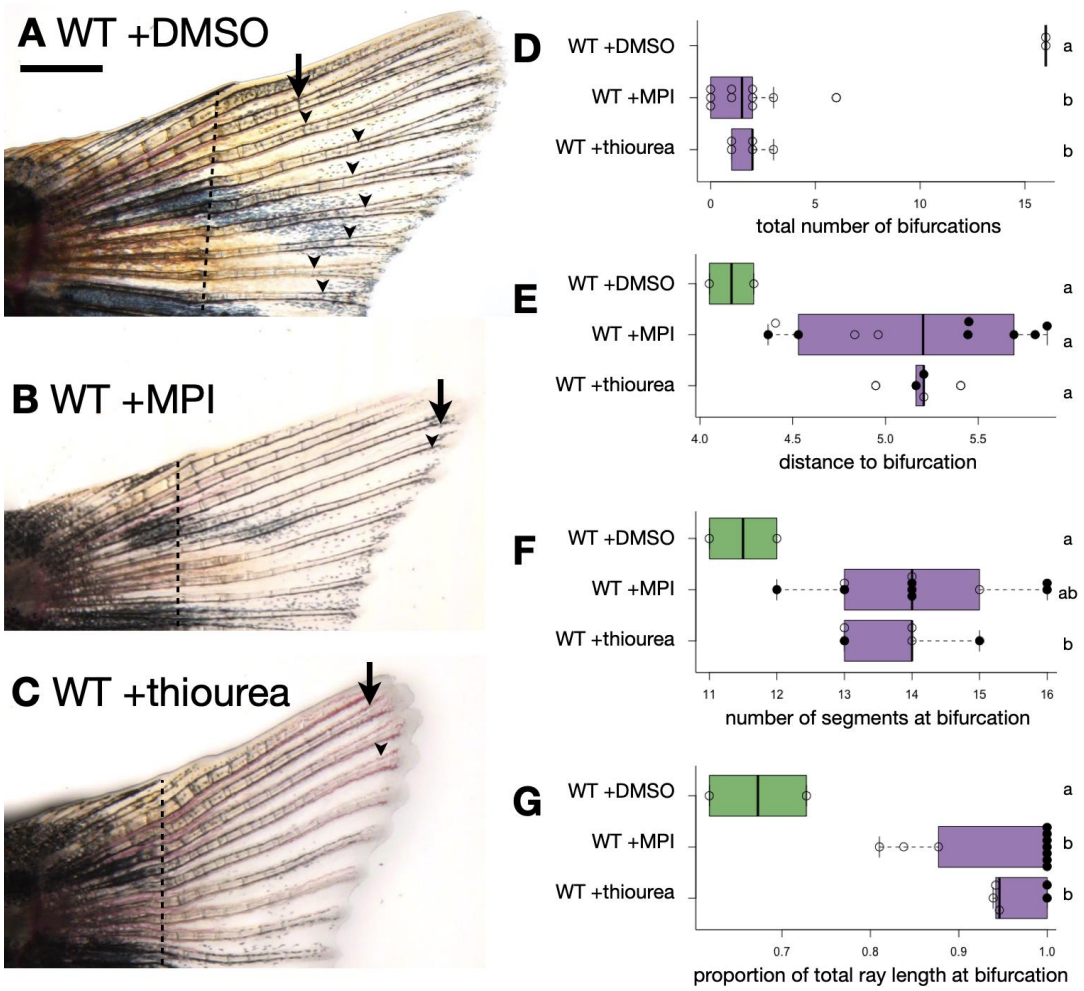

Supplemental Figure 2.17 Pharmacologically-induced hypothyroidism proximalizes fin rays during regeneration. Regenerated fins of WT zebrafish treated with (*A*) vehicle control or goitrogenic drug treatments (*B*) MPI cocktail or (*C*) thiourea throughout the regenerative period. Arrows indicate primary bifurcations of the 2nd dorsal ray, arrowheads indicate all other primary bifurcations. (Scale bar, 1 mm). Boxplots showing (*D*) the total primary bifurcations of each fin, and (*E*) the absolute distance to bifurcation of the 2nd dorsal ray (or the total ray length for non-bifurcating rays), (*F*) the number of segments proximal to the bifurcation (or the total number of segments for non-bifurcating rays), and (*G*) the proportion of the total ray length at the bifurcation. In *E-G*, Filled circles represent measurements from non-bifurcating rays, empty circles represent measurements from bifurcating rays. Significance determined by ANOVA followed by Tukey's HSD.

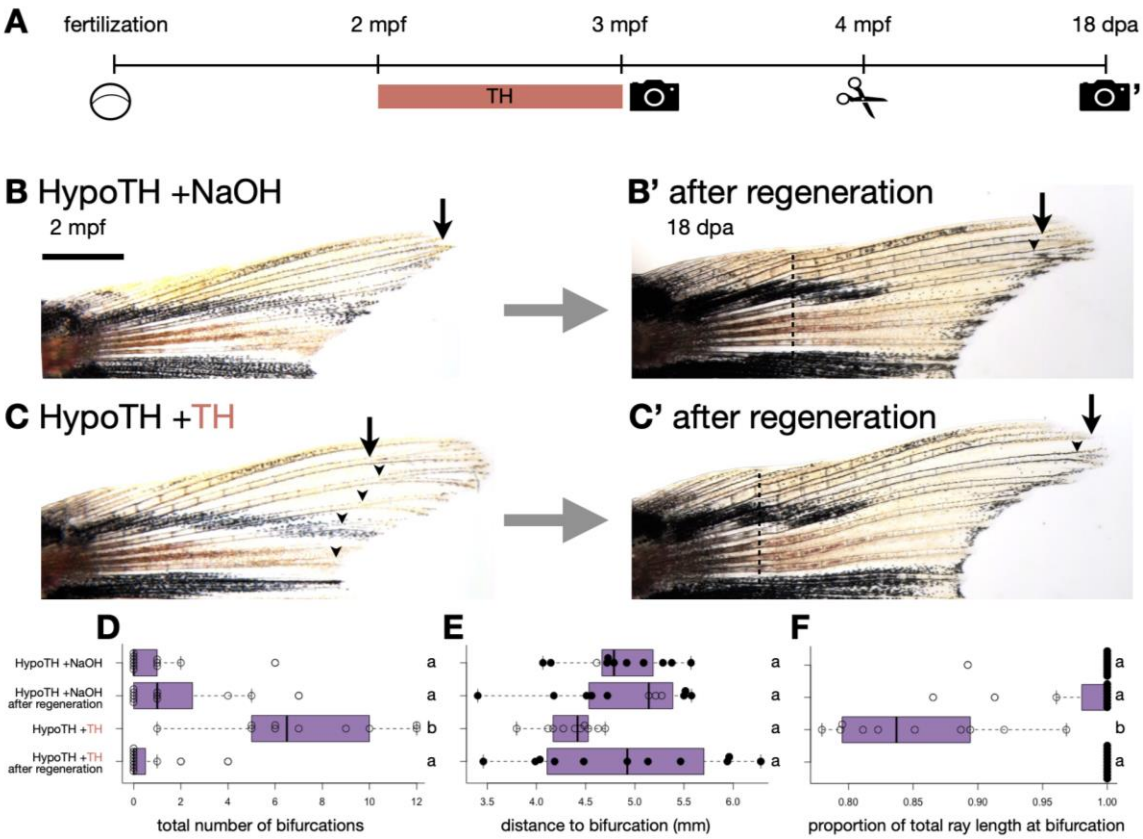

Supplemental Figure 2.18 Developmental rescue is not remembered during regenerative patterning. (*A*) Timeline of experimental treatment. Fish treated with (*B*) vehicle or (*C*) 5nm T4 for one month, starting at 2mpf. After developmental rescue, fish were returned to system water for one month before amputation, amputated and allowed to regenerate (*B'*, *C'*). Arrows indicate primary bifurcations of the 2nd dorsal ray, arrowheads indicate all other primary bifurcations. (Scale bar, 1 mm). Boxplots showing (*D*) the total primary bifurcations of each fin, (*E*) the absolute distance of the ray up to the bifurcation (or the total ray length for non-bifurcating rays), and (*F*) the proportion of total ray length at bifurcation. Filled circles represent measurements from non-bifurcating rays, empty circles represent measurements from bifurcating rays. Significance determined by an ANOVA followed by Tukey's HSD.

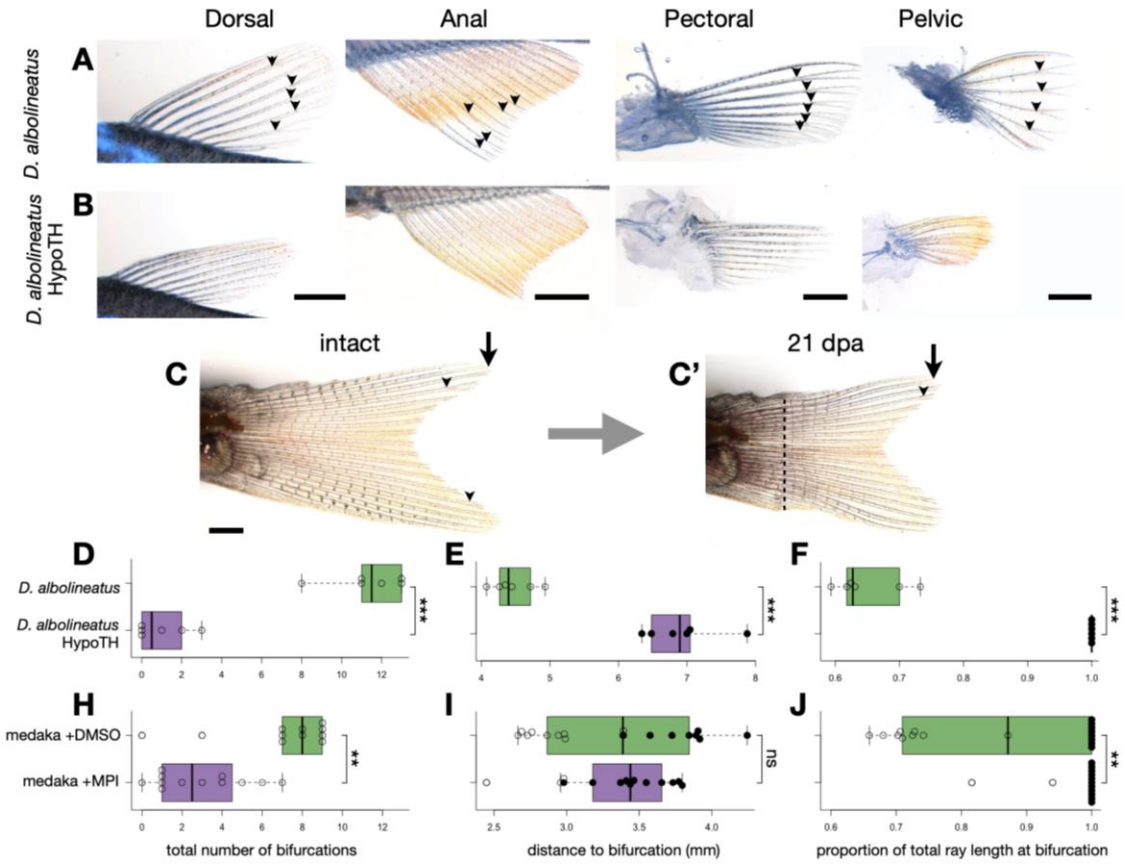

Supplemental Figure 2.19 Thyroid hormone promotes ray bifurcation in other teleost species. *D. albolineatus* were reared under WT conditions or else thyroid-ablated at 4dpf, then reared under HypoTH conditions. (*A*, *B*) Two medial fins (dorsal and anal) and two paired fins (pectoral and pelvic) of adult *D. albolineatus* reared under two TH profiles. (*C*) *D. albolineatus* caudal fins regenerate with original patterning: individual fin (C) before amputation and (C') after regeneration. Arrows indicate primary bifurcations of the 2nd dorsal ray in *C*, arrowheads indicate all other primary bifurcations. (Scale bars, 1 mm). Boxplots showing (*D*, *H*) the total primary bifurcations of each fin, (*E*, *I*) the absolute distance of the ray up to the bifurcation, (or the total ray length for non-bifurcating rays), and the proportion of total ray length at bifurcation in (*F*) *D. albolineatus* 2nd dorsal ray or (*J*) *O. latipes* (medaka) 3rd dorsal ray. Caudal fins of medaka were amputated and regenerating individuals were treated either with a vehicle control or TH-inhibiting cocktail (MPI) during regeneration. In graphs, filled circles represent measurements from non-bifurcating rays, empty circles represent measurements from bifurcating rays. Significance determined by a Welch two-sample *t* test.

CHAPTER 3

Growth patterns of caudal fin rays are informed by both external signals from the regenerating organ and remembered identity autonomous to the local tissue

The material in this chapter was adapted from:

Autumn, M., Hu, Y., Zeng, J., & McMenamin, S. K. (2024). Growth patterns of caudal fin rays are informed by both external signals from the regenerating organ and remembered identity autonomous to the local tissue. Developmental Biology, 515, 121–128. https://doi.org/10.1016/J.YDBIO.2024.07.008

3.1 INTRODUCTION

3.1.1 Fin rays are an excellent regenerative model.

To restore the original morphology of an appendage, regeneration must faithfully rebuild lost tissue. The morphology and size to which regenerating tissue grows must be determined by positional information (Wolpert, 1969). Such cues could be informed by remembered positional identity or could be interpreted from environmental cues from surrounding tissue (e.g. diffusible or spatially distributed factors). However, these two potential inputs can be difficult to disentangle.

Zebrafish fins are powerful models for studying regeneration and can provide new insights into the nature of positional memory and the pathways that regulate regional growth and patterning. The caudal fin is made up of symmetrical dorsal and ventral lobes, each composed of nine segmented fin rays. Upon amputation, a blastema of de-differentiated cells forms (Knopf et al., 2011; Tu & Johnson, 2011), and each ray regrows from the wound site to rebuild its original morphology (reviewed in Harris et al., 2021; I. M. Sehring & Weidinger, 2020).

3.1.2 Known proximodistal-dependent features of fin ray tissue.

Regeneration rate is informed by the relative proximodistal location of the regenerating tissue on the fin (Lee et al., 2005). Distal amputations are followed by slow regenerative growth, while proximal amputations close to the body initiate rapid growth that progressively slows as the regenerate approaches the original size (Akimenko et al., 1995; Banu et al., 2022; Lee et al., 2005; Uemoto et al., 2020). Regardless of how much tissue is removed, regeneration restores the organ to its original size within three weeks (Wehner et al., 2014).

Intact fin rays exhibit morphological differences along the proximodistal axis. At the proximal base, ray segments are longest and widest, tapering and shortening progressively towards the distal edge; rays also form bifurcations at specific locations along the axis (Harper et al., 2023). Components of proximodistal patterning are regulated by thyroid hormone (TH), which induces distal features (Harper et al., 2023). Proximal and distal tissues from intact adult fins show unique transcriptomic profiles (Rabinowitz et al., 2017), and these expression patterns are regulated by developmental TH (Harper et al., 2023). Here, we tested if transcriptomic differences are apparent during the regeneration of proximal compared to distal regions of the fin.

3.1.3 Previous transplant experiments indicate memory of ray length.

The relative length of individual rays appears to be remembered autonomously by tissues (Uemoto et al., 2020). Fin rays differ in length from the central to the peripheral regions of the fin, giving the organ an overall forked shape. Previous transplantation experiments demonstrate that when short central rays are swapped with long peripheral rays, the tissue regenerating in the new environment produces a ray of intermediate length (Shibata et al., 2018). However, it remains unclear whether proximodistal location along an intact ray imprints remembered positional information that could inform morphology during regeneration.

Transplants of blastema cells from different proximodistal locations were not able to influence lengths of regenerates (Shibata et al., 2018). Further, hemi-rays—the apposed contralateral bones that make up individual ray segments—can be transplanted to different proximodistal locations; the resulting recombinant rays regenerate with morphologies expected for the regenerating environment (Murciano et al., 2007). Nonetheless, given the notable differences in gene expression and morphology along the intact proximodistal axis, we asked if entire ray segments could remember

proximodistal identity, and we tested the ability of this memory to influence gene expression, regrowth rates, ultimate length and patterning of regenerating rays.

3.2 RESULTS

3.2.1 Regenerating fin tissue shows unique proximodistal transcription.

Many genes show proximodistal differences in expression as the caudal fin regenerates (Akimenko et al., 1995; Lee et al., 2005), and we aimed to capture trends across the transcriptome during the regeneration of the organ. Amputating at a consistent proximal location, we evaluated expression from three regions as they regenerated a proximal region collected after the blastema had already formed (Wang et al., 2019; 4 days post amputation, dpa), a middle region midway through regeneration as the ray bifurcations were forming (7 dpa), and a distal region (15 dpa; see Supplementary Fig 3.1C). We identified 489 transcripts that were differentially expressed between proximal and distal regenerating tissue (Fig 3.1A-B): 29 genes were proximally enriched and 460 were distally enriched. GO term analysis of differentially expressed transcripts along the proximodistal axis showed enrichment of genes involved in pigmentation, likely reflecting differentiation of pigment cells (Supplementary Fig 3.1G). Transcripts dependent on thyroid hormone were enriched for gas transport GO terms, potentially reflecting shifts in circulation and metabolism (Supplementary Fig 3.1H). In our regenerates, ray bifurcations were actively forming during the middle time point (7 dpa). While this tissue had significantly different expression from either proximal *or* distal tissue, there were no middle tissue unique transcripts that were differentially expressed when compared to both proximal *and* distal tissue.

3.2.2 Hypothyroid tissues lose proximodistal differential expression of many genes.

Developmental hypothyroidism proximalizes both transcriptional expression and ray morphology in intact fins (Harper et al., 2023), and we asked if fins regenerating in a hypothyroid context also showed proximalized gene expression patterns. We reasoned that transcripts with a TH-regulated expression differential would be strong candidates as mediators of proximodistal

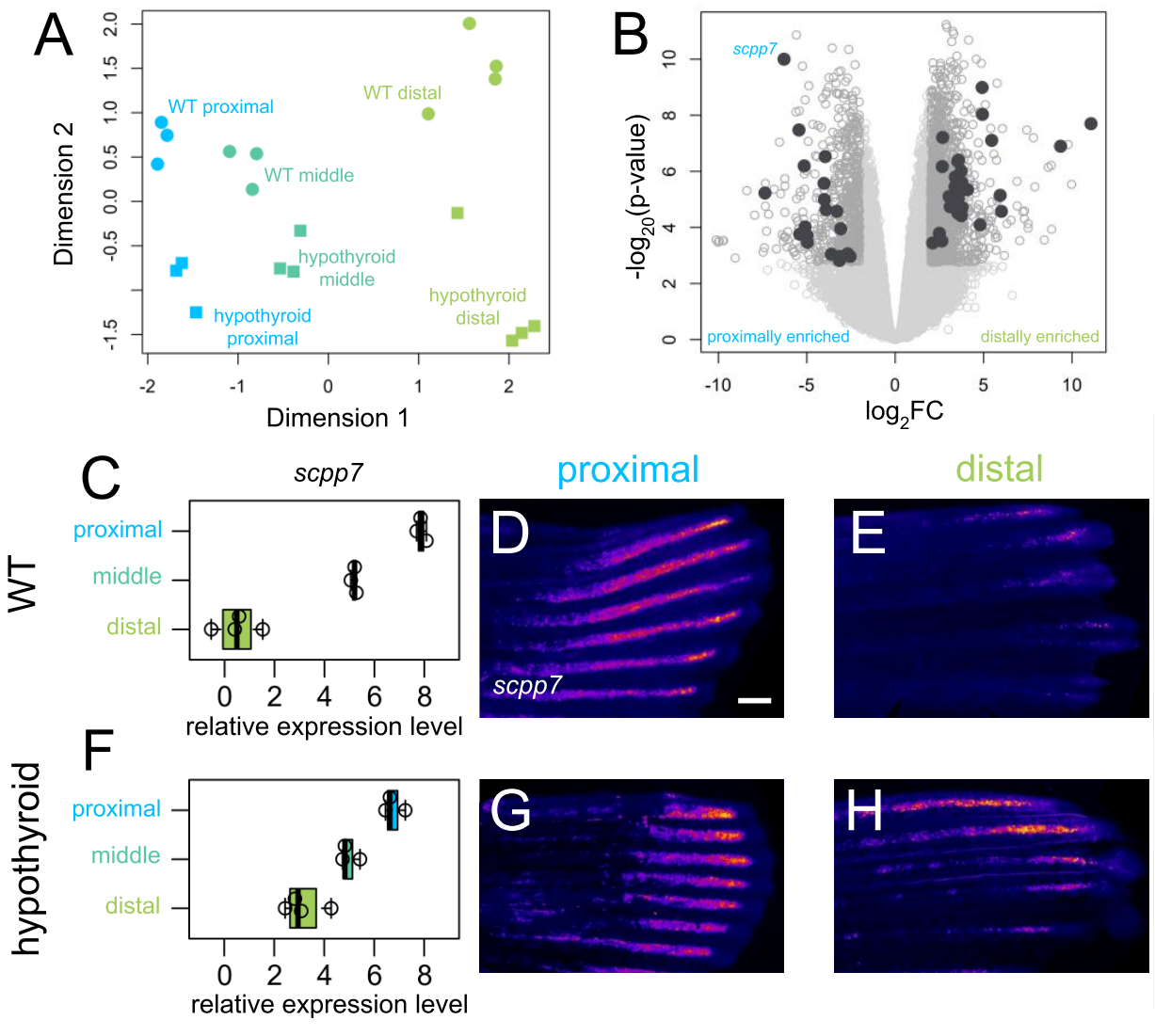

Figure 3.1 Thyroid hormone distalizes gene expression patterns during regeneration. (A) Multidimensional scaling plot comparing gene expression profiles in different regions (proximal, 4

dpa; middle, 7 dpa; distal, 15 dpa) of regenerating tissue from WT and hypothyroid fish; each data point represents one biological replicate. (B) Volcano plot showing differential gene expression between regenerating proximal and distal regions in WT. Filled grey circles indicate thyroid hormone-dependent genes. (D, F) *scpp7* relative expression in (C) WT and (F) hypothyroid tissue samples. Note increased proximal expression in hypothyroid distal tissues. Whole mount fluorescent *in situ* hybridization using custom *scpp7* RNAscope probe on (D-E) WT and (G-H) hypothyroid tissue regenerating (D, G) proximal or (E, H) distal fin tissues. Warm colors indicate highest regions of expression. Scale bar, 200 μm.

patterning and distal identity. Analyzing the transcriptomes holistically, the major axes of variation robustly captured proximodistal location (dimension 1) and TH condition (dimension 2), but there was little apparent correlation between the two (Fig 3.1A). Nonetheless, certain transcripts showed a proximodistal differential in expression that was dependent on the presence of TH. Indeed, of the 489 differentially expressed genes found in WT tissue, 364 lost proximodistal specificity in hypothyroid tissue: ~86% (25/29) of proximally enriched and ~76% (349/460) of distally enriched genes lost proximodistal differential expression in a hypothyroid context.

3.2.3 *scpp7* is proximally enriched during regeneration.

Of the transcripts showing TH-dependent proximal enrichment, secretory calcium-binding phosphoprotein 7 (*scpp7*) could be robustly visualized using RNAscope (Fig 3.1D-E, G-H). Along with other SCPP factors, SCPP7 is involved in bone mineralization (Kawasaki, 2009), and is strongly upregulated during scale regeneration (Bergen et al., 2022). Proximal tissues showed robust expression of *scpp7* in both WT and hypothyroid backgrounds, but the gene was more strongly expressed in distal tissue from hypothyroid regenerates compared to those of WT (Fig 3.1C-H).

We asked if the variation in *scpp7* expression in the different regions could be attributed to differences in the time since injury rather than proximodistal position of regeneration. To test this possibility, we performed distal amputations on WT fins (see

Supplementary Fig 3.1D) and assessed *scpp7* expression in 4 dpa distally-regenerating tissue. *scpp7* expression was similar to that of 15 dpa distally-regenerating tissues (Supplementary Fig 3.1E-F), suggesting that this expression differential indeed characterizes distal regenerating tissue.

3.2.4 scpp7 expression in regenerating tissues reflects original proximodistal location rather than regenerative environment.

We asked whether attenuated *scpp7* expression would be remembered by distal tissues if they regenerated in a proximal context. To test this, we designed a distal-to-proximal ray

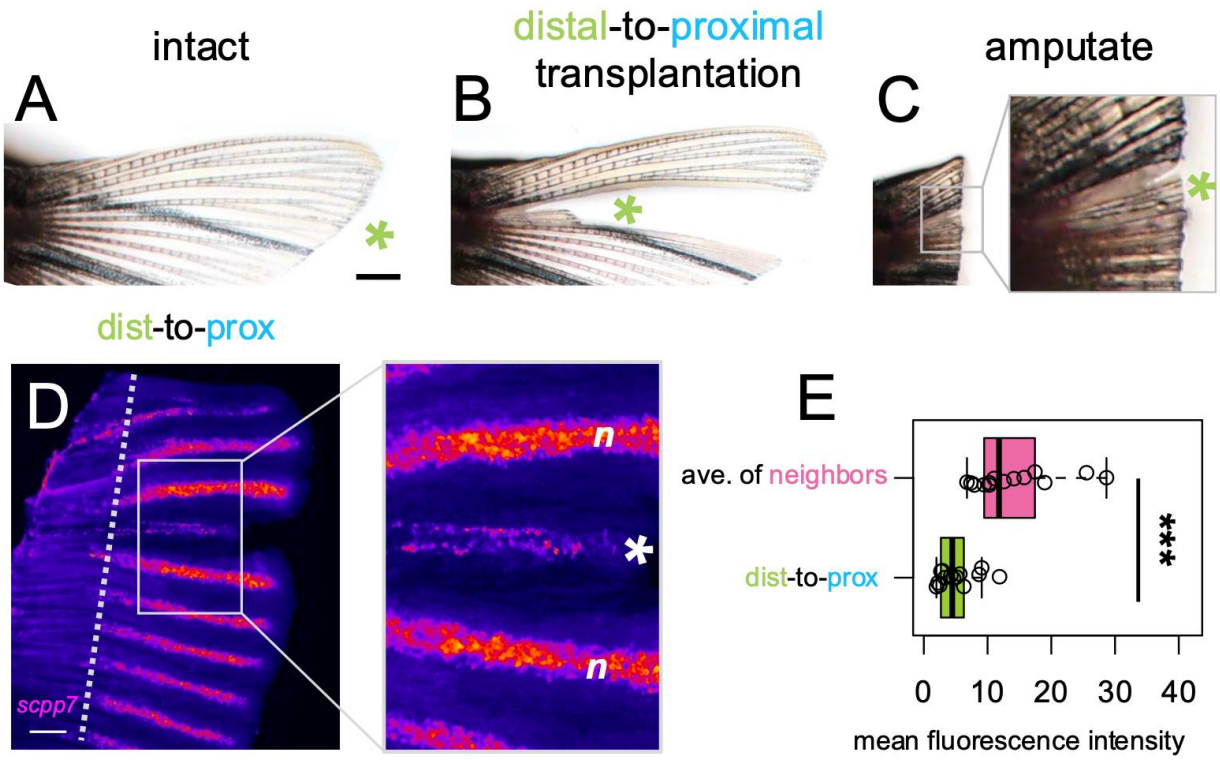

Figure 3.2 *scpp7* expression in regenerating tissues reflects original position rather than current environment. (A-C) Example of a fin lobe subjected to the distal-to-proximal transplantation procedure. (D) Whole mount fluorescent *in situ* hybridization with *scpp7* RNAscope probe on dist-to-prox regenerating fins at 4 dpa. Warm colors indicate highest regions of expression. (E) Boxplot showing mean fluorescence intensity of dist-to-prox transplant tissue (asterisk) and the average intensity of its peripheral-most and center-most neighbors (n). Significance determined by a Welch two-sample paired t test. Scale bars, (A) 1 mm; (D) 200 μm.

transplantation procedure in which a ray was removed from the fin, and a distal portion of the extirpated ray was transplanted into the proximal position. After the distal transplant integrated into the proximal location, the entire fin was amputated (through the transplant) to allow distal tissue to regenerate alongside proximal tissue (“dist-to-prox”, Fig 3.2A-C; see Methods and Supplementary Fig 3.10 for additional details). A completely extirpated ray with no transplant produced no regeneration (Supplementary Fig 3.2). We assessed *scpp7* expression in the regenerate originating from the dist-to-prox transplant and found expression was significantly reduced compared to those of neighboring proximal rays at 4 dpa (Fig 3.2D-E). This recapitulation of distal-like expression while regenerating in a proximal context suggests that expression level of this transcript is informed by original tissue identity.

3.2.5 Distal-to-proximal transplanted tissue restores shorter fin rays.

We predicted that if dist-to-prox transplanted tissue possessed remembered positional identity, precocious distal features should be apparent in the resulting regenerate. To adequately evaluate subtle differences in regrowth, we needed a comparison that had undergone identical microsurgery without introducing a major axis translocation. Thus, we performed control “prox-to-prox" transplants, extirpating a ray, then grafting the entire tissue back into its position (Fig 3.3A-D). Interestingly, these prox-to-prox rays were not able to regenerate to the same length as the corresponding rays on the ventral lobe (Supplementary Fig 3.3K) and were ultimately slightly shorter than undisturbed neighboring rays. During microsurgery, prox-to-prox rays inevitably lost 1-3 segments and about a mm in length (Supplementary Fig 3.3I), so the change in ultimate length may reflect a slight positional shift. Additionally (or alternatively), the manipulation of the microsurgery itself may be sufficient to affect patterns of regeneration.

Compared to the microsurgery-controlled baseline of prox-to-prox rays, rays originating from dist-to-prox transplants were consistently shorter, through eleven weeks after amputation (Fig 3.3I). Dist-to-prox regenerates were obviously shorter than both neighboring rays (Fig 3.3G-H) and the corresponding ray on the ventral lobe (Supplementary Fig 3.3G-H). These differences in ultimate length suggest that the dist-to-prox transplants autonomously retain memory of their original proximodistal identity.

3.2.6 Growth rates during regeneration reflect both intrinsic identity and environmental context.

Since the dist-to-prox regenerates were significantly shorter compared to prox-to-prox regenerates, we asked whether these regenerates grew at a relatively slower pace. During the first week of regeneration (weeks 0-1), prox-to-prox transplants regenerated rapidly, adding 2.6 mm (0.37 mm per day); in contrast, dist-to-prox regenerates grew much more slowly, adding only 2.0 mm during this first week (0.27 mm per day; Fig 3.3J-K). By the second week (weeks 1-2), the two types of transplants were growing at comparable speeds, adding 1.9 mm length (0.27 mm per day). Through the remainder of the eleven-week period, dist-to-prox and prox-to-prox rays maintained similar regrowth speeds (Fig 3.3J-K). Growth rates plateaued after week nine, as the regenerates reached isometric growth (Fig 3.3J-K). Prox-to-prox rays' regrowth speed was reduced in comparison to corresponding ventral rays during the first week of regeneration but by the second week they kept pace (Supplementary Fig 3.3J-K).

3.2.7 Fin ray patterning is environmentally coordinated.

Bifurcations are a discrete indicator of proximodistal morphology (Harper et al., 2023). We asked whether the origin of tissue (distal versus proximal) would influence the

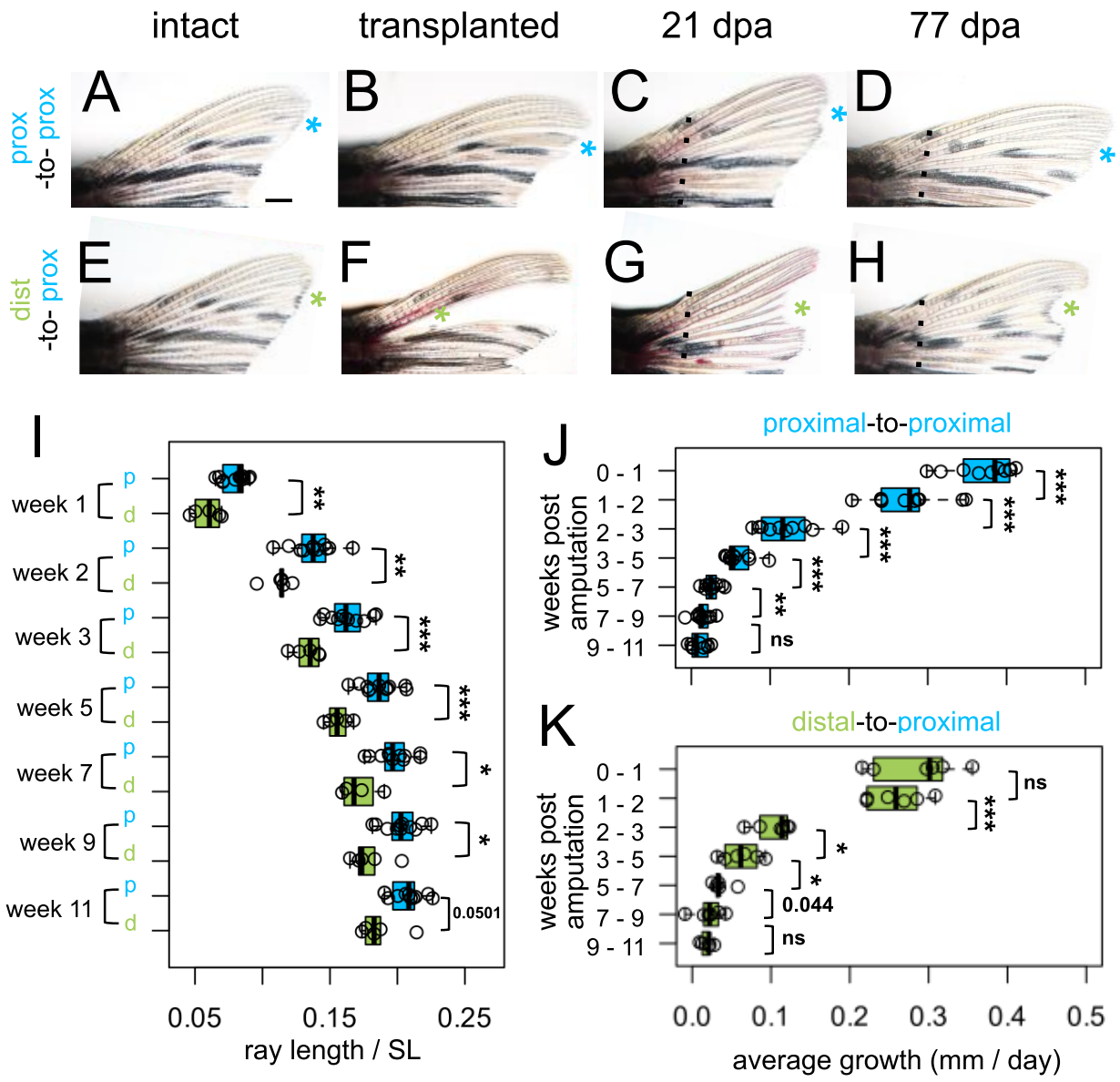

Figure 3.3 Regrowth rate reflects both intrinsic identity and the regenerative environment. Dorsal fin lobes of (A-D) proximal-to-proximal (blue asterisk) or (E-H) distal-to-proximal (green asterisk) transplantation: (A, E) intact pre-transplantation, (B-F) one day post-transplantation, (C-G) regenerating at 21 dpa, (D, H) regenerating at 77 dpa. Amputation plane, dashed line. (I) Prox-to-prox versus dist-to-prox ray length (measured from amputation plane) normalized by standard length (SL) for each week. Average amount of growth per day during different growth periods for (J) prox-to-prox or (K) dist-to-prox rays. Significance determined by (J-K) paired or (I) unpaired Welch two-sample t tests. Scale bar, 1 mm.

location of the bifurcation in a regenerate, and we quantified the bifurcation position in dist-to-prox and prox-to-prox rays. Bifurcations formed in the location expected for the

environment regardless of transplant type (Fig 3.4C), suggesting bifurcation position is the result of globally coordinated cues (Dagenais et al., 2021; Murciano et al., 2002, 2007) rather than being locally regulated by tissues based on remembered identity.

In evaluating appropriate controls for our dist-to-prox transplants, we discovered that while ray length is similar between dorsal and ventral lobes, the proximodistal patterning differs between the dorsal and ventral lobes of uninjured fins (Supplementary Fig 3.4). Further, regenerated ray segments were somewhat longer and wider than segments of the intact fin, with bifurcations farther from the body (Supplementary Fig 3.5E-F; Supplementary Fig 3.6I-J; also see Azevedo et al., 2012). Therefore, we the prox-to-prox transplants were used as the best comparisons for dist-to-prox proximodistal patterning. While dist-to-prox rays regrew marginally thinner segments, segment length was comparable to that of prox-to-prox ray segments (Fig 3.4D-E).

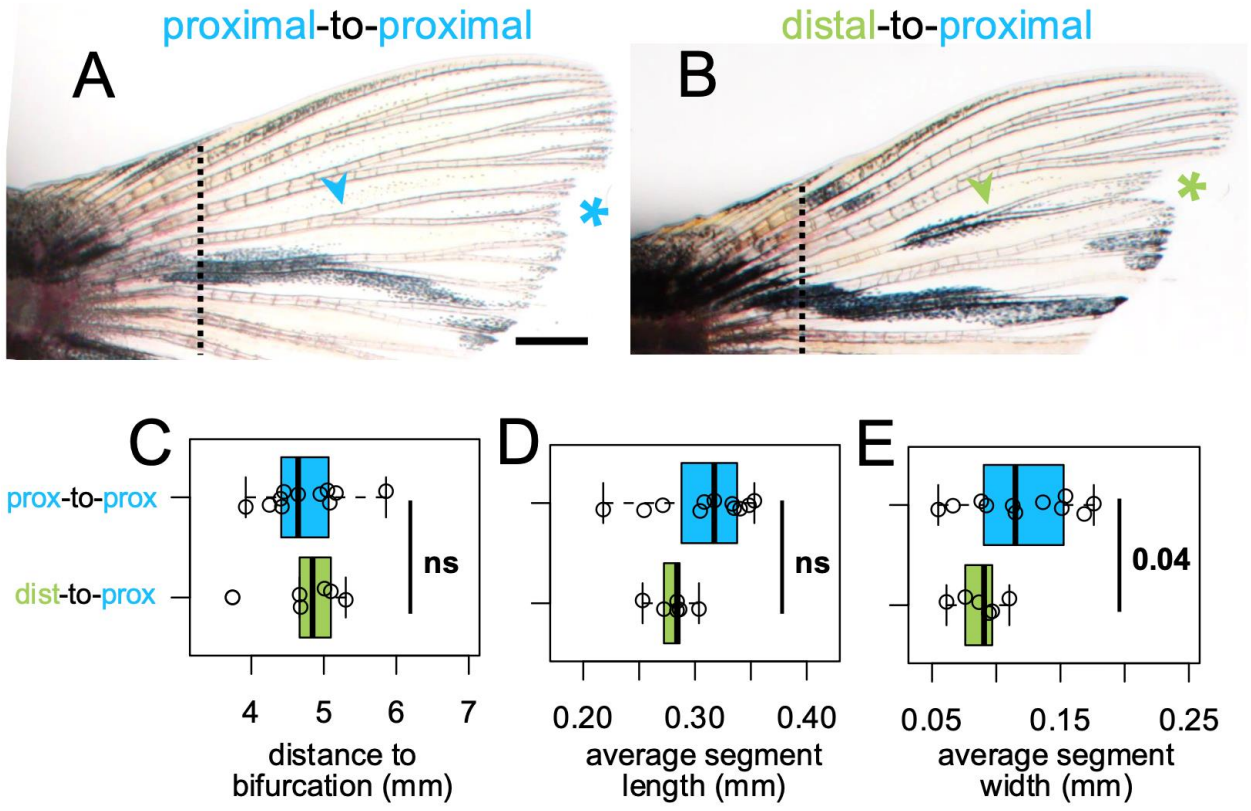

Figure 3.4 Fin ray patterning matches environment. Dorsal fin lobe at 35dpa after either (A) proximal-to-proximal (blue asterisk) or (B) distal-to-proximal (green asterisk) transplantation. Amputation plane shown with dashed line. Arrowheads indicate primary bifurcations. Boxplots showing the (C) proximodistal position of the bifurcation, (D) average segment length, and (E) average segment width in regenerate. Significance determined by a Welch two-sample t test. Scale bar, 1 mm.

The total length of a regenerating fin can be increased by treating with a calcineurin inhibitor, but these treatments do not alter positional memory and rays return to their WT baseline upon regeneration (Daane et al., 2018). We asked if regenerating from a pharmacologically-lengthened segment would alter the patterning of a regenerating ray; however, once calcineurin inhibition was removed, segment length and location of bifurcation were indistinguishable from control regenerates (Supplementary Fig 3.8).

3.2.8 Rays originating from distal transplants remember their length through multiple rounds of regeneration.

To test whether the intermediate length of dist-to-prox rays would be remembered, we performed multiple rounds of regeneration, amputating distal to the previous amputation plane (Fig 3.5A-D). Even after three rounds of regeneration, rays originating from dist-to-prox transplants were always significantly shorter than corresponding ventral rays (Fig 3.5E-G).

3.3 DISCUSSION

3.3.1 Transcriptional differences across the PD axis.

Intact fins show transcriptomic differences across the proximodistal axis (Harper et al., 2023; Rabinowitz et al., 2017), and here we identified a suite of genes that shift as the

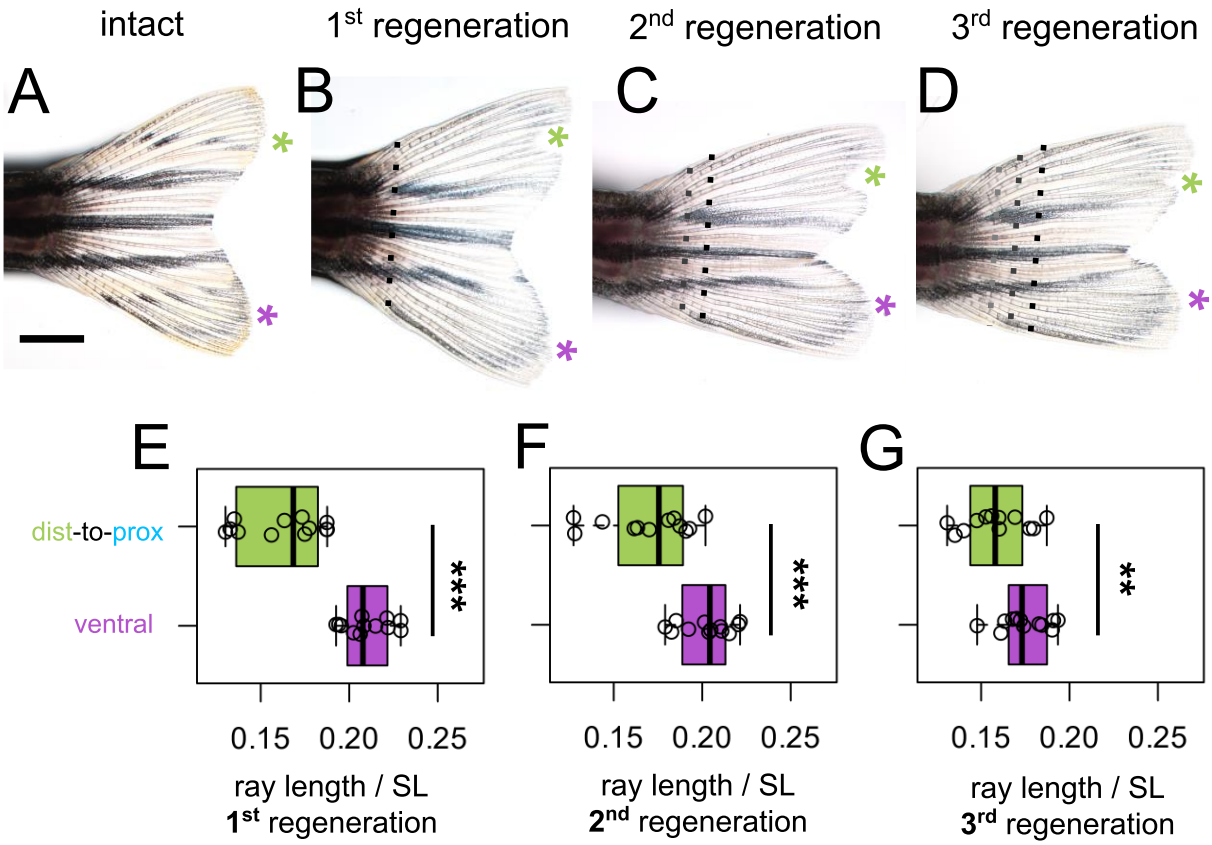

Figure 3.5 Shorter ray length is remembered through multiple regeneration cycles. (A) Intact fin. (B-D) Regenerating fin after distal-to-proximal transplantation: (B) 28 days post first amputation, (C) 28 days post second amputation, (C) 28 days post third amputation. Green asterisk, dist-to-prox; purple asterisk, ventral ray. Black dashed line, most recent amputation. Grey dashed lines, previous amputation planes. Boxplots showing the total length standardized by SL after (E) first, (F) second, and (G) third regeneration. Ray length was measured from the most recent amputation plane. Significance determined by paired Welch two-sample t test. Scale bar, 2 mm.

fin regenerates different proximodistal regions. Previous transcriptomic analyses of regenerating fins have focused on the early shifts in expression as the tissue initiates regenerative regrowth (Li et al., 2021; Nauroy et al., 2019); we found that there are substantial shifts in expression patterns even after regeneration is underway, corresponding with different stages of outgrowth proceed (see Akimenko et al., 1995; Lee et al., 2005). Indeed, we found ten times as many distally- as compared to

proximally-enriched transcripts; this may reflect the increased number of differentiated cells in the more mature regenerate (Nauroy et al., 2019).

3.3.2 Thyroid hormone induced transcriptional differences.

The presence of TH throughout development distalizes gene expression patterns as fins develop (Harper et al., 2023); however, during regeneration, hypothyroidism did not proximalize pattern of gene expression. It is possible that temporal shifts in the regenerating transcriptome overwhelmed any TH-dependent proximodistal pathways in our analysis, since the three stages analyzed vary in both time since injury and proximodistal regions of regeneration. Nevertheless, we identified many genes expressed in a proximodistal differential that was dependent on TH, and these are strong candidates for mediators of distal patterning. Notably, we did not identify any genes or pathways that were differentially expressed in the middle of the fin where bifurcations formed. This suggests that there are not unique pathways underlying bifurcation, and that expression patterns become progressively distalized as the proximodistal axis grows.

3.3.3 Growth and ultimate ray length regulation in zebrafish.

We showed that proximally-transplanted distal portions of zebrafish fin ray tissue produced regenerates that were informed by retained memory of their original distal identity. Regenerates originating from dist-to-prox transplants retained a distal pattern of gene expression for a proximally-enriched transcript, initiated regeneration at a markedly slower pace, and regrew to a shorter length than expected for their location. Dist-to-prox transplanted rays regenerated much longer than the original size of the transplanted tissue, indicating that the proximal environment can induce considerable growth in a regenerate. Notably however, dist-to-prox regenerates grew to an ultimately much

shorter length than was appropriate for their regenerating environment, and this altered length was remembered through multiple rounds of regeneration. In contrast to the regenerate length, however, we found no evidence that proximodistal patterning was remembered by dist-to-prox transplanted tissue, as these produced regenerates with segment patterning and bifurcation placement appropriate for their environmental context.

Speed of regeneration is specific to proximodistal location: proximal tissue regrows quickly while distal tissue regrows at a slower rate (Banu et al., 2022; Lee et al., 2005; Uemoto et al., 2020). Dist-to-prox transplanted rays regenerated at a slower pace during the first week of regrowth, suggesting a retained memory of distal identity. Thinner, smaller dist-to-prox rays provide fewer cells for the initial proliferation of the blastema; this smaller pool of cells may depress the initial speed of regeneration and ultimately shorten the total regenerated ray length through multiple rounds of regeneration (as in Wang et al., 2019).

Although fin rays are known to retain memory of their original length (Shibata et al., 2018), the existence of remembered identity along the proximodistal axis of the fin rays has not previously been demonstrated. Previous proximodistal transplants of blastema cells or hemi-rays did not demonstrate any retained memory of these tissues, however these transplants grafted a much smaller portion of distal tissue (Murciano et al., 2007; Shibata et al., 2018, see experimental setup diagram in Supplementary Fig 3.9). There may be a threshold cell number required to specify proximodistal identity not met in these previous experiments. Our dist-to-prox transplantation relocates large numbers of numerous cell types, presumably including osteoblasts, fibroblasts, ectoderm, blood vessels, nerve tissue and other cell types—intra-ray fibroblasts are the likely mediators of positional information (Perathoner et al., 2014). Our transplant

translocated sufficient types and/or numbers of cells into a proximal location to permanently alter positional memory in the regenerate.

3.4.4 Regenerating fin ray tissue along the proximodistal axis is unique.

In all, regenerating caudal fins show progressive changes in expression along the proximodistal axis, and many of these progressive changes are dependent on TH. We have shown that proximodistal gene expression patterns can be remembered autonomously by fin tissues, with dist-to-prox transplants producing regenerates with attenuated, distally-appropriate levels of *scpp7* expression. Initial rates of regenerative growth are further informed by remembered tissue identity: dist-to-prox rays begin regeneration at a slow (distally appropriate) rate. This early setback maintains the ray originating from the transplant at a shorter length than neighboring rays, and this decrease in length is remembered even through multiple rounds of regeneration.

3.4 MATERIALS AND METHODS

3.4.1 Fish rearing conditions.

Zebrafish were reared at 28°C with a 14:10 light:dark cycle. Hypothyroid fish and their WT controls were *Tg(tg:nVenus-2a-nfnB)* (McMenamin et al., 2014). All other fish were WT (Tübingen line). WT fish were fed marine rotifers, *Artemia*, Gemma Micro (Skretting, Stavanger, NOR) and Adult Zebrafish Diet (Zeigler, Gardners PA, USA) 2-3 times per day. Hypothyroid fish and their WT controls were fed a diet of Spirulina flakes (Pentair, London, UK) and live *Artemia*.

3.4.2 Thyroid follicle ablations.

To generate hypothyroid individuals, we performed transgenic thyroid ablations (as in McMenamin et al., 2014). Briefly, to ablate the thyroid follicles of *Tg(tg:nVenus-2a-nfnB)*, 4-5dpf larvae were incubated overnight in 10 mM metronidazole (Thermo Scientific Chemicals) dissolved in 1% dimethyl sulfoxide (DMSO, Sigma) in larval water, and controls with just 1% DMSO in larval water.

3.4.3 RNA Sequencing.

Regenerating caudal fin tissue was collected from sibling adults (>18 standard length; SL) reared under wildtype or hypothyroid conditions during regeneration of three different regions. To minimize enrichment of genes involved in blastema formation (Li et al., 2021; Nauroy et al., 2019), we chose 4 dpa regenerates to represent proximal outgrowth. Tissue was collected at 4 dpa (proximal tissue), 7 dpa (middle tissue) or 15 dpa (distal tissue). Fish were anesthetized with tricaine (MS-222, Pentair; ~0.02% w/v in system water), the distal-most portion of the regenerating fin (~3 segments closest to the leading edge) was collected and immediately flash frozen in a dry ice / ethanol bath. Three or four biological replicates, each containing tissue from six individual fins, were collected at each time point and TH condition. Total RNA was extracted immediately with Zymo Quick-RNA Microprep kit R1050 (Zymo Research, Irvine CA, USA). Quality check, library preparation, and sequencing were performed by Genewiz (Cambridge, MA). Sample libraries were made with Illumina Truseq RNA Library Prep kit and sequenced on an Illumina HiSeq platform with 150bp paired-end sequence reads. Raw sequence reads were aligned to Zebrafish GRCz11 using STAR version 2.7.3 and gene counts were called with Ensembl GRCz11 gene annotation. Differential gene expression analyses were performed with Bioconductor package limma (Michaud et al., 2008). All transcriptomes were analyzed by a multidimensional scaling plot to detect overall differences in the transcriptomes. Subsequently, comparisons were made between

proximal and distal regenerating regions in both WT and hypothyroid backgrounds; these were subsequently compared to identify the subset of differentially expressed genes that lost differential expression in a hypothyroid context. Genes were considered significantly expressed if they showed a $\log_2$ fold difference higher than 2 and a false discovery rate lower than 0.01.

3.4.4 Microsurgeries.

Transplantation was most reliable using larger adults. Tracking individuals for months necessitated a wider range of fish standard length (SL), as fish grew within the course of the experiment: individuals that began and ended within a range of 25-40mm SL were sampled. For ray extirpation, the interray tissue on both sides of dorsal ray four (DR4) was cut (using Surgical Grade Blades #11) to separate the ray from its neighbors. The entire ray was then plucked from the peduncle, by securing the zebrafish body with General-Purpose Broad-Tipped Forceps (Fisher Scientific) while using Dumont #5 Forceps (Fine Science Tools, 1125240) to grasp the base of the ray. For dist-to-prox transplants, DR4 was extirpated from the fin, ~2 mm of the distal tip was clipped off, and this portion was grafted back into the now-empty DR4 site (see Supplementary Fig 3.10 for further detail). For prox-to-prox transplants, DR4 was extirpated and then re-inserted in its native position (Supplementary Fig 3.11). Directly after transplantation, fish were maintained in a lightly anesthetized state for 30-60 minutes using ~0.01% tricaine and 3PPM clove bud oil (Sigma-Aldrich). One day post-transplant, we assessed fins for graft success: dist-to-prox transplants grafted ~80% of the time while prox-to-prox transplants only grafted in ~60% of microsurgeries. After allowing 24 hours for recovery and for the graft to fuse with neighboring tissues, fish were again anesthetized with tricaine, and the entire fin (including the transplanted graft) was amputated along a single plane with a razor blade.

3.4.5 RNAscope whole mount *in situ* hybridization.

Regenerating fins were collected at 4 dpa (proximal tissue or dist-to-prox tissue) or 15 dpa (distal tissue) and fixed for 30 minutes in 4% PFA at room temperature. Fins were stained as described in (I. Sehring et al., 2022) with the modification that all 0.2x SSCT washes were only performed twice. We used the RNAscope Multiplex Fluorescent Reagent Kit v2 (ACD Bio-techne, 323100) to screen seven candidate probes (ACD Bio-techne: *scpp7* 1265951-C1, *rhbg* 1315181-C2, *kcnma1a* 1315191-C3, *nfil3-6* 1265961-C2, *noxo1a* 1265971-C3, *defbl1* 1265981-C4, *olfml2ba* 1315201-C4) in proximal and distal regenerating tissue. Only the *scpp7* probe was able to reliably label transcripts in our whole mount tissues. Selecting candidates with known function, gene targets were manually curated from the 45 transcripts that showed proximal or distal enrichment was dependent upon TH.

3.4.6 Imaging.

For brightfield images, zebrafish were lightly anesthetized with tricaine and imaged on an Olympus SZX16 stereoscope with an Olympus DP74 camera. This set-up allowed for whole-fin imaging while preserving the resolution to identify individual segments of each ray. For fluorescent imaging, an Olympus IX83 inverted microscope with a Hamamatsu ORCA Flash 4.0 camera was used to achieve greater resolution of individual rays. Identical microscope settings (including exposure and magnification) were used for all samples within each fluorescent *in situ* experiment. Images were transformed in FIJI with the Fire LUT for visualization. For fluorescent quantifications, we used FIJI to capture mean fluorescent intensity of the blastema by sampling the distal end of dorsal ray three, dorsal ray four transplant, and dorsal ray five (DR3, DR4, and DR5).

3.4.7 Analyses.

All analyses were done in R 4.2.2. DR4 was used for all transplant procedures, with non-transplanted ventral ray four (VR4) serving as an internal comparison. Any damaged rays were excluded from analysis. Fin ray morphology was quantified with the StereoMorph R package (Olsen & Westneat, 2015) as described in (Harper et al., 2023). We used paired or unpaired Welch two-sample t tests or a paired repeated samples ANOVA followed by pairwise *t* tests to account for the two rays from a single fin or multiple time points assessed. Significance was marked as: $p < 0.05$, *; $p < 0.01$, **; $p < 0.001$, ***.

3.4.8 Pharmacological treatments.

FK506 (Selleck Chemicals) was suspended in DMSO, then diluted to 200 nM FK506 and 0.02% DMSO. Controls were treated with 0.02% DMSO. ~70% water changes were performed every other day throughout the treatment before washout. Fish recovered for seven days, then were amputated a second time with no drug treatment.

3.5 SUPPLEMENTAL DATA

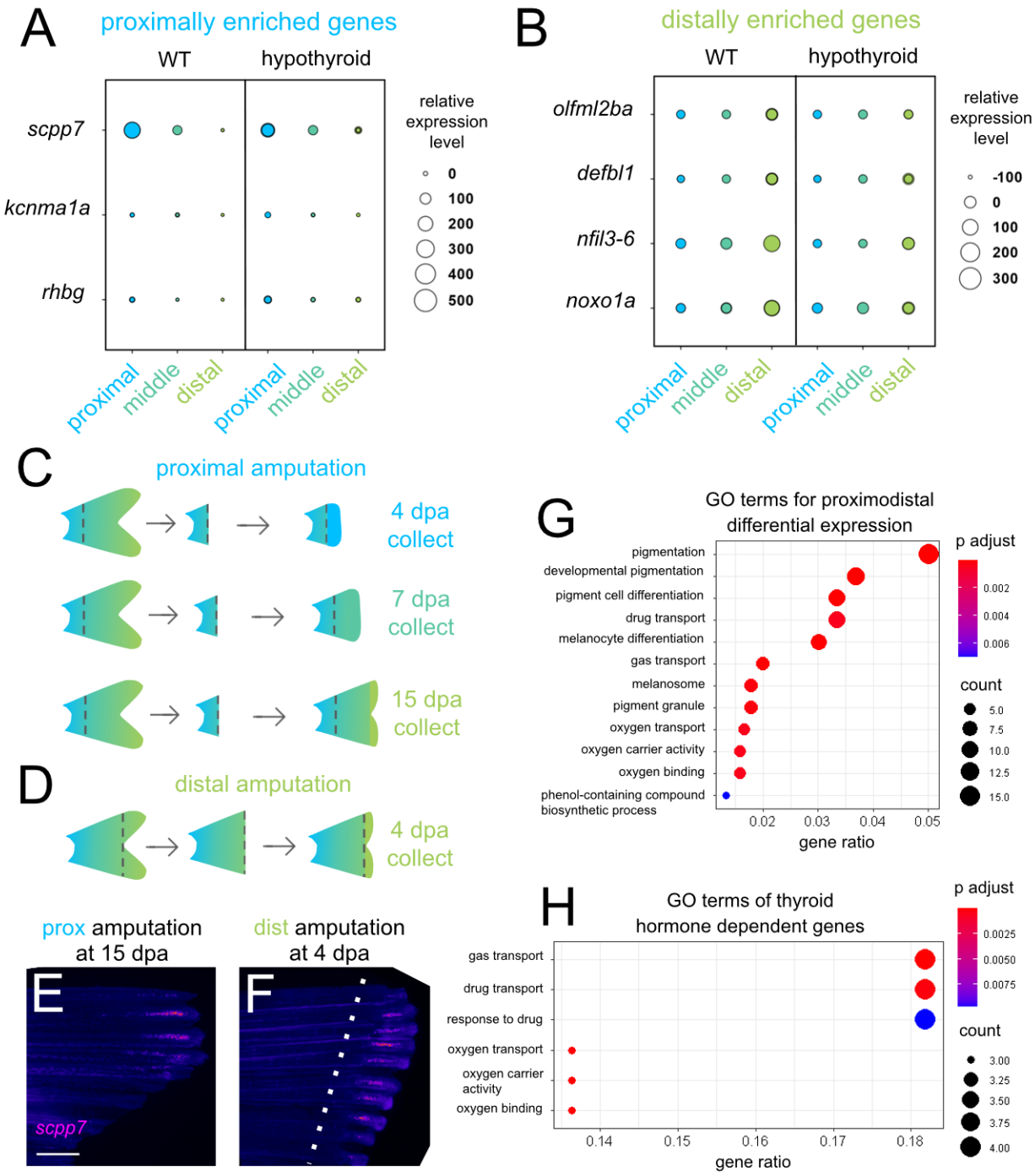

Supplementary Figure 3.1 Differentially expressed gene candidates for fluorescent *in situ* hybridization. Thyroid hormone-dependent gene candidates that are either (A) proximally enriched or (B) distally enriched in WT tissues. Custom RNAscope probes were made and tested for all genes, but only the *scpp7* probe showed specific staining. (C-D) Schematic showing sample collection with (C) proximal or (D) distal amputation. (E) Proximally amputated at 15dpa

or (F) distally amputated 4dpa tissue stained for *scpp7*. Amputation plane, dashed line. Warm colors indicate highest regions of expression. (G) GO enrichment of the 489 genes proximodistal differentially expressed in WT. (H) GO enrichment of the 45 genes that were thyroid hormone dependent and proximodistal differentially expressed in WT. Scale bar, 400 μm.

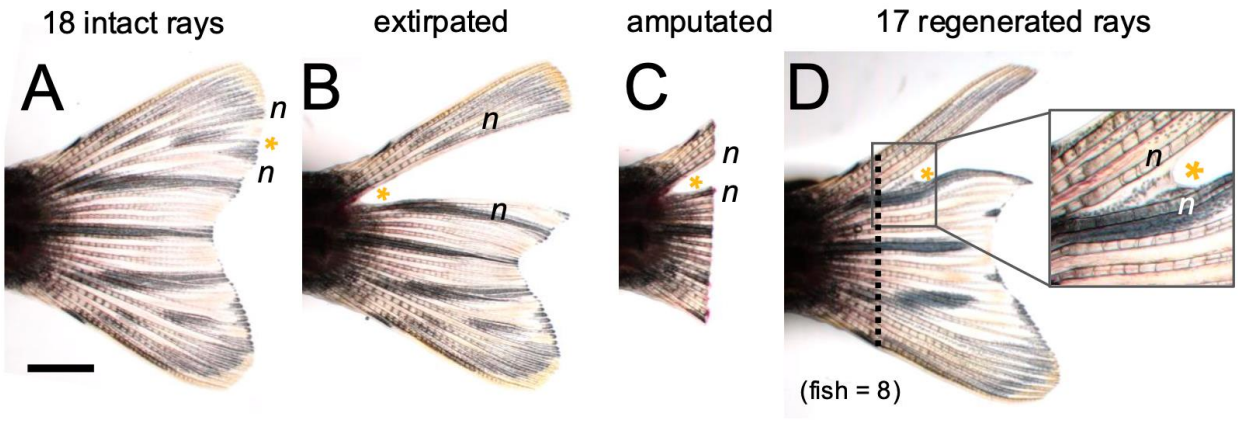

Supplementary Figure 3.2 Regeneration does not originate from an extirpated ray. (A) Intact fin with 18 rays, dorsal ray 4 (D4) marked with yellow asterisk. (B) Fin one day post D4 extirpation. (C) Freshly amputated fin, one day post D4 extirpation. (D) Fin regenerates with 17 rays (one-less ray than original, intact fin). n indicates neighboring dorsal rays 3 and 5. Amputation plane, dashed line. Scale bar, 2 mm.

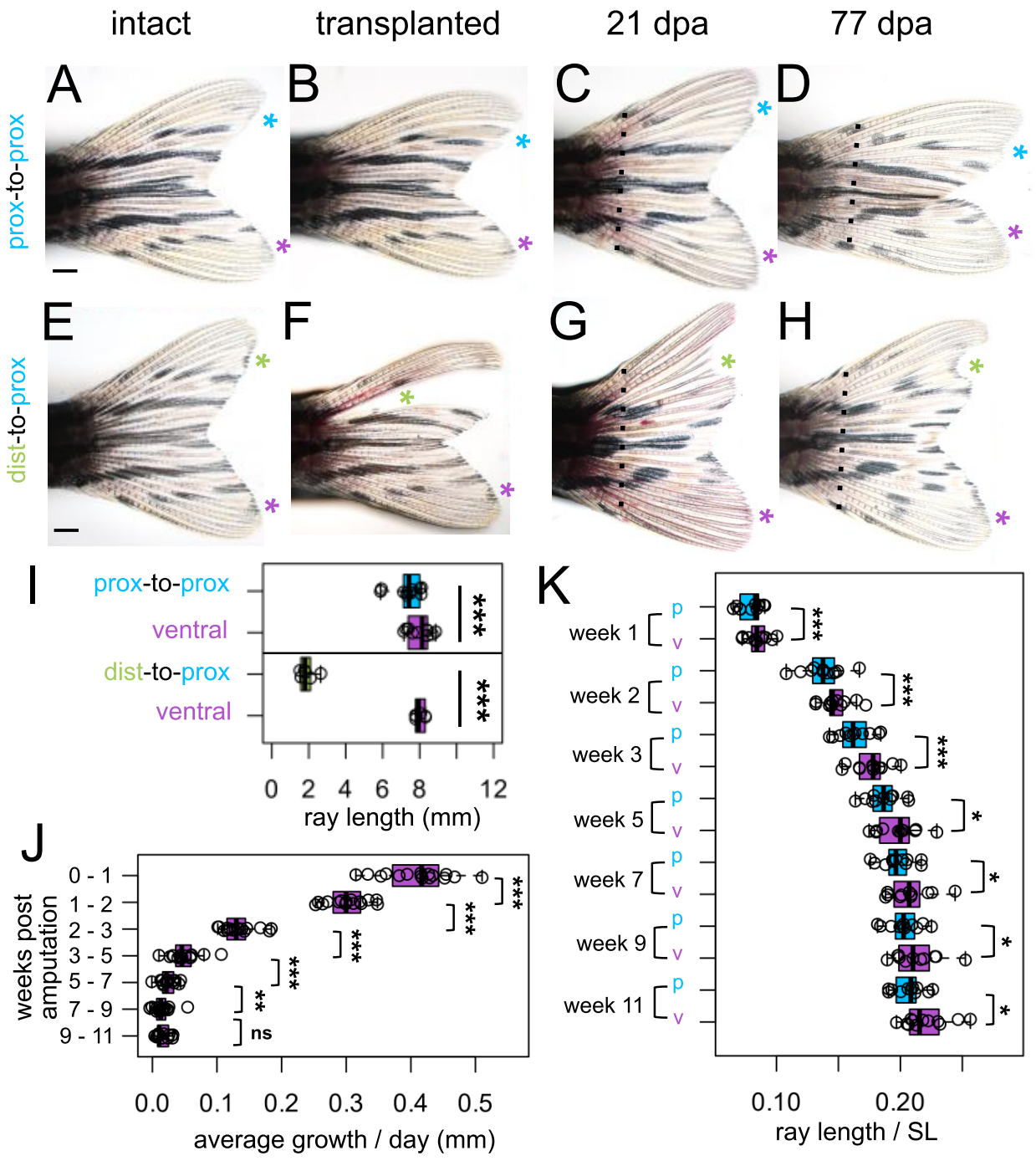

Supplementary Figure 3.3 Non-transplanted rays regenerated faster than transplanted rays. Fins of (A-D) proximal-to-proximal (blue asterisk) or (E-H) distal-to-proximal (green asterisk) transplantation: (A, E) intact pre-transplantation, (B-F) one day post-transplantation, (C-G) regenerating at 21 dpa, (D, H) regenerating at 77 dpa. Ventral rays indicated with purple asterisks. Amputation plane, dashed line. (I) Length of the rays after transplantation, as measured from the peduncle. (J) Average amount of growth per day during a one/two week periods for all the ventral ray comparisons. (K) Prox-to-prox rays versus ventral ray comparisons, ray length

(measured from amputation plane) divided by SL at each week. Significance determined by paired Welch two-sample t tests. Scale bar, 1 mm.

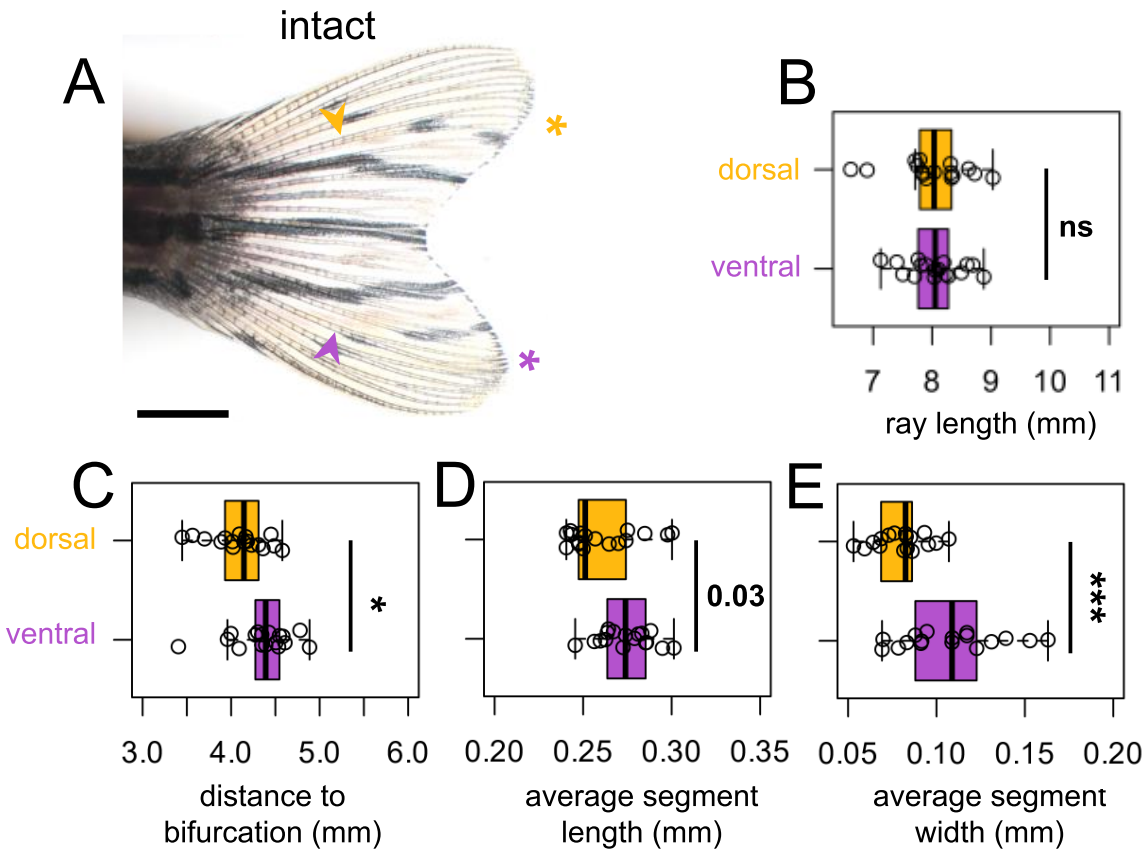

Supplementary Figure 3.4 Dorsal ray patterning is unique from ventral ray patterning. (A) Intact fin. A yellow or purple asterisk indicates dorsal ray 4 or ventral ray 4, respectively. Arrowheads, primary bifurcations. Boxplots showing the (B) total length of the ray, (C) proximodistal position of the bifurcation, (D) average segment length, and (E) average segment width measured from a set distance from the peduncle. Significance determined by a paired Welch two-sample t test. Scale bar, 2 mm.

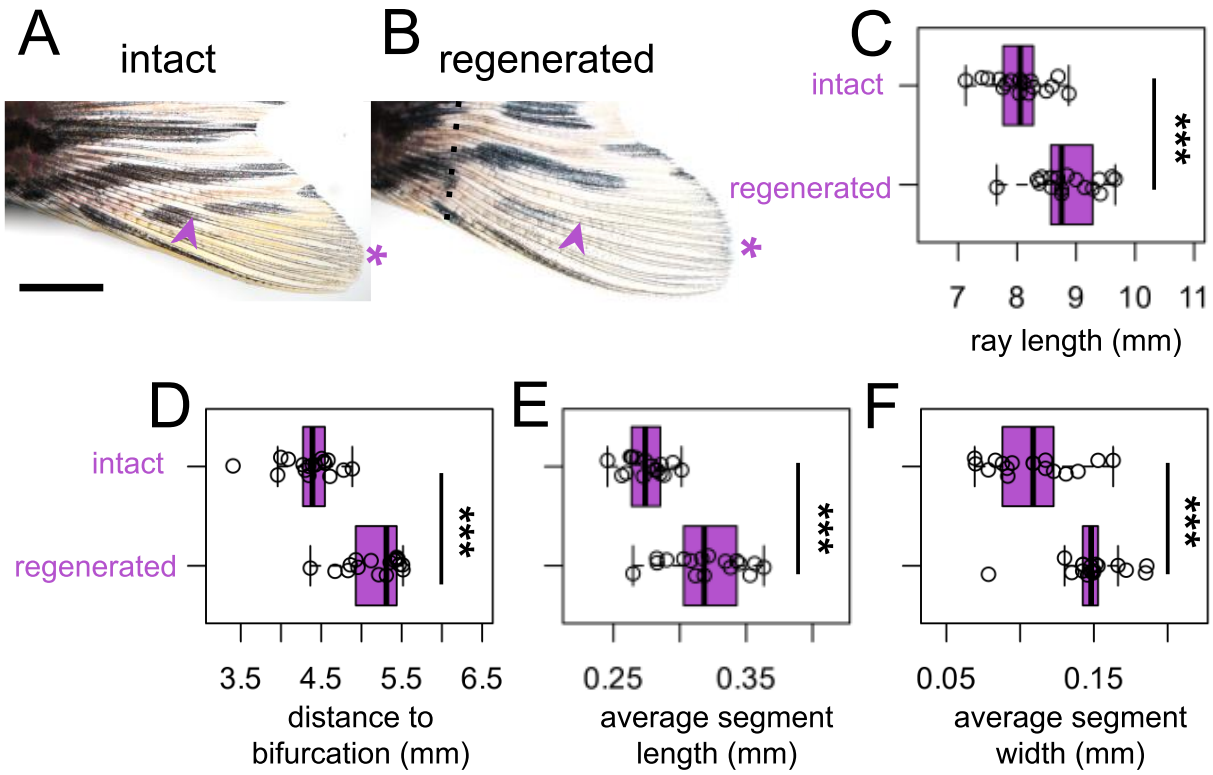

Supplementary Figure 3.5 Intact and regenerated ray patterning are different. (A-B) Ventral lobe of (A) intact or (B) regenerating fin at 35dpa. Purple asterisks indicate ventral ray 4. Arrowheads, primary bifurcations. Amputation plane, dashed line. Boxplots showing the (C) total length of the ray, (D) proximodistal position of the bifurcation, (E) average segment length, and (F) average segment width measured from a set distance from the peduncle. Significance determined by a paired Welch two-sample t test. Scale bar, 2 mm.

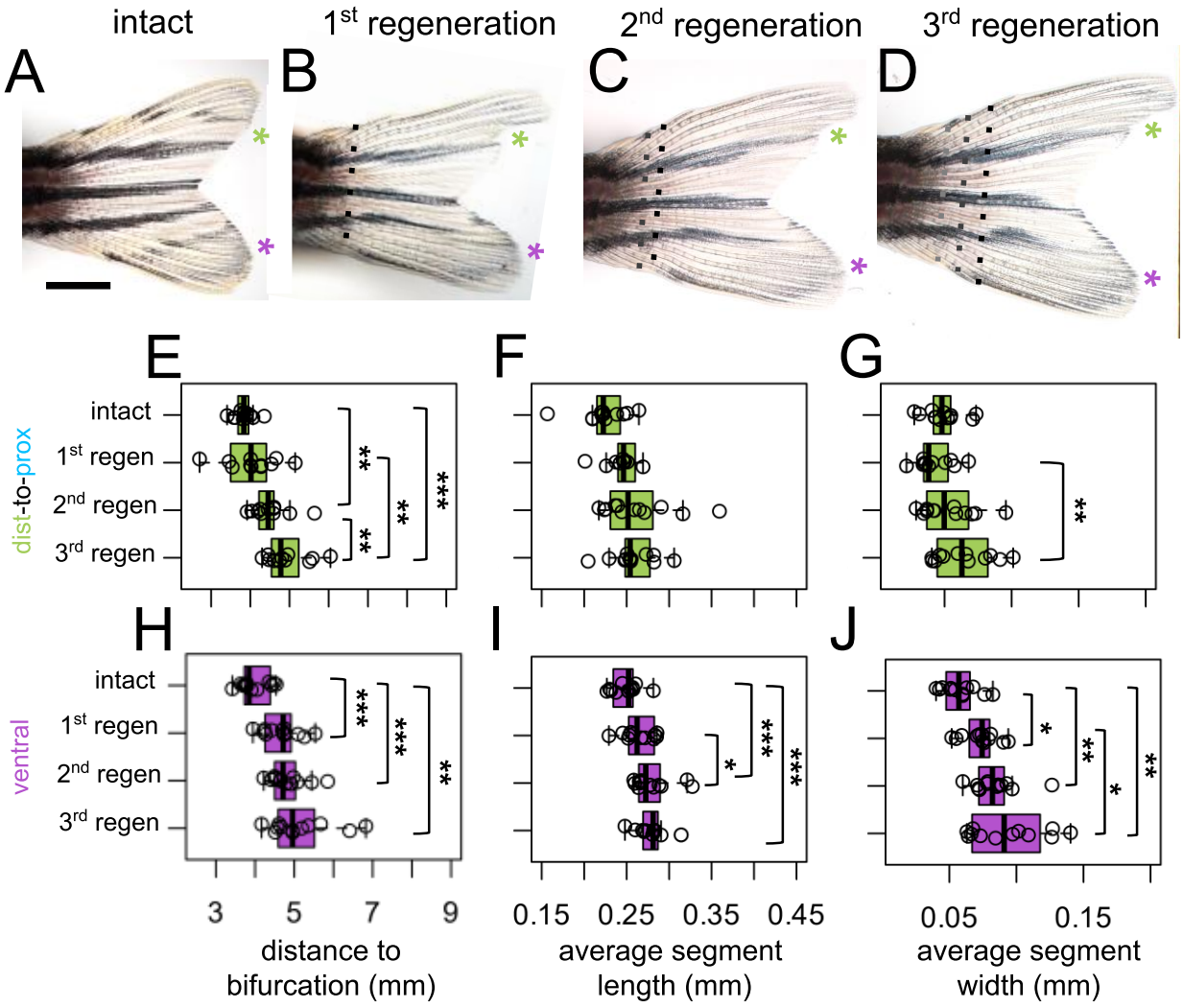

Supplementary Figure 3.6 Regenerative ray patterning differs from previous regenerated morphology. (A) Intact fin. (B-D) Regenerating fin after distal-to-proximal transplantation: (B) 28 days post first amputation, (C) 28 days post second amputation, (C) 28 days post third amputation. Green or purple asterisks indicate dist-to-prox or ventral ray, respectively. Black dashed line, most recent amputation. Grey dashed lines, previous amputation planes. (E, H) Boxplots showing the proximodistal position of the bifurcation. Note that bifurcations form at increasingly distal location after each amputation, as previously described . Boxplots showing (F, I) average segment length, and (G, J) average segment width. All measurements were taken from a set distance from the peduncle. Significance determined by paired repeated samples ANOVA followed by pairwise t tests. Scale bar, 2 mm.

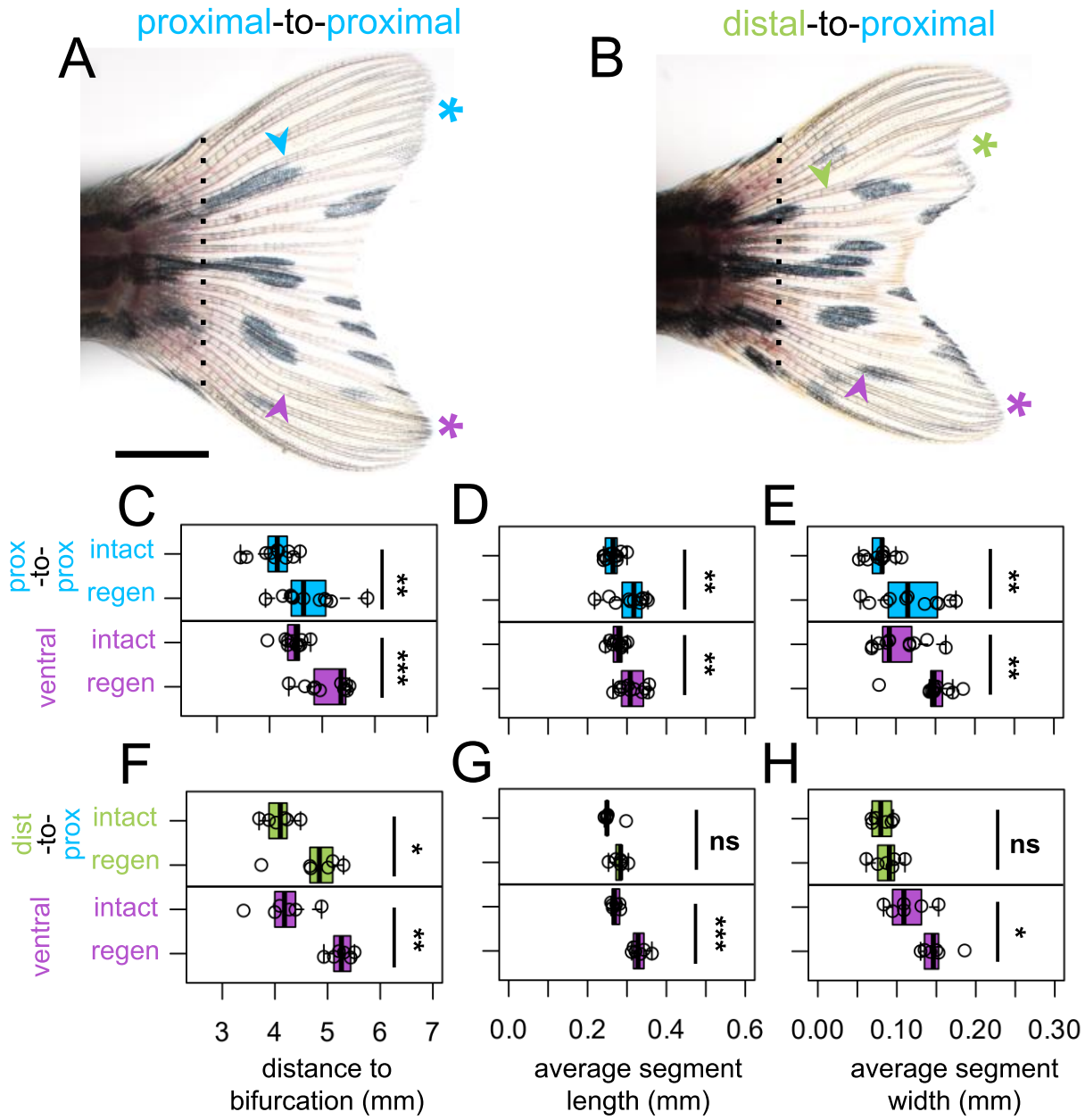

Supplementary Figure 3.7 Proximodistal patterning is dependent upon the current regenerative environment. Regenerating fins at 35dpa after either (A) proximal-to-proximal (blue asterisk) or (B) distal-to-proximal (green asterisk) transplantation. Purple asterisks indicate ventral ray comparison. Amputation plane shown with dashed line. Arrowheads indicate primary bifurcations. C-H) Boxplots showing the (C, F) proximodistal position of the bifurcation, (D, G) average segment length, and (E, H) average segment width of intact or regenerated rays, measured from a set distance from the peduncle. (C-E) Prox-to-prox or dist-to-prox ray measurements are shown alongside their ventral ray comparisons. Significance determined by a paired Welch two-sample t test. Scale bar, (A-B) 2 mm.

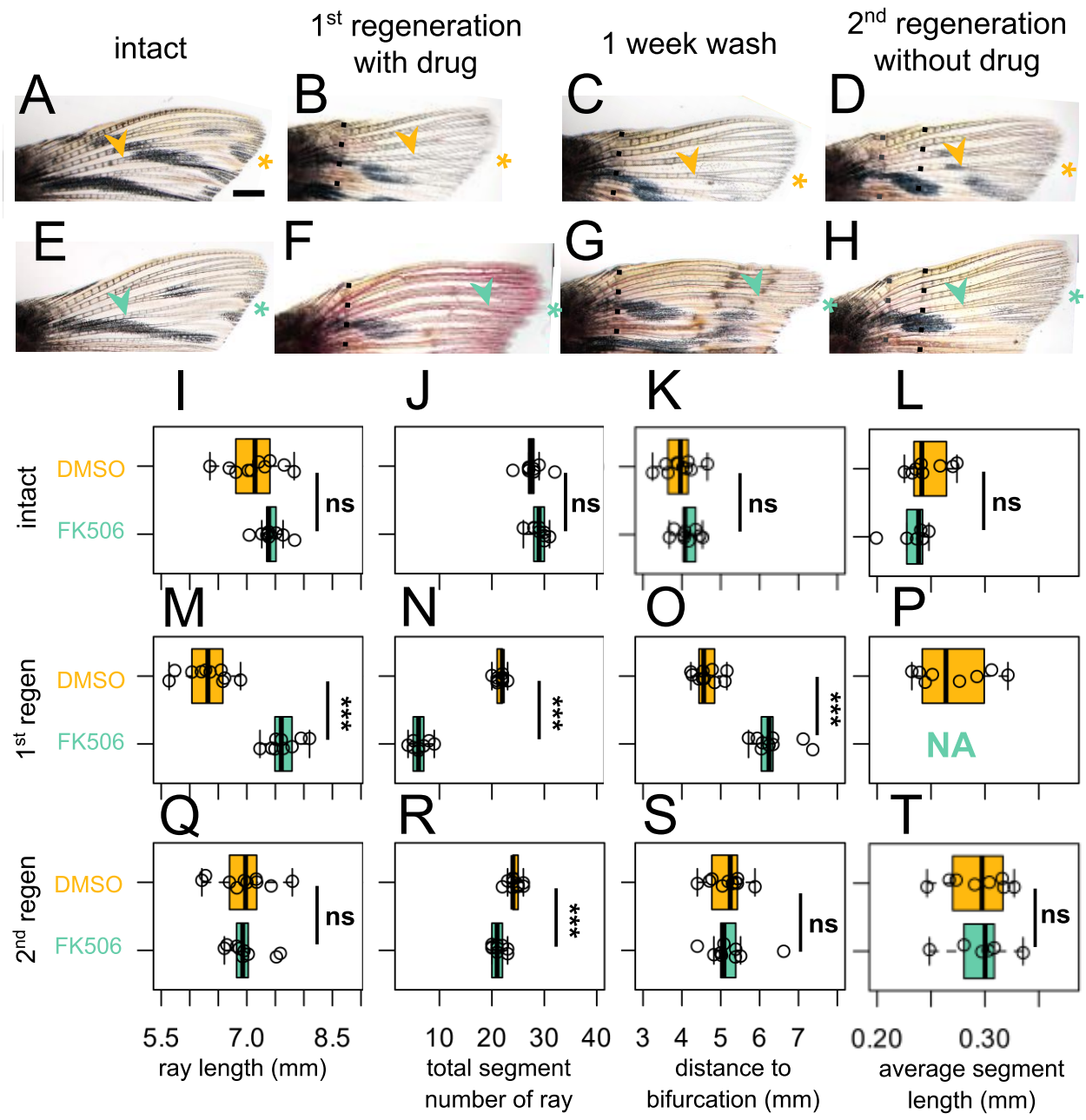

Supplementary Figure 3.8 Calcineurin inhibition-induced morphologies are not remembered in subsequent regeneration cycles. (A, E) Intact dorsal lobe before treatment. (B, F) Regenerated fin after (B) DMSO (yellow asterisk) or (F) 200 nM FK506 (turquoise asterisk) treatment, 21 days post amputation. (C, G) Fins after one week wash to clear remaining drug from water. (D, H) Regenerated fin 21 days post second amputation with no treatment. Black dashed line, most recent amputation. Grey dashed lines, previous amputation plane. Boxplots showing (I, M, Q) total ray length, (J, N, R) total number of segments of the ray, (K, O, S) bifurcation position, and (L, P, T) average segment length for (I-L) intact, (M-P) first regeneration with respective drug treatment, and (Q-T) second regeneration with no drug treatment. All measurements were taken from a set distance from the peduncle. Note in (P), rays were built from only ~5 segments, making segments lengths so long that none were contained by the

standard region of interest measured. Significance determined by unpaired Welch two-sample t test. Scale bar, 1 mm.

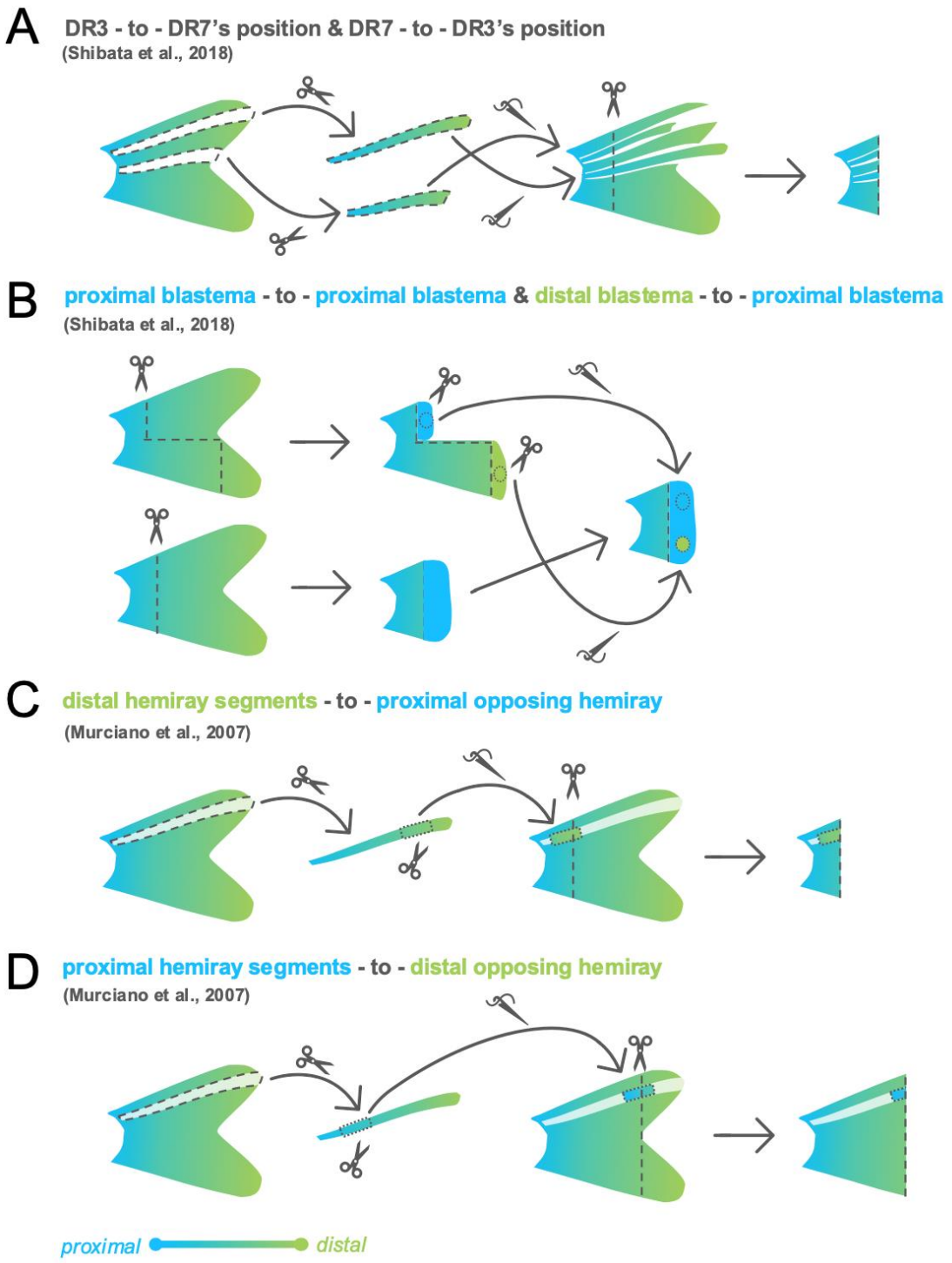

Supplementary Figure 3.9 Historical transplantation experiments. (A) Shibata et al., 2018 performed full ray transplantations, moving dorsal ray 3 into dorsal ray 7 position and vise versa.

After successful grafting, they amputated the entire. (B) Shibata et al., 2018 also made a proximal and distal amputation in a fin, collected blastema tissue from each region, and then transplanted these tissues into a proximally regenerating fin. (C) Murciano et al., 2007 extirpated an entire distal hemiray from the fin. A distal hemiray segment was grafted onto a proximal region to appose a proximal hemiray segment, then the entire fin was amputated through the graft. (D) Murciano et al., 2007 further extirpated a single hemiray, then grafted a proximal hemiray segment onto a distal region to appose a distal hemiray, then the entire fin was amputated through the graft.

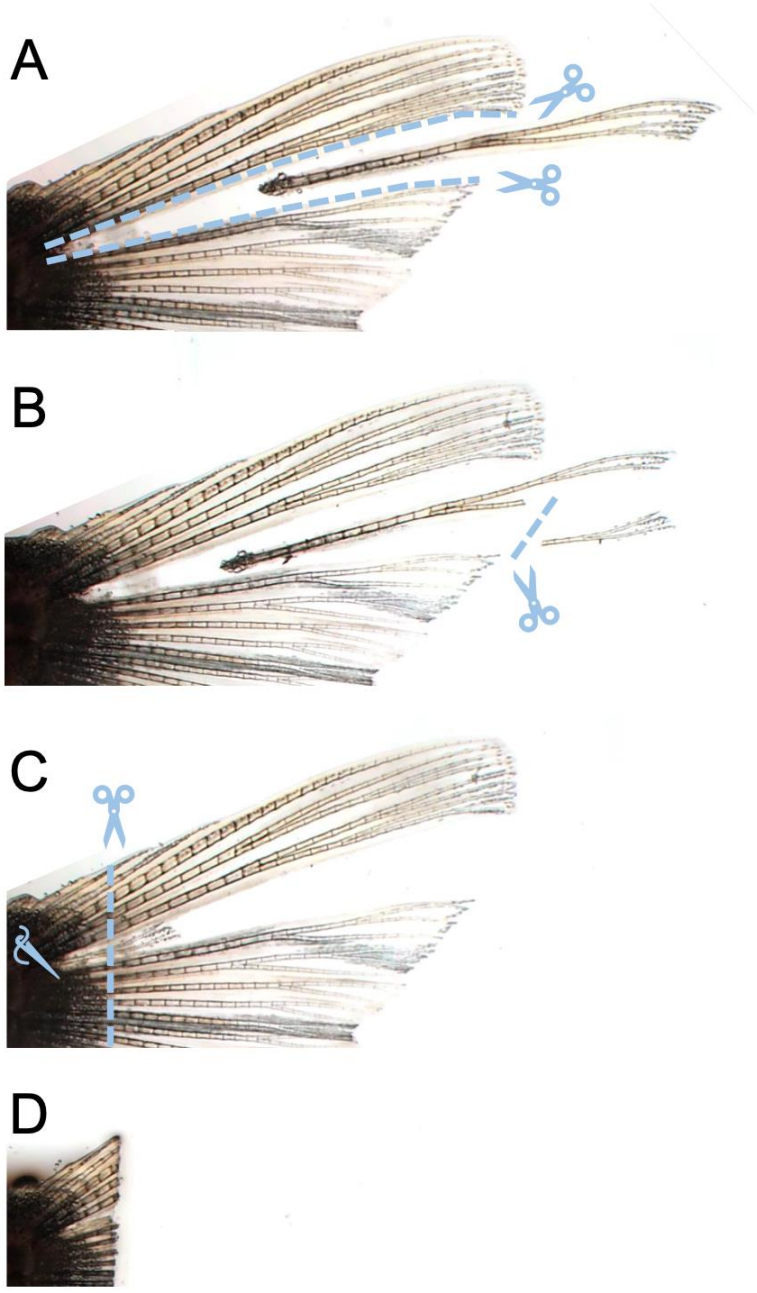

Supplementary Figure 3.10 Distal-to-proximal transplantation. (A) Interray tissue is cut sliced on either side of dorsal ray 4, permitting the ray to be cleanly plucked out of the peduncle. (B)

Distal ray tissue is removed from the rest of the ray. (C-D) After allowing 24hrs for the transplanted tissue to graft, the entire fin is amputated.

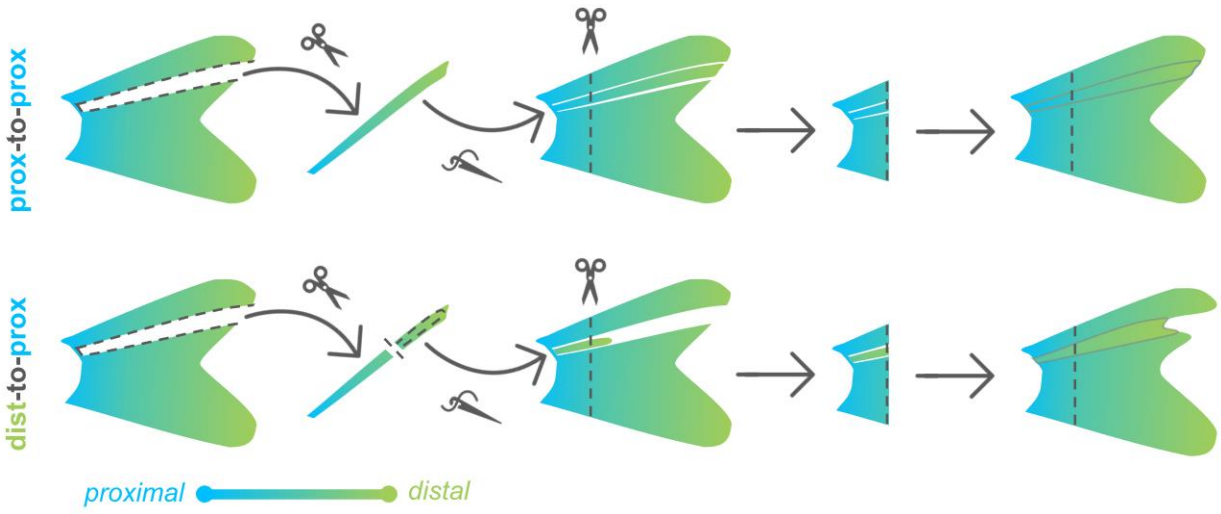

Supplementary Figure 3.11 Graphical abstract of transplantation procedures.

CHAPTER 4

Notch activity in peripheral rays of zebrafish caudal fin requires nuclear thyroid hormone signaling

The material in this chapter was adapted from:

Autumn, M., Zeng, J., & McMenamin, S. K. Notch activity in peripheral rays of zebrafish caudal fin requires nuclear thyroid hormone signaling (in preparation)

4.1 INTRODUCTION

4.1.1 Fin rays regenerate skeletal patterning that reflects original identity.

Complex tissues require precise guidance to generate functional shapes and identities. In regeneration-competent species, developed identities can be remembered upon injury and used to recreate original shape. The external fin skeleton of zebrafish (*Danio rerio*) allows for straightforward investigation of tissue morphogenesis and the emergence of shape during both development and regeneration. The caudal fin is composed of two symmetrical lobes, each supported by a skeleton of nine fin rays (dorsally, DR1-DR9 and ventrally VR1-VR9). After injury or amputation, each ray forms an individual blastema and regrows from the distal edge to restore its initial skeletal patterning and length (Lee et al., 2005; Uemoto et al., 2020), the entire fin regrowing to its original shape and size within three weeks (Wehner et al., 2014).

4.1.2 Peripheral-most rays are morphologically and transcriptionally unique from other rays in the fin skeleton.

The peripheral-most rays of each lobe of the caudal fin (DR1 and VR1; "peripheral rays" see Fig 1.1) develop and regenerate characteristics that distinguish them from all other rays of the fin. While internal rays (DR2-DR9 and VR2-VR9) branch into daughter rays, the peripheral rays never form these bifurcations and are slightly thicker than the central rays. The peripheral rays further show pathway activity unique from other rays in the fins: DR1 and VR1 show the highest expression of *aristaless* 4 (*alx4,* known to define pectoral ray identity) during development (Desvignes et al., 2022; Nachtrab et al., 2013). Along with the next most peripheral rays (DR2-DR3 and VR2-VR3), the distal portions of peripheral rays have white pigment cells called leucophores (Lewis et al., 2019).

4.1.3 Thyroid hormone activity and Notch activity are required for fin regeneration.

TH is a globally circulating endocrine factor, crucial for a diverse array of functions across vertebrates, including in fishes (McMenamin & Parichy, 2013; Porazzi et al., 2009). In zebrafish and other fishes, the hormone coordinates proximodistal patterning of fin rays during both development and regeneration (Harper et al., 2023). Seemingly independent of its role as a distalizing factor, TH shows uniquely high activity in the peripheral rays (Harper et al., 2023).

In contrast to the circulating endocrine factor TH, Notch activity is locally regulated by the physical interaction of transmembrane receptors and ligands (see Hamada et al., 2014). In the regenerating zebrafish caudal fin, Notch signaling maintains the plasticity of pre-osteoblasts, stimulating proliferation and self-renewal while inhibiting terminal differentiation during ray formation (Grotek et al., 2013; Münch et al., 2013). Further, we found novel peripheral ray-specific Notch activity in developed and regenerating fins.

Despite peripheral ray morphology being distinct from all other rays of the fin, little is known about the mechanisms that permit these differences. Here we investigate the function and interaction of peripheral TH and Notch activity, assessing them alongside the rays' marker *alx4*. Using ray transplants, we asked if peripheral ray patterning is regulated in a similar manner as central rays. Through this work we seek to establish the developmental signaling pathways that orchestrate peripheral ray formation.

4.2 RESULTS

4.2.1 High thyroid hormone activity characterizes peripheral ray.

The transgenic line *6xTRE-bglob:egfp* reports nuclear TH activity (Matsuda et al., 2017) and shows uniquely high expression in the peripheral rays of the adult caudal fins (Harper et al., 2023; Fig 4.1A). The nuclear TH receptor Thrab inhibits distalization of fin rays in the absence of the TH ligand (Harper et al., 2023), and we asked whether high TH activity in the peripheral rays was dependent on Thrab. Indeed, TH activity in the peripheral rays was severely reduced in *thrab*-/- mutants (Fig 4.2B). Deiodinase enzymes locally modulate the nuclear activity of the hormone (Orozco & Valverde-R, 2005), and we found deiodinase 2 (Dio2) to be coincidently enriched in the peripheral rays (Supplementary Fig 4.1).

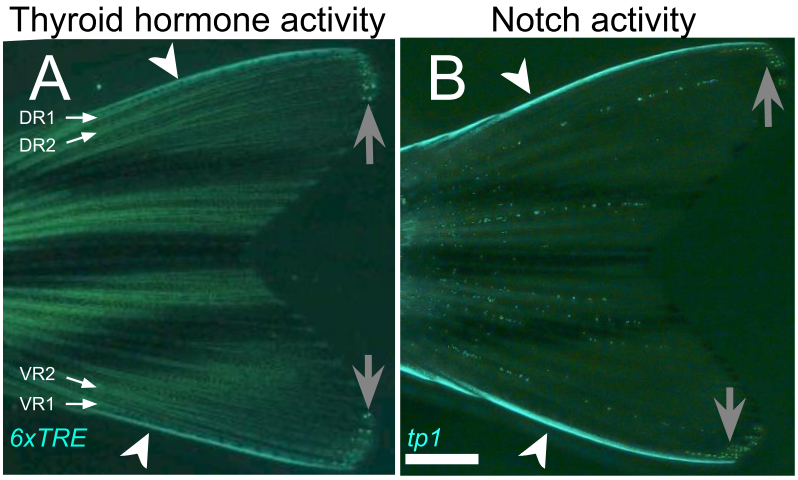

Figure 4.1 High activity of thyroid hormone and Notch in the peripheral rays of the caudal fin. Intact caudal fins (A) *6xTRE-bglob1:eGFP* reporting TH activity, (B) *Tg(Tp1bglob:eGFP^{um13})* reporting Notch activity. Arrowheads, peripheral rays. Grey arrows, leucophores. Scale bar, 1 mm.

We asked if the external hydrodynamic environment at the peripheral edge of the fin might directly induce the increased TH activity. To test this possibility, we trimmed the peripheral rays of intact fins over 47 days so they could not regrow, making the next-most-peripheral rays (DR2 or VR2) would be exposed to the external environment. Although deprived of a peripheral neighbor, the exposed DR2 and VR2 did not show TH activity to match an intact peripheral ray (Fig 4.2C, E). To test the possibility that ray

growth in the external environment might establish high TH activity, we amputated the entire fin and continued to trim the peripheral rays throughout regeneration: this did not induce DR2 or VR2 to acquire high TH activity (Fig 4.2D, F). Even in the absence of the peripheral rays, exposed DR2 rays can form bifurcations: 2/3 exposed DR2 rays bifurcated, although none of the three exposed VR2 rays formed bifurcations.

To test if high TH activity is autonomously remembered by peripheral ray tissues, we transplanted peripheral rays into central positions. Once successfully grafted, fins were amputated through the graft and allowed to regenerate. These peripheral-to-central transplants regenerated tissue showing high TH activity despite the new central position (Supplementary Fig 4.2A). The transplanted peripheral rays grew to lengths expected for their new environment, and they were shorter than peripheral rays regenerated at the edge of the fin (Supplementary Fig 4.3C-D). This stands in contrast to transplants using branching rays. When transplanted to central regions of the fin, DR2 and VR2 grow excessively relative to their neighbors, suggesting that positional information autonomous to the rays influences ultimate length (Shibata et al., 2018; also see Supplementary Fig 4.3G). Certain components of the peripheral rays were maintained even in peripheral-to-central transplanted regenerates. These regenerates did not form bifurcations (Supplementary Fig 3C)—although a single bifurcation (out of four transplants) was observed forming in a transplanted ray after a second round of regeneration (Supplementary Fig 4.3D''). Peripheral-to-central transplanted regenerates also restored leucophore pigment cells (Supplementary Fig 2A', B'), which are not normally found in central tissues. We asked whether leucophores originating from other medial fins could be rebuilt in the caudal fin. Indeed, when dorsal rays were transplanted to the caudal fin, they regenerated with both leucophores and uniquely dorsal pigment patterns (Supplementary Fig 4.4).

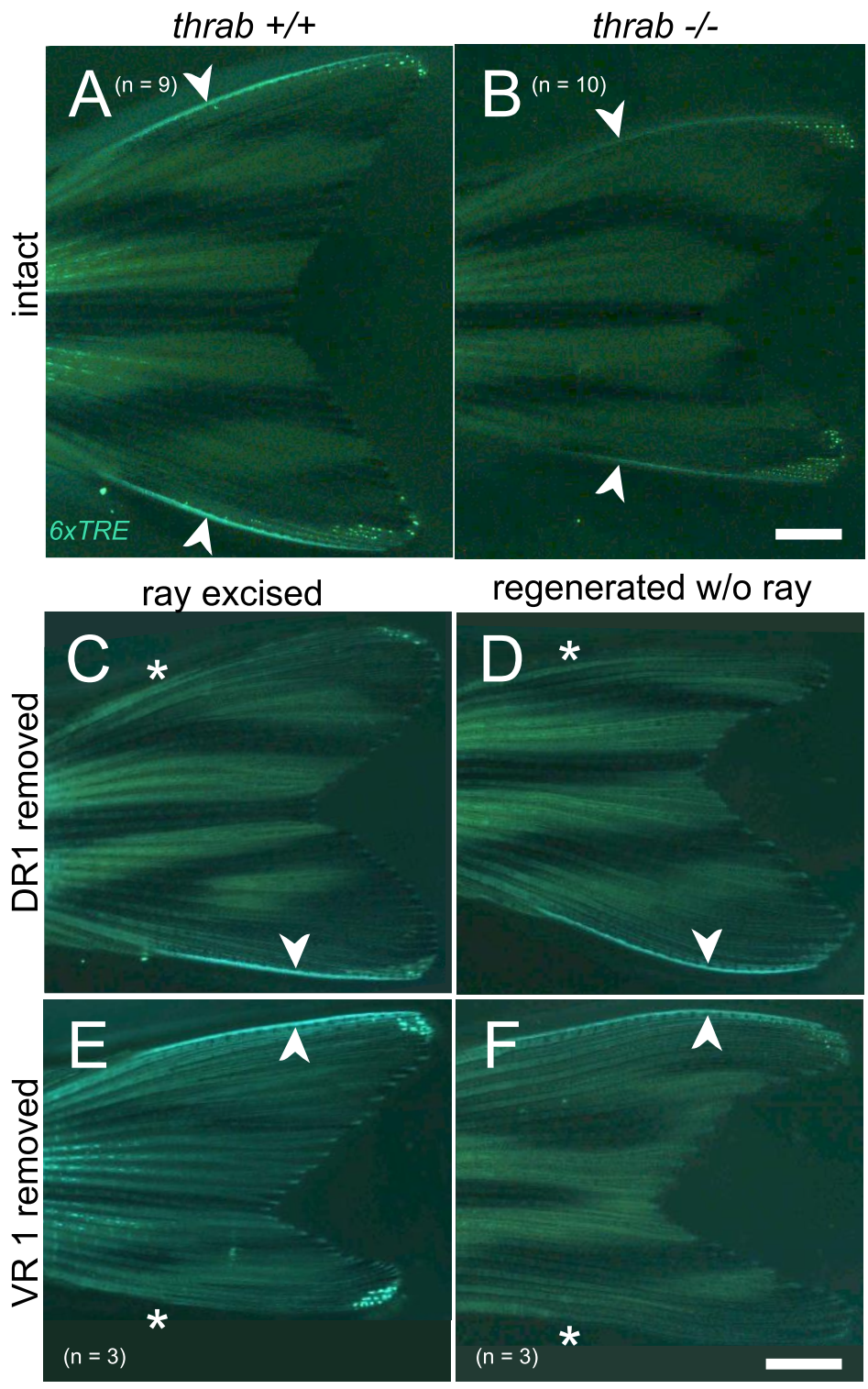

Figure 4.2 Thyroid hormone activity specific to the peripheral rays. *6xTRE-bglob1:eGFP* reports TH activity. Full sibling comparison (A) thrab +/+ (WT) or (B) *thrab-/-* fish highlight peripheral activity dependency on the nuclear receptor. Intact fin after 47 days of (C) dorsal or (E) ventral ray 1 removal. Regenerated fin at 47 dpa with continuous (D) dorsal or (F) ventral ray 1 removal. Arrowheads, peripheral-associated TH activity. Asterisk, excised ray. Scale bars, 1 mm.

4.2.2 Thyroid hormone activity colocalizes with *alx4* expression.

alx4 is expressed in fibroblasts and osteoblasts and is known to localize to peripheral rays of the caudal fin, as well as the leading rays of pectoral, pelvic, dorsal and anal fins (Desvignes et al., 2022; Nachtrab et al., 2013), and we found that TH activity was high in these anterior rays as well (Supplementary Fig 4.5). TH activity is present in several different cell types in the rays (see Harper et al., 2023), and the highest activity was detected in inter ray mesenchyme adjacent to the ray; this region overlapped with *alx4* positive tissue (Fig 4.3).

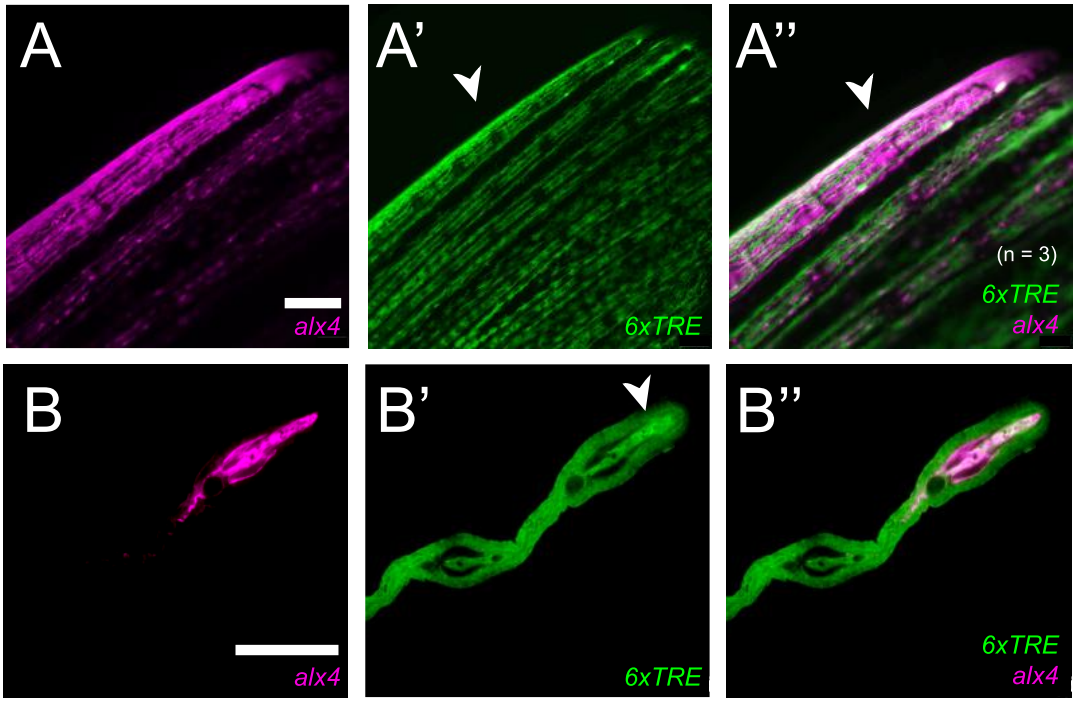

Figure 4.3 *alx4* is expressed in thyroid hormone active tissue. (A) *alx4:dsRed* and *6xTRE-bglob1:eGFP* reports *alx4* expression and TH activity in intact fin. Shown in (B) is a transverse section of an intact ray stained with secondary antibodies against the fluorophores. Arrowheads, peripheral TH activity. Scale bars, 100 μm.

4.2.3 High Notch activity characterizes but is not remembered by peripheral rays.

We evaluated activity of the Notch pathway using the *Tp1bglob:eGFP*^{um13} line (Parsons et al., 2009). Notch activity was notably high in the peripheral rays (Fig 4.1B). In contrast, Wnt activity (Wang et al., 2012) and expression of *shh* (Neumann & Nuesslein-

Volhard, 2000) do not show enrichment in the peripheral rays, suggesting that enrichment in the peripheral rays is not generic to all developmental signaling pathways (Supplementary Fig 4.6). To test if Notch activity was remembered by peripheral ray tissues, we again performed peripheral-to-central transplants. In contrast to TH activity, which was reestablished in transplants, Notch activity was abolished in regenerated peripheral-to-central transplants (Supplementary Fig 4.2B'). We asked if peripheral activity was also associated with *alx4* expression. However, Notch activity was restricted to the epithelium and did not overlap with *alx4* in the mesenchyme (Fig 4.4). Despite this, Notch activity was present along with *alx4* in all paired and medial fins (Supplementary Fig 4.9).

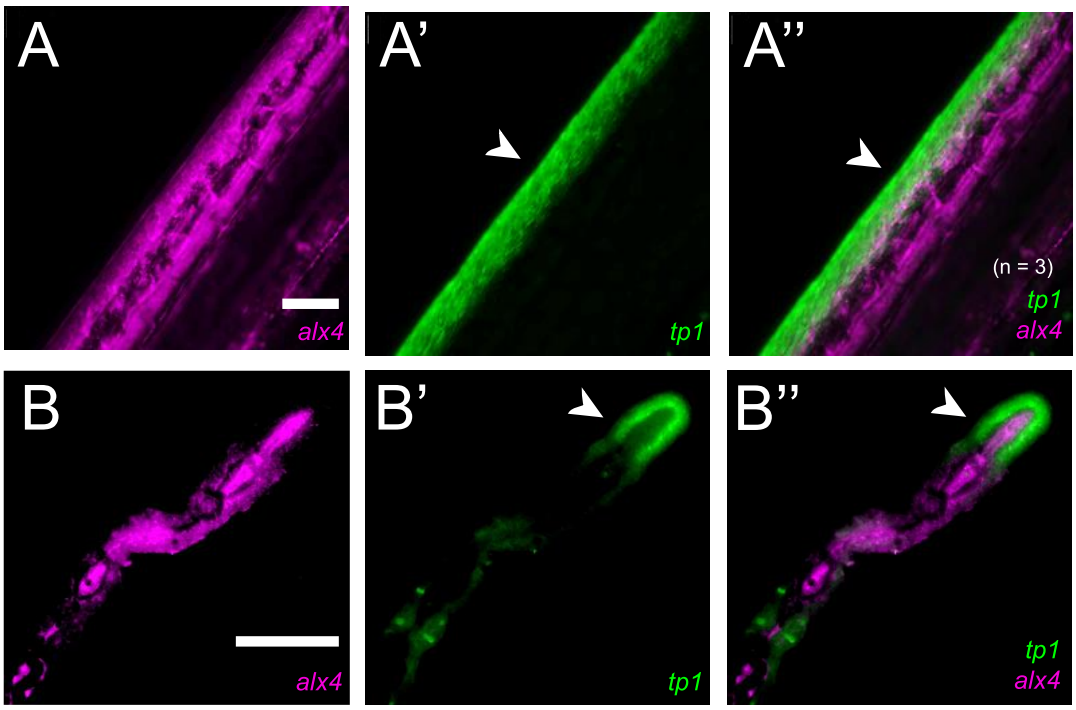

Figure 4.4 Notch activity is superficial to *alx4*-expressing tissue. (A) *alx4:dsRed* and *Tg(Tp1bglob:eGFP^{um13})* reports *alx4* expression and Notch activity in intact fin. Shown in (B) is a transverse section of an intact ray stained with secondary antibodies against the fluorophores. Arrowheads, peripheral Notch activity. Scale bars, 100 μm.

4.2.4 Notch activity in peripheral rays is downstream of TH signaling.

To test if TH activity is regulated by Notch, we treated fish with LY411575, a γ-secretase inhibitor that reduces Notch signaling (Grotek et al., 2013). When Notch was inhibited, TH activity in the peripheral rays was maintained (Supplementary Fig 4.8), suggesting that peripheral TH activity does not require Notch signaling.

To test if Notch activity is regulated by TH, we examined the Notch reporter line in a thyroid-ablated background and found that peripheral ray Notch activity was lost in hypothyroid conditions (Fig 4.5A-B). Despite the striking reduction in Notch signaling in the absence of TH, Notch activity was still present in neuromasts. Actinodins are structural proteins essential for outgrowth and patterning of regenerating rays (Nakagawa et al., 2022), with *and1* is known to be up regulated by Notch (Grotek et al., 2013), and we did not observe a reduction of *and1* in a hypothyroid context (Supplementary Fig 4.9).

To determine if TH was sufficient to rescue Notch activity during regeneration, we treated regenerating fins of hypothyroid fish with exogenous TH (thyroxine; T4). Peripheral-specific Notch activity was dependent on TH, as T4 treatment was sufficient to restore peripheral Notch activity in regenerating fins of hypothyroid fish (Fig 4.5E').

4.3 DISCUSSION

4.3.1 Transplanted peripheral rays restore a morphology that reflects their original identity and the central environment.

Many peripheral ray features were remembered and restored by peripheral-to-central transplants: transplants formed leucophores and did not bifurcate. In contrast to branching rays transplanted to central positions in the fin (Shibata et al., 2018), peripheral rays restored lengths appropriate to their new central location, rather than restoring the longer lengths predicted by their original position. Previous work showed

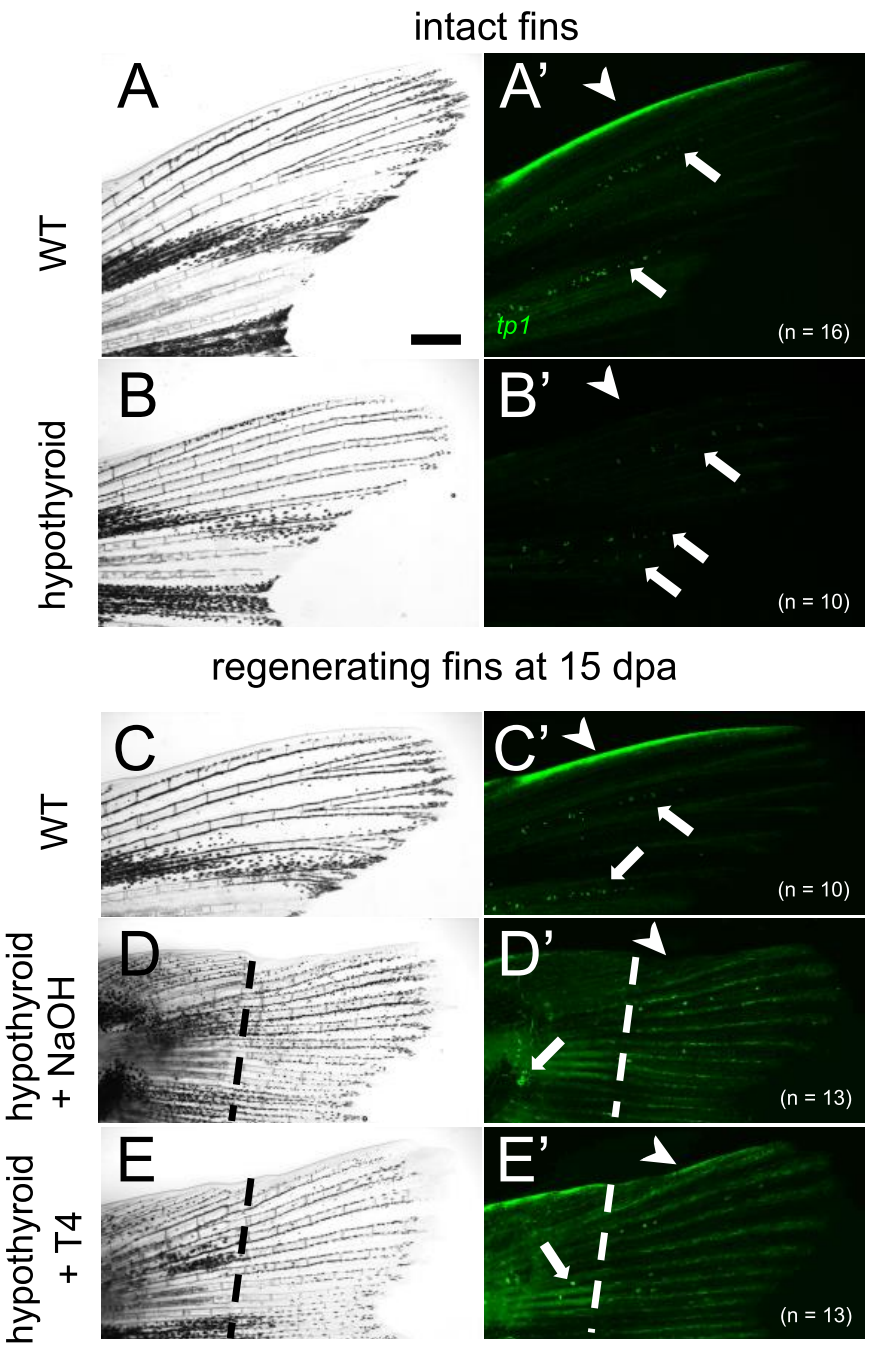

Figure 4.5 Thyroid hormone stimulates peripheral Notch activity. *Tg(Tp1bglob:eGFP^{um13})* reports Notch activity. (A-B) Intact dorsal lobe of a (A) WT or (B) hypothyroid fish. (C-E) Regenerated dorsal lobe of (C) WT fish or hypothyroid fish after treatment with (D) vehicle control or (E) thyroxine (T4). Neuromasts, sensory cells of the lateral line system, are known to be Notch-dependent (Matsuda & Chitnis, 2010). Note the distal ends of regenerating fins maintained considerable Notch activity most likely supporting osteoblast proliferation as previously described in (Grotek et al., 2013; Münch et al., 2013). Arrowheads, peripheral Notch activity. Arrows, neuromasts. Dashed line, amputation plane. Scale bar, 400 μm.

peripheral tissue transplanted centrally is competent to initiate bifurcations (Murciano et al., 2002), but we observed occasional branching only after a second amputation (Supplementary Fig 4.3D). These findings suggest peripheral rays retain and deploy identity differently than central, branching rays.

4.3.2 Thyroid hormone is necessary and sufficient to induce competent peripheral ray-specific Notch activity.

We found peripheral TH activity—but not Notch activity—was restored in regenerated peripheral-to-central transplants. Previous work with inter-individual fin ray transplants show ray grafts contribute tissue to the regenerating mesenchyme, while epithelial tissue is replaced by host tissues (Shibata et al., 2018). However, tissue replacement may be less prevalent in self-self-transplants than between two different individuals. Perhaps TH activity was restored because transplanted mesenchymal cells contribute to the regenerate, while Notch activity was lost due to transplanted epithelium being replaced by central host tissue. TH activity was not sufficient to impart peripheral Notch activity to central tissue; this suggests epithelial tissue must be predisposed to respond to the hormonal signal. Nevertheless, Exogenous TH was sufficient to restore peripheral activity, indicating peripheral epithelium is competent to respond appropriately to TH signaling.

4.3.3 Peripheral ray patterning appears Thrab independent.

While peripheral ray segments are TH-responsive, bifurcations never form in peripheral rays under hypothyroid or hyperthyroid conditions (Harper et al., 2023). Previous work demonstrates that Thrab serves to gate the functions of TH in the developing pigment pattern (Saunders et al., 2019), squamation (Aman et al., 2021), and the patterning of the rays (Harper et al., 2023). Although proximodistal patterning is

altered in a hypothyroid context, peripheral rays appear morphologically indistinguishable regardless of TH titer; I speculate that Thrab-mediated TH activity is not required for bone morphogenesis.

4.3.4 Thyroid hormone's induction of Notch activity is peripheral ray specific.

The Notch pathway is crucial in the development of numerous morphological structures (reviewed by Kopan & Ilagan, 2009), and the pathway is involved in regeneration in both vertebrate and certain invertebrate systems (Beck et al., 2003; Mashanov et al., 2020). Additionally, TH induction of Notch activity has been robustly documented in other systems (Hasebe et al., 2017; Morte et al., 2018; Silva et al., 2017; Sirakov et al., 2015), and here we report a novel instance of TH dependent Notch activity. High TH activity does not appear to colocalize with Notch; nonetheless, TH regulates Notch activity specifically in the peripheral rays. Notch activation requires a physical interaction of membrane-bound ligand and receptor between adjacent cells, so colocalization is not necessary for their interaction.

TH-regulation of Notch appears exclusive to the peripheral activity, as we don't note reduced Notch blastema activity in regenerating hypothyroid rays. Further, Notch activity, which also promotes the expression of structural proteins (actinodins) critical for ray outgrowth (Grotek et al., 2013), are not reduced by hypothyroid conditions (Supplementary Fig 4.9).

4.3.5 *alx4* may interact with thyroid hormone or Notch.

In peripheral tissue, *alx4* and highest TH activity appear in the same region of the inter ray mesenchyme, whereas Notch activity is external to and more superficial than either *alx4* or TH activity (as modeled in Supplementary Figure 4.10). Nonetheless, Notch and TH signaling are active in *alx4*-positive rays in all zebrafish fins, hinting at the

possibility of regulatory interactions. As *alx4* defines pectoral fin ray identity and shows robust expression throughout caudal fin development, perhaps this transcription factor also serves to dictate peripheral identity. Unlike TH and Notch peripheral activity, which are exclusive to DR1 and VR1 and persist throughout adulthood, *alx4* transcription is often restricted to the ventral lobe in later adulthood (Desvignes et al., 2022; Nachtrab et al., 2013). As *alx4* defines pectoral fin ray identity and shows robust expression throughout caudal fin development, perhaps this transcription factor also serves to dictate peripheral identity. Future work will unravel the regulatory interactions between TH, Notch, and *alx4*, and will determine whether *alx4* is necessary for proper ray patterning during fin regeneration.

4.4 MATERIALS AND METHODS

4.4.1 Fish rearing conditions.

Zebrafish were reared at 28°C with a 14:10 light:dark cycle and fed 2-3 times per day. Wild-type zebrafish were fed marine rotifers, *Artemia*, Gemma Micro (Skretting, Stavanger, NOR) and Adult Zebrafish Diet (Zeigler, Gardners PA, USA). HypoTH and their controls were fed a TH-free substitute of Spirulina flakes (Pentair, London, UK) and Artemia.

4.4.2 Fish lines.

Fish lines used in this study were Tg(tg:nVenus-v2a-nfnB) (McMenamin et al., 2014), Tg(6xTRE-bglob1:eGFP) (Matsuda et al., 2017), *Tg(Tp1bglob:eGFP^{um13})* (Parsons et al., 2009), *Tg(−2.7shha:GFP)* (Neumann & Nuesslein-Volhard, 2000), *Tg(alx4a:DsRed2)^{pd52}* (Nachtrab et al., 2013), *Tg(7xTCF-Xla.Siam:GFP)^{ia4}* (Wang et al., 2012), *Tg(2Pand1:eGFP)* (Lalonde et al., 2016), or wild-type (Tübingen).

4.4.3 Thyroid follicle ablations. Thyroid follicles ablations of *Tg(tg:nVenus-2a-nfnB)* were performed (as in McMenamin et al., 2014). Larvae were incubated overnight in 10 mM metronidazole (MTZ) dissolved in 1% dimethyl sulfoxide (DMSO; Sigma) in larval water, with controls treated with 1% DMSO in larval water.

4.4.4 Imaging.

Zebrafish were anesthetized with tricaine (MS-222; Pentair, ~0.02% w/v in system water) then imaged on an Olympus SZX16 stereoscope with an Olympus DP74 camera or an Olympus IX83 inverted microscope using a Hamamatsu ORCA Flash 4.0 camera. Identical microscope settings (exposure, magnification, gain) were used for experimental and controls; image processing was performed in ImageJ.

4.4.5 Peripheral-to-central ray transplantation.

Microsurgery was performed as in (Autumn et al., 2024). Dorsal or ventral ray 1 (DR1, VR1) was clipped off at the base and dorsal or ventral ray 5 (DR5, VR5) was extirpated from the peduncle. DR1 or VR1 was then transplanted into the DR5 or VR5 position, respectively. We note that peripheral rays could not be extirpated, and the residual ray base allowed DR1/VR1 rays to regenerate completely. For bifurcating ray transplantations, DR2 and R rays were transplanted into the positions of DR7 and VR7. After the transplanted ray was secured in its new location 24 hours after transplant, the entire fin was amputated, allowing transplant and native central tissues to regenerate side by side.

4.4.6 Dorsal fin ray to caudal fin transplantation.

Dorsal fin ray 3 (counting from the leading edge) was clipped off at the base and caudal fin ray (DR4) was extirpated from the peduncle. The dorsal ray was grafted into the caudal fin. The entire caudal fin was amputated 24 hours later, allowing dorsal fin ray tissue to regenerate alongside caudal fin ray tissue.

4.4.7 Fin amputation.

After anesthetizing fish with tricaine, we performed a full amputation between the 4-5th segment away from the peduncle with a razor blade. Second amputations were made distal to original amputation plane.

4.4.8 Drug treatments.

L-thyroxine (T4; Sigma-Aldrich, St. Louis MO, USA) was diluted into 0.5 M sodium hydroxide (NaOH; Sigma-Aldrich), this working stock further diluted into fish system water for a final concentration of 10 μM T4 with 194 nM NaOH. Controls were treated with 194 nM NaOH in fish system water. 50% water changes were performed every other day throughout treatment. and LY411575 (TargetMol, T6063) was diluted with DMSO into a 10mM stock, and then further diluted with fish water to final concentrations of 5uM.

4.4.9 Immunohistochemistry.

Whole-mount fins were stained for Dio2 using Deiodinase Type II (Antibodies-Online.com, ABIN652664). Longitudinal cryosections were stained for transgenically expressed eGFP and dsRed using anti-GFP(Sigma Aldrich, Burlington MA, USA, SAB4301138) and anti-mCherry (Novus Biologicals, Minneapolis MN, USA, NBP2-25158), respectively. Secondary antibodies used were AffiniPure Alexa Fluor 488 Anti-

Rabbit and Alexa Fluor 594 Anti-Chicken (Jackson ImmunoResearch, West Grove PA, USA, 711-545-152 and 703-585-155).

4.5 SUPPLEMENTAL DATA

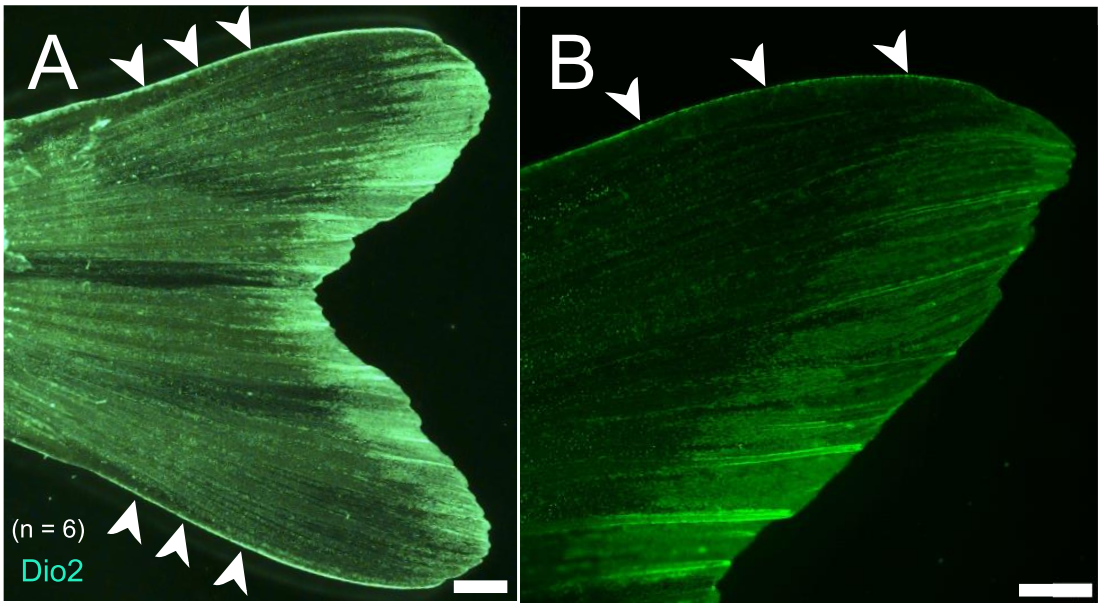

Supplementary Figure 4.1 Dio2 localizes to peripheral and distal tissues. Whole-mount intact fin stained for deiodinase 2 (Dio2). Arrows, peripheral-associated Dio2. Scale bars, (A) 2 mm; (B) 400 µm.

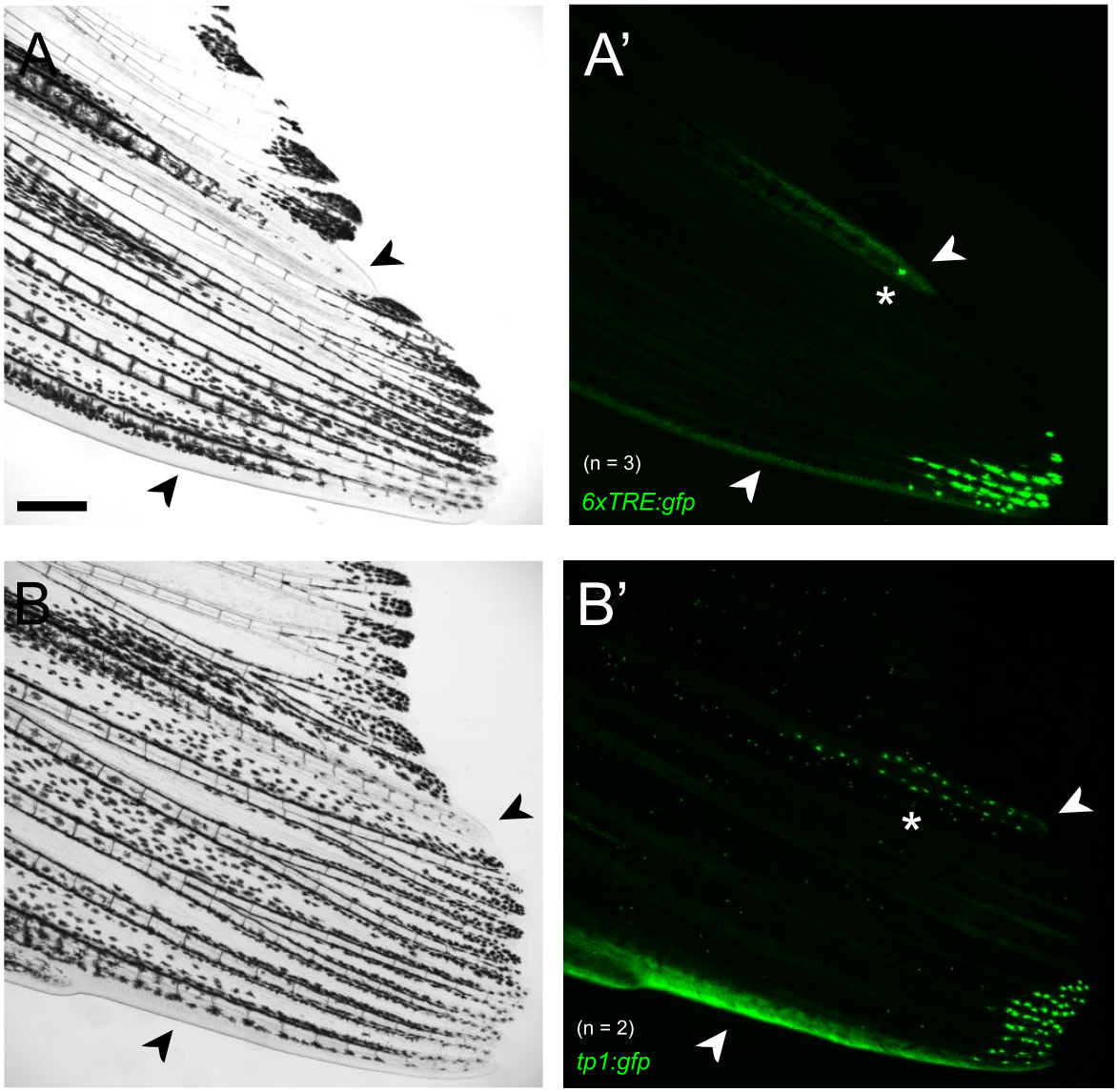

Supplementary Figure 4.2 Peripheral-to-central transplants only restore TH activity. *6xTRE-bglob1:eGFP* reports TH activity in regenerated fin. (A) Regenerated fin after peripheral-to-central ray transplantation and regeneration. Note that both the regenerated peripheral ray and the ray originating from the transplanted stump of peripheral ray tissue both show TRE activity and leucophore pigmentation. *Tg(Tp1bglob:eGFP^{um13})* reports Notch activity. (B) Regenerated fin after peripheral-to-central ray transplantation and regeneration. Note that only the regenerated peripheral ray shows Notch activity. Arrowheads, peripheral rays. Asterisks, leucophores pigment cells. Scale bar, 400 μm.

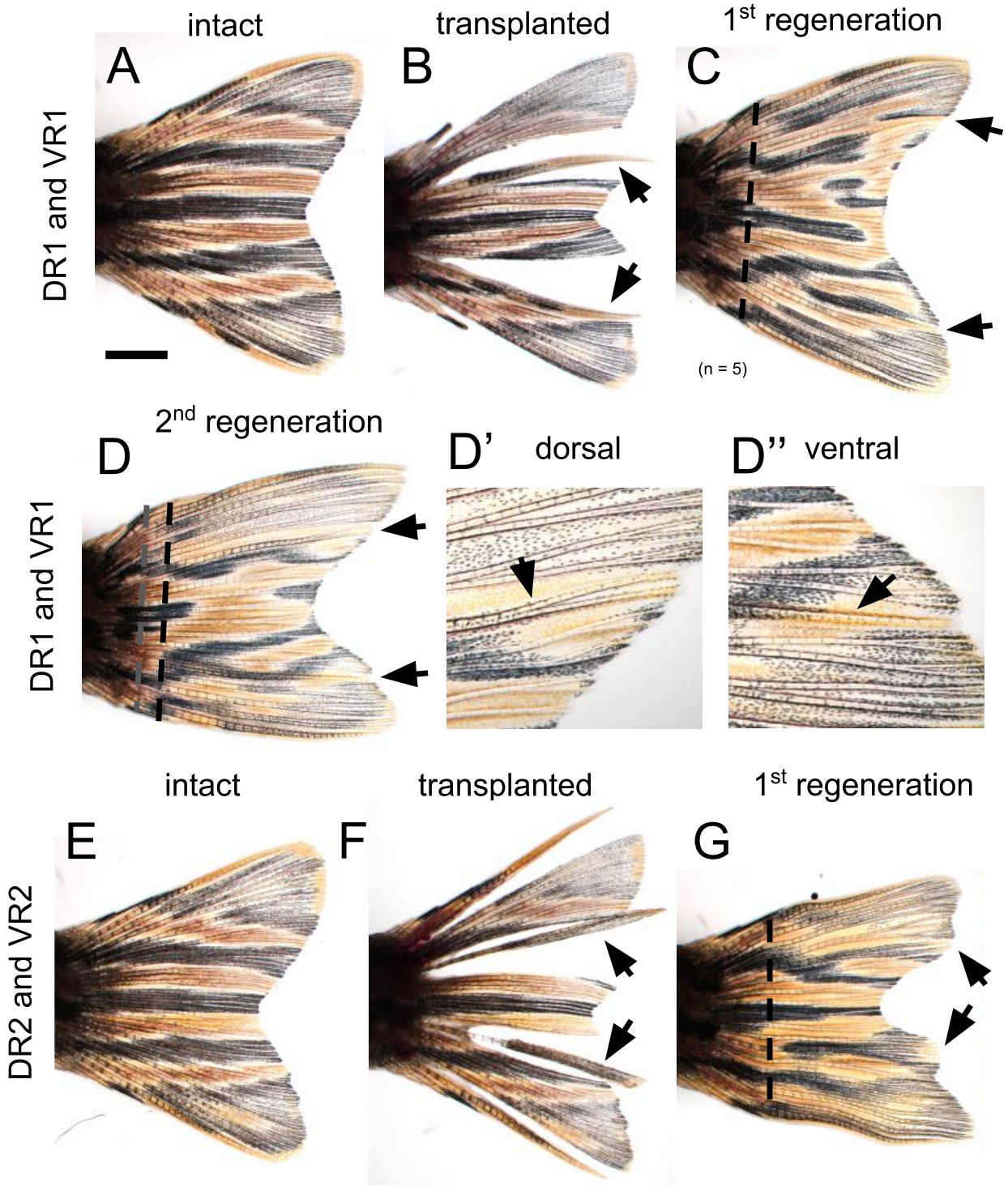

Supplementary Figure 4.3 Peripheral-most rays regenerate central-appropriate lengths. (A, E) Intact fins. (B, F) Fin one day post transplantation of (B) DR1 and VR1 or (F) DR2 and VR2 to central positions. (C, G) Regenerated fin 54 days after amputation. Note only DR2/VR2 transplanted rays grow longer than neighboring rays. (D) Regenerated D1/V1 fin was amputated a second time and assessed at 35 dpa. Note aberrant bifurcation formed in the dorsal lobe's peripheral transplant. Arrows, transplanted rays. Dashed line, amputation plane. Scale bar, 2 mm.

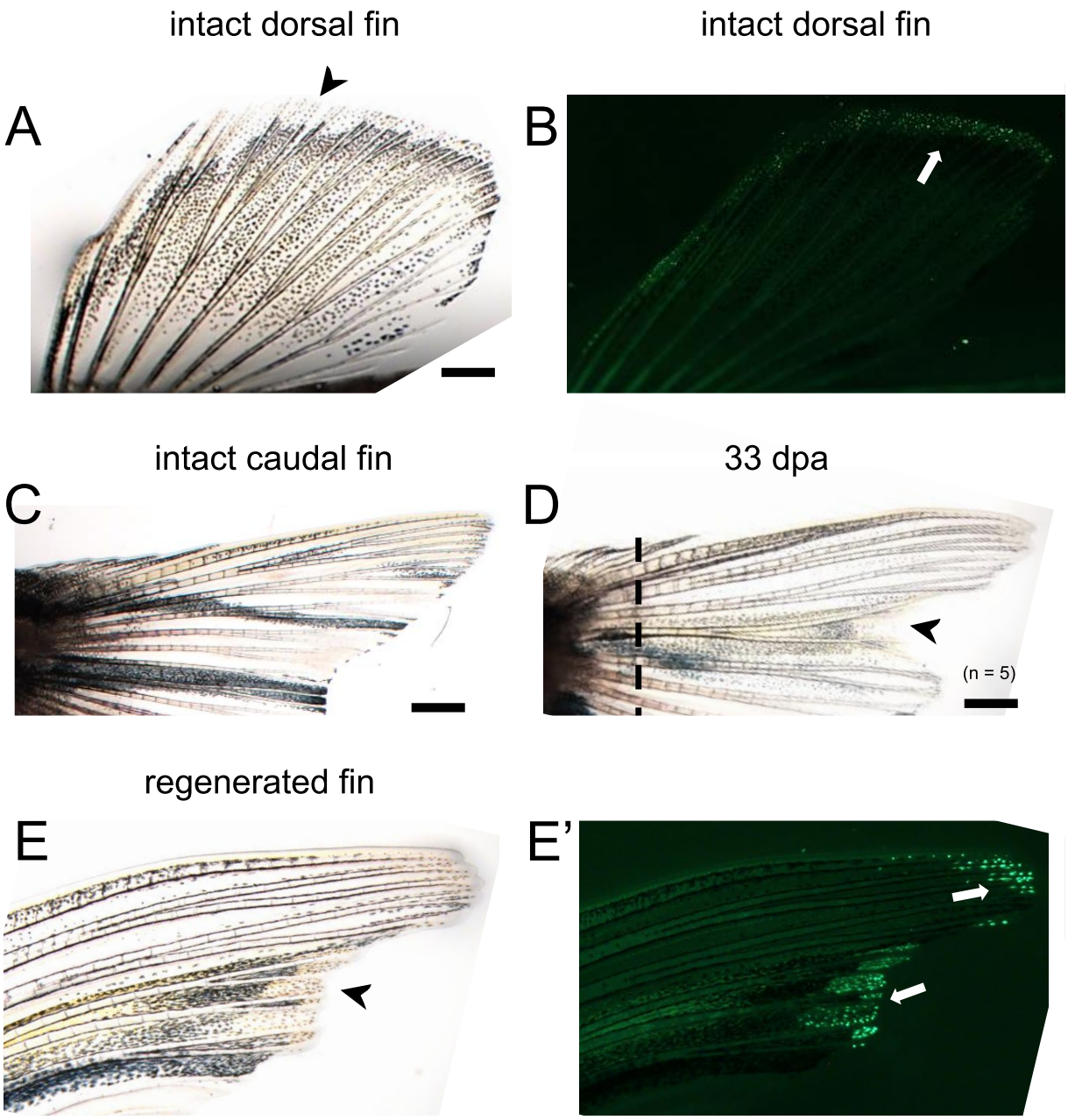

Supplementary Figure 4.4 Dorsal fin ray pigment cells restore origin pattern in a caudal fin environment. (A) Intact dorsal fin. (B) Intact WT dorsal fin. Note autofluorescence of leucophores. (C) Intact dorsal lobe of caudal fin. (D) A dorsal fin ray 3 was transplanted into the caudal fin and then the all rays were amputated to allow rays from different fins to regenerate together. (E) Dorsal fin ray to caudal fin regenerated fin. Note dorsal fin-like speckled melanophore pattern and leucophores. Dashed line, amputation plane. Arrowheads, dorsal fin ray. Arrows, leucophores. Scale bars, 1 mm.

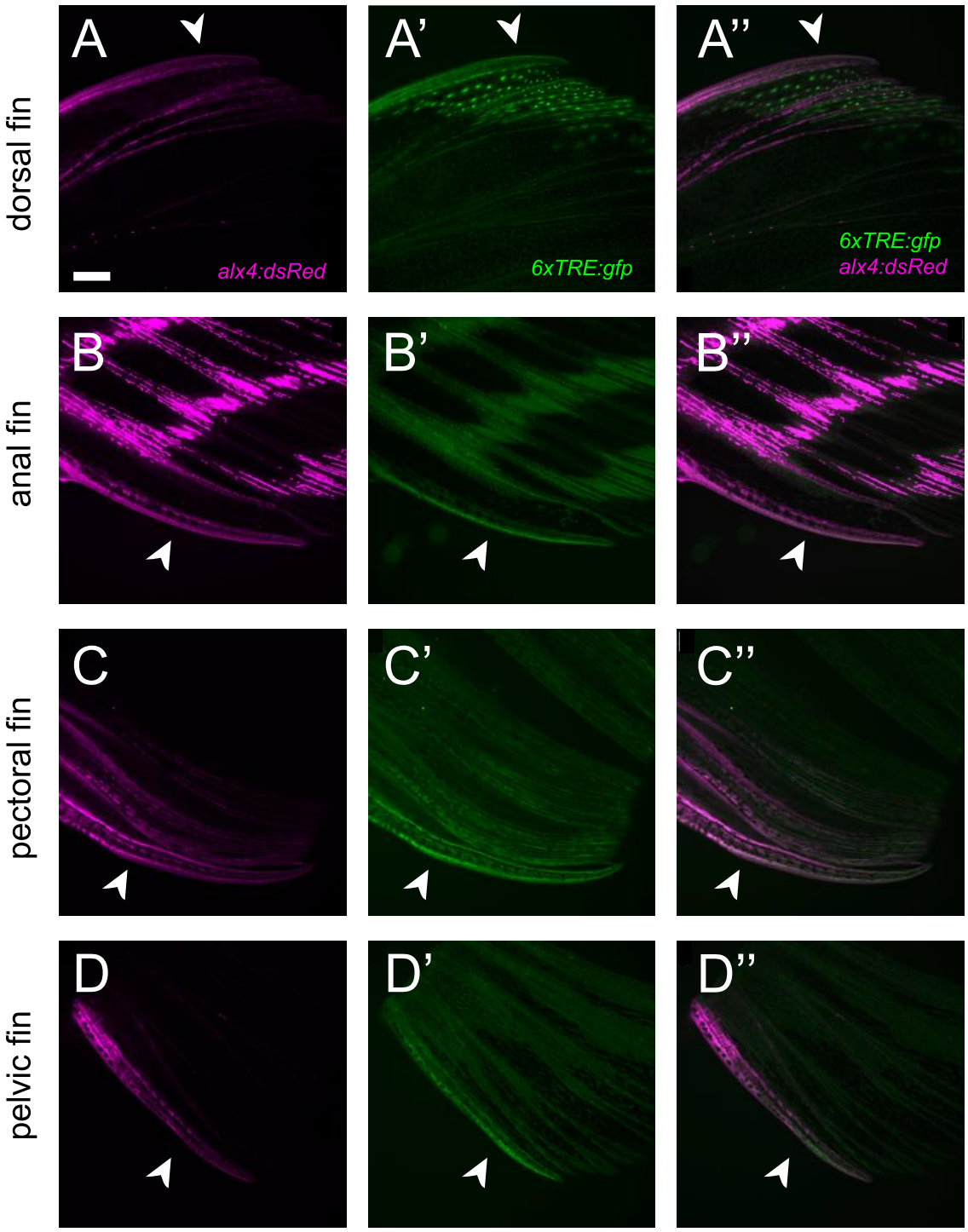

Supplementary Figure 4.5 *alx4* and TH activity each localize to anterior and leading rays of fins. *alx4:dsRed* and *6xTRE-bglob1:eGFP* reports *alx4* expression and TH activity in intact medial (A) dorsal and (B) anal fins and paired (C) pectoral and (D) pelvic fins. Arrowhead, anterior or leading ray of fin. Scale bar, 400 μm.

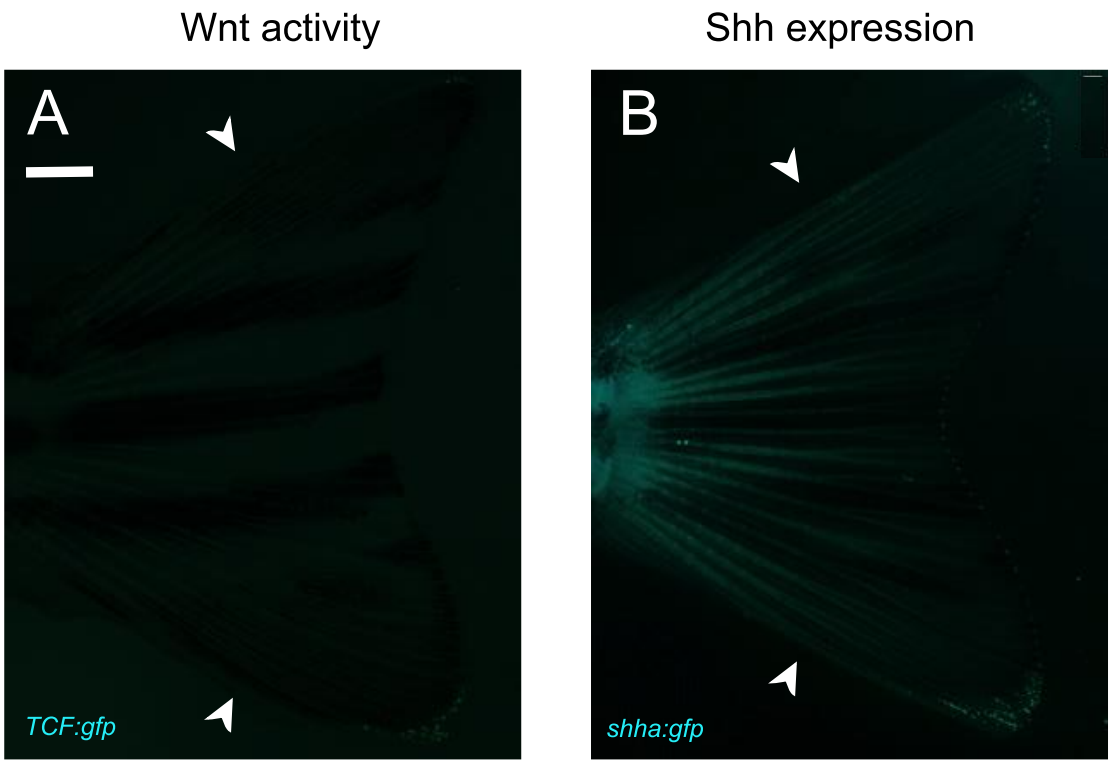

Supplementary Figure 4.6 Peripheral rays do not show enriched Wnt activity or *shh* expression. (A) *Tg(7xTCF-Xla.Siam:GFP)*^{ia4} reporting Wnt pathway activity and (B) *Tg(−2.7shha:GFP)* showing sonic hedgehog ligand expression. Arrowheads, peripheral rays. Scale bar, 1 mm.

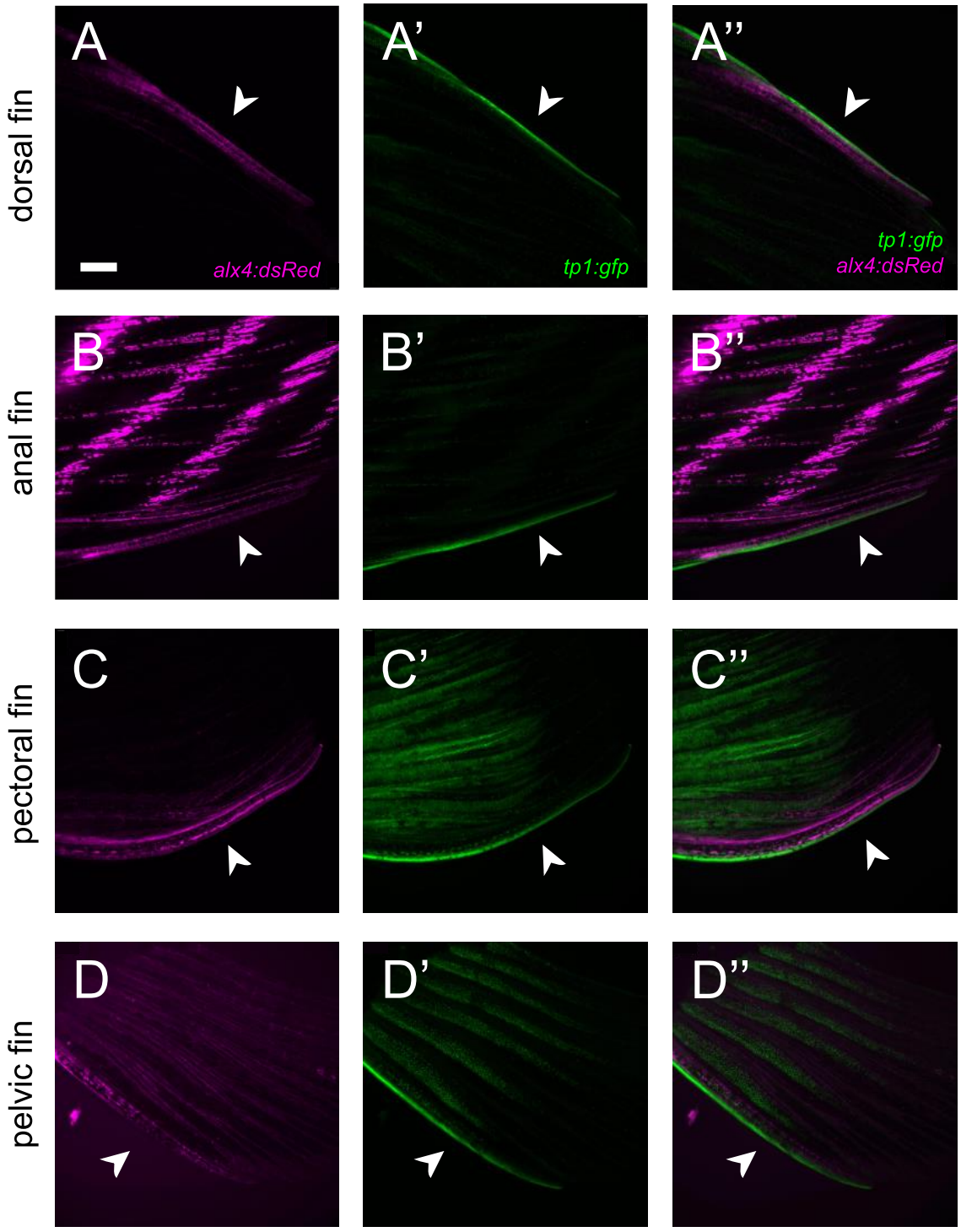

Supplementary Figure 4.7 *alx4* and Notch activity each localize to anterior and leading rays of fins. *alx4:dsRed* and *Tg(Tp1bglob:eGFP^{um13})* reports *alx4* expression and Notch activity in intact medial (A) dorsal and (B) anal fins and paired (C) pectoral and (D) pelvic fins. Arrowhead, anterior or leading ray of fin. Scale bar, 400 μm.

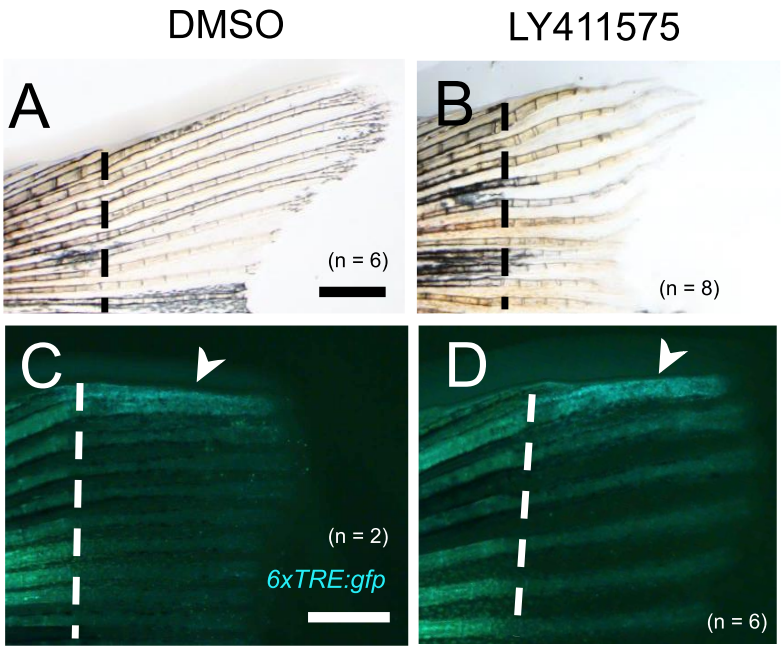

Supplementary Figure 4.8 Thyroid hormone activity is not dependent upon Notch signaling. Regenerated fins at 21 dpa after continuous treatment with (A) vehicle control (DMSO) or (B) Notch inhibitor (LY411575). *6xTRE-bglob1:eGFP* reports TH activity in regenerating dorsal lobe at 6 dpa after 2 days treatment with (C) vehicle control or (D) Notch inhibitor. Arrowheads, peripheral activity. Dashed line, amputation plane. Scale bars, 500 μm.

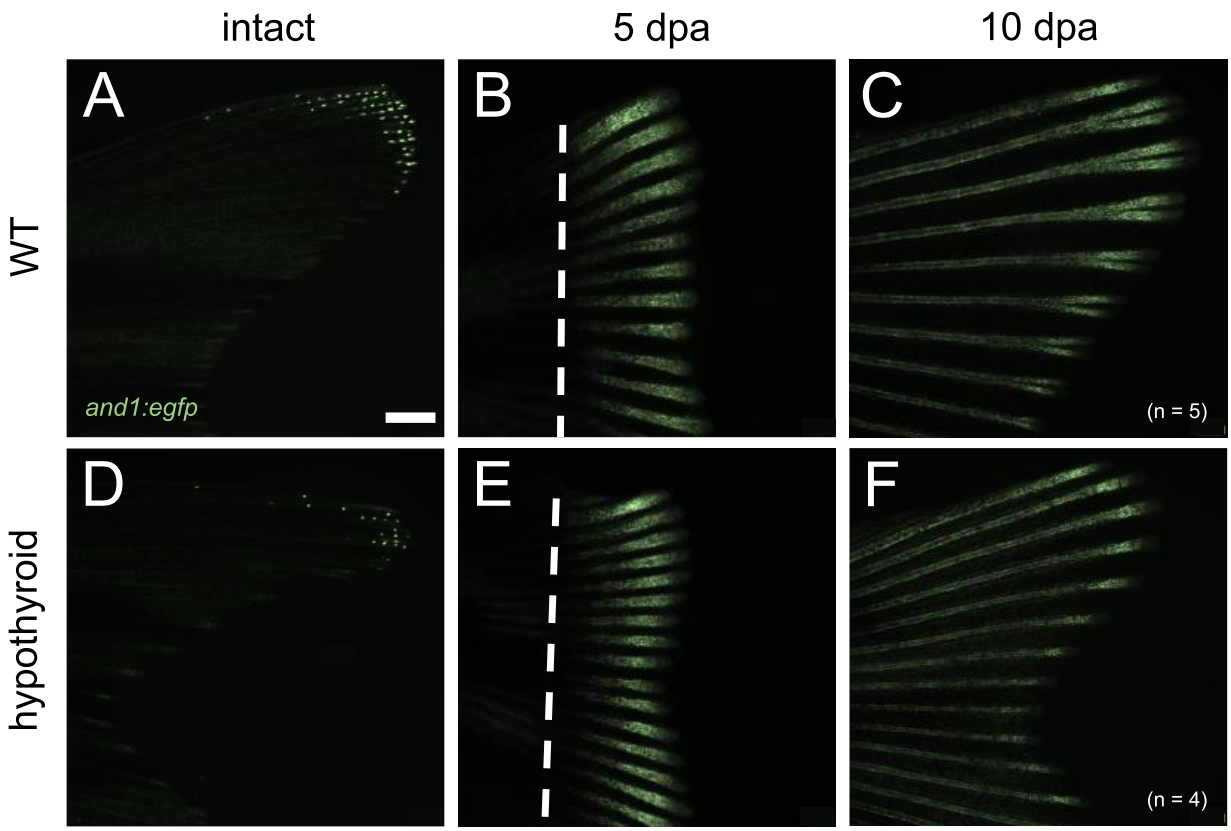

Supplementary Figure 4.9 Actinodin expression is not thyroid hormone dependent. *Tg(2Pand1:eGFP)* reports actinodin expression. Notch activity promotes the expression of actinodins, structural proteins necessary for bone formation, as reported in (Grotek et al., 2013). Intact caudal fin of a (A) WT or (D) hypothyroid fish. Regenerated fins at (B, E) 5 dpa and (C, F) 10 dpa. Dashed line, amputation plane. Scale bar, 400 μm.

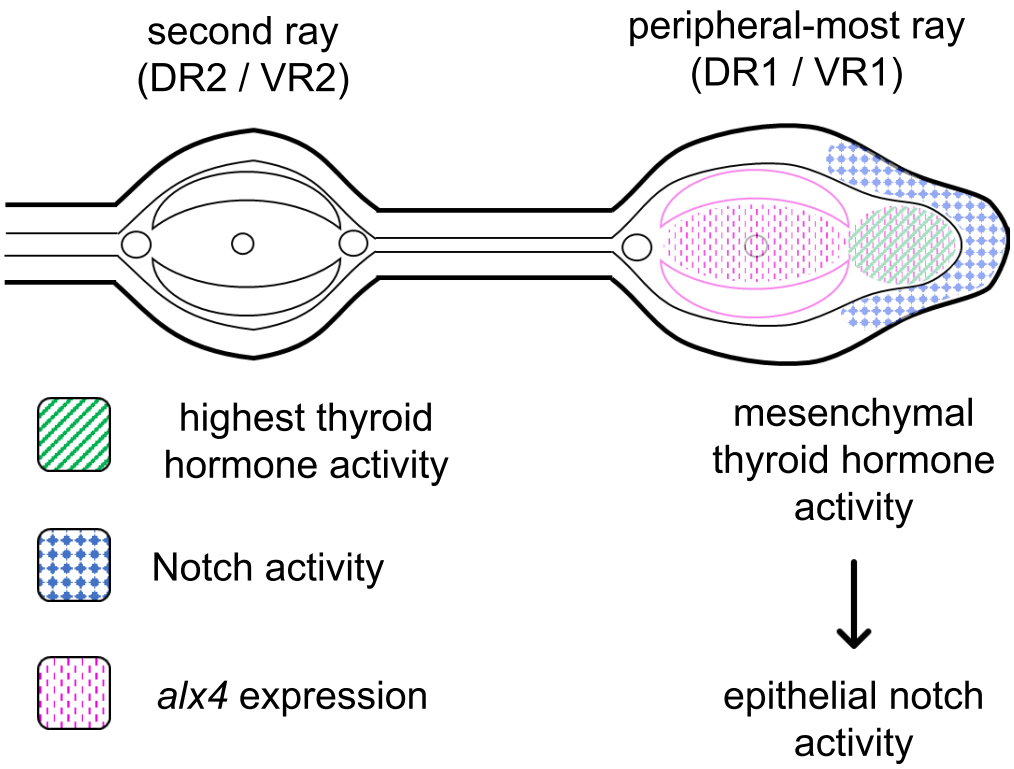

Supplementary Figure 4.10 Peripheral thyroid hormone activity stimulates Notch. Proposed model in which mesenchymal enrichment of TH activity stimulates Notch signaling in epithelial tissue in peripheral rays.

CHAPTER 5

Discussion: Thyroid hormone's direction of ray pattering

5.1 RESEARCH SUMMARY AND FUTURE DIRECTIONS

5.1.1 Research goals.

My three goals in this thesis were (1) To resolve TH's direction of proximodistal patterning along the fin ray axis during development and regeneration; (2) To disentangle the different aspects of positional memory that inform regenerative ray patterning; and (3) To characterize Notch-mediated TH signaling in peripheral rays.

5.1.2 Thyroid hormone regulates distal patterning of the appendicular skeleton.

Processes that regulate size and patterning along an axis must be highly integrated to generate robust shapes; relative changes in these processes underlie both congenital disease and evolutionary change. Fin length mutants in zebrafish have provided considerable insight into the pathways regulating fin size, with alterations in segment size (Perathoner et al., 2014) and number (Goldsmith et al., 2003) contributing to novel lengths, yet signals underlying patterning have remained less clear. The bony rays of the fins possess distinct patterning along the proximodistal axis, reflected in the location of ray bifurcations and the lengths of ray segments, which show progressive shortening along the axis (Christou et al., 2018).

In Chapter 2, we showed that TH regulates aspects of proximodistal patterning of the caudal fin rays, regardless of fin size. Not only does TH coordinate ray bifurcations and segment shortening with skeletal outgrowth along the proximodistal axis, but we also discovered it promotes distal gene expression patterns, suggesting a genuine role for the hormone in inducing distal identity. This distalizing role for TH is conserved between development and regeneration, in all fins (paired and medial), and between *Danio* species as well as distantly-related medaka. Further, we found TH acutely induces Shh-mediated skeletal bifurcation (Armstrong et al., 2017) during regenerative

outgrowth. Zebrafish have multiple nuclear TH receptors (Darras et al., 2011; Takayama et al., 2008), and we discovered that unliganded Thrab—but not Thraa or Thrb—inhibits the formation of distal features. Broadly, our results have demonstrated that proximodistal morphology is regulated independently from size-instructive signals. Modulating proximodistal patterning relative to size—either through changes to TH metabolism or other hormone-independent pathways—can shift skeletal patterning in ways that recapitulate aspects of fin ray diversity found in nature.

As bifurcations serve as one of the most discrete indicators of proximodistality, further work should elucidate how TH times this morphological event. Recent studies highlight osteoclast/osteoblast interplay as a physical regulator of bifurcation (Cardeira-Da-Silva et al., 2022), so the next step would be to investigate how TH interacts with the prevalence and/or activity of these two cell populations.

Previous caudal fin models include defined roles and activity domains for many developmental signaling pathways (Shh, RA, Notch, BMP, Wnt, ect; Wehner & Weidinger, 2015). With this work we introduced TH and comprehensibly defined its action, adding another signaling factor to the model of known actors. Indeed, we identified the driver of proximodistal-specific gene expression and showed TH regulates the location of bifurcations. Not only did we establish TH to be critical for zebrafish skeletal patterning, but our work in medaka and *D. albolineatus* suggests the TH's action is conserved across teleosts.

5.1.3 Regeneration speed is remembered autonomously by fin ray tissue.

Regenerating tissues must remember or interpret their spatial position, using this information to restore original size and patterning. The external skeleton of the zebrafish caudal fin is composed of 18 rays; after any portion of the fin is amputated, position-dependent regenerative growth restores each ray to its original length (Lee et al., 2005;

Uemoto et al., 2020). In Chapter 3, we tested for transcriptional differences during regeneration of proximal versus distal tissues and identified 489 genes that differed in proximodistal expression. TH directs multiple aspects of ray patterning along the proximodistal axis, and we identified 364 transcripts showing a proximodistal expression pattern that was dependent on thyroid hormone context.

Next, we disentangled which aspects of ray positional identity are directed by extrinsic cues versus remembered identity autonomous to the tissue itself with distal-to-proximal transplanted rays. Evaluating *scpp7*, a transcript with TH-regulated proximal enrichment, in regenerating distal-to-proximal transplants, we found neighboring proximal tissue showed robust expression while regenerating rays originating from transplanted distal tissue showed reduced (distal-like) expression during outgrowth. Despite this transcriptional remembrance, we discovered most aspects of fin ray morphology –bifurcation and segment length– were determined by the environment with only segment width showing a minor reduction in regenerated width.

However, these distal-to-proximal transplants regenerated far beyond the length of the graft itself, which indicated cues from the proximal environment can promote additional growth. Nonetheless, these transplants initially regenerated at a much slower rate compared to controls, which suggests retained memory of distal identity. We found this early growth retardation caused rays that originated from transplants to become noticeably shorter than their native neighboring rays. Lastly, we determined that regeneration speed and ray length are remembered autonomously by tissues, as it persisted across multiple rounds of amputation and regeneration.

Bioelectric mutants (Perathoner et al., 2014) and previous transplantation experiments (Shibata et al., 2018) implicate mesenchymal fibroblasts as sufficient to retain ray length positional identity. Distal-to-proximal transplants did not appear to retain memory of distal patterning features, only ray length information, so perhaps

mesenchymal osteoblasts are also responsible for carrying proximodistal ray length information.

Here our findings reinforce the model of progressive distalization established in Chapter 2: distal patterning features are not remembered but must be induced. Regardless, distal tissue retains distal-like transcription and initiates growth with a slower regeneration rate despite a proximal environment. Most excitingly, this suggests regeneration speed is not arbitrary, instead, it is highly regulated to determine ray morphology. Indeed, slowing proliferation slows ultimate ray length (Wang et al., 2019), so perhaps encoded regeneration speeds cause the extended/truncated regenerated ray lengths documented in other transplant experiments (Birnie, 1947; Murciano et al., 2002; Shibata et al., 2018).

5.1.4 Thyroid hormone dependent Notch activity is exclusive to peripheral rays.

Accurate readout of positional identity is required for proper tissue patterning during skeletal development and regeneration. The rays at the edge of the caudal fin, the peripheral rays, differ from the more central rays in several respects: the peripheral rays never form bifurcations and show differences in gene expression. In Chapter 4, we found TH activity–mediated by TH receptor Thrab–is enriched in peripheral ray tissue, reiterating the transcription pattern of *alx4*, which was previously identified as being highly expressed in peripheral rays (Desvignes et al., 2022; Nachtrab et al., 2013). Transplanting peripheral rays to central locations, we found TH activity, as well as other peripheral ray features, were restored upon amputation, even in a novel central environment. Further, by amputating and regenerating fins without peripheral rays, we discovered second-most peripheral rays do not acquire TH activity.

Next, we discovered epithelial Notch pathway activity corresponded with TH peripheral activity during development and regeneration. Indeed, TH activity, Notch

activity and *alx4* expression were all high in specific rays in all paired and medial fins of the zebrafish. In hypothyroid conditions, Notch activity was substantially reduced, and exogenous TH supplementation was sufficient to restore Notch signaling. This TH-dependence of Notch appeared exclusive to peripheral rays, as other domains of Notch activity are unaffected in a hypothyroid context. The signals that regulate and define the identity of the peripheral rays are still poorly defined, making this Notch-mediated TH activity a strong candidate for further investigation. The critical next step of this project would be to determine if *alx4* interacts with this novel peripheral activity, and if *alx4* alone is sufficient to imbue peripheral identity.

By discovering two new locally expressed actors in peripheral rays, we lay the groundwork for understanding how TH, Notch, and *alx4* form these unique structures. Additionally, our Notch findings show a possible explanation for how TH can differentially produce peripheral or central ray guidance cues. Further, we present evidence that peripheral ray identity is regulated differently than central rays. Peripheral rays have long been overlooked for their central counterparts, so this work highlights them as an exciting model for discovering novel mechanisms regulating caudal fin development and regeneration.

5.1.5 Summary.

In this dissertation, each chapter increasingly reveals TH's action upon the fin ray skeleton. Additionally, we have discovered many aspects of patterning and ray identity are independent upon this global endocrine factor. First, I established TH is necessary for the formation of distal features in fin rays, with exogenous TH sufficient to rescue developing and regenerating morphologies. Next, I discovered the majority of proximodistal fin ray patterning is not remembered autonomously, the regenerating fin environment overrides tissue identity to rebuild properly shaped bones. Lastly, I found an

additional, precise role for TH in regulating Notch activity that may define peripheral ray identity. Together these findings have expanded the field's knowledge of TH's action (Borisov & Shkil, 2024; Miyamoto et al., 2024; Qu et al., 2024; Roux et al., 2024; Zwahlen et al., 2024) and furthered work in regenerative patterning mechanisms (Ortega Granillo et al., 2024; VanWinkle, Lee, et al., 2024; VanWinkle, Wynn, et al., 2024).

5.1.6 Interpretation and speculation.

As HypoTH skeletal patterning was proximalized, I first evaluated the transcriptome along the proximodistal axis in both intact and regenerating tissues. Gene expression is position dependent along the axis, with TH necessary for maintaining this differential expression, so I confirmed TH was functioning via canonical signaling using dual receptor *thrab* loss-of-function mutants. As this mode of TH action drives gene expression through the epigenetic modification of chromatin, I assessed whether TH could impart lasting distal identity into tissue. I found that distal patterning is not remembered tissues: distal patterning features only form in the active presence of TH, and distal tissue regenerates proximal features when grafted to a proximal position. Additionally, I found bioelectric regulation of segment length is not TH-dependent, and, unlike sonic hedgehog inhibition, HypoTH conditions do not prevent bifurcation morphogenesis.

As the physical mechanisms that permit fin ray patterning morphogenesis appear independent of TH signaling, I believe TH acts as a global coordinator to regulate the time in which distal patterning is initiated. Distal tissue transplants build properly patterned rays along the proximodistal axis, reiterating this idea of TH action being a fin-wide coordinator that progressively distalizes tissue during outgrowth. Removing Thrab alleviates HypoTH phenotypes and induces proximalized fin rays in WT conditions, so TH is likely required for both the suppression of this default proximal gene programs and

the activation of a distalizing gene suite. Further, many distal-enriched genes are not upregulated in HypoTH distal tissues and HyperTH conditions induce only marginal precocious distalization. Therefore, I speculate that proximal morphologies may be encoded as the default patterning information in fin ray tissue.

Caudal fin tissue remains receptive to TH signaling, as distal features can be induced at any point during regeneration in a HypoTH context (peripheral-specific TH activity maintains receptivity as well). The transcriptome is progressively distalized along the proximodistal axis, with a myriad of genes showing TH-dependent proximodistal differential expression, and I have not found evidence of a single downstream distalizing agent. Likely, TH signaling stimulates a multitude of distalizing factors. Canonical TH signaling acts through chromatin acetylation, so I believe interrogating the chromatin landscape across the proximodistal axis and in different TH backgrounds will provide further resolution of TH-induced patterning.

REFERENCES

Akimenko, M. A., Johnson, S. L., Westerfield, M., & Ekker, M. (1995). Differential induction of four msx homeobox genes during fin development and regeneration in zebrafish. *Development*, *121*(2), 347–357.

Aman, A. J., Kim, M., Saunders, L. M., & Parichy, D. M. (2021). Thyroid hormone regulates abrupt skin morphogenesis during zebrafish postembryonic development. *Developmental Biology*, *477*, 205–218. https://doi.org/10.1016/J.YDBIO.2021.05.019

Armstrong, B. E., Henner, A., Stewart, S., & Stankunas, K. (2017). Shh promotes direct interactions between epidermal cells and osteoblast progenitors to shape regenerated zebrafish bone. *Development (Cambridge)*, *144*(7), 1165–1176. https://doi.org/10.1242/dev.143792

Autumn, M., Hu, Y., Zeng, J., & McMenamin, S. K. (2024). Growth patterns of caudal fin rays are informed by both external signals from the regenerating organ and remembered identity autonomous to the local tissue. *Developmental Biology*, *515*, 121–128. https://doi.org/10.1016/J.YDBIO.2024.07.008

Autumn, M., Zeng, J., Ranieri, I., & McMenamin, S. K. (2025). Experimentally manipulating the thyroid hormone axis in zebrafish. In *Methods Molecular Biology*. Springer Nature.

Azevedo, A. S., Grotek, B., Jacinto, A., Weidinger, G., & Saúde, L. (2011). The regenerative capacity of the zebrafish caudal fin is not affected by repeated amputations. *PLoS ONE*, *6*(7). https://doi.org/10.1371/journal.pone.0022820

Azevedo, A. S., Sousa, S., Jacinto, A., & Saúde, L. (2012). An amputation resets positional information to a proximal identity in the regenerating zebrafish caudal fin. *BMC Developmental Biology*, *12*, 24. https://doi.org/10.1186/1471-213X-12-24

Banu, S., Gaur, N., Nair, S., Ravikrishnan, T., Khan, S., Mani, S., Bharathi, S., Mandal, K., Kuram, N. A., Vuppaladadium, S., Ravi, R., Murthy, C. L. N., Quoseena, M., Babu, N. S., & Idris, M. M. (2022). Understanding the complexity of epimorphic regeneration in zebrafish caudal fin tissue: A transcriptomic and proteomic approach. *Genomics*, *114*(2), 110300. https://doi.org/10.1016/J.YGENO.2022.110300

Beck, C. W., Christen, B., & Slack, J. M. W. (2003). Molecular pathways needed for regeneration of spinal cord and muscle in a vertebrate. *Developmental Cell*, *5*(3), 429–439. https://doi.org/10.1016/S1534-5807(03)00233-8

Bergen, D. J. M., Tong, Q., Shukla, A., Newham, E., Zethof, J., Lundberg, M., Ryan, R., Youlten, S. E., Frysz, M., Croucher, P. I., Flik, G., Richardson, R. J., Kemp, J. P., Hammond, C. L., & Metz, J. R. (2022). Regenerating zebrafish scales express a subset of evolutionary conserved genes involved in human skeletal disease. *BMC Biology 2021 20:1*, *20*(1), 1–25. https://doi.org/10.1186/S12915-021-01209-8

Bertrand, S., Thisse, B., Tavares, R., Sachs, L., Chaumot, A., Bardet, P.-L., Escrivà, H., Duffraisse, M., Marchand, O., Safi, R., Thisse, C., & Laudet, V. (2007). Unexpected Novel Relational Links Uncovered by Extensive Developmental Profiling of Nuclear Receptor Expression. *PLoS Genetics*, *3*(11), e188. https://doi.org/10.1371/journal.pgen.0030188

Bhattacharya, S., Hyland, C., Falk, M. M., & Iovine, M. K. (2020). Connexin 43 gap junctional intercellular communication inhibits evx1 expression and joint formation in regenerating fins. *Development (Cambridge)*, *147*(13). https://doi.org/10.1242/DEV.190512/266936/AM/CONNEXIN43-GAP-JUNCTIONAL-INTERCELLULAR

Birnie, J. (1947). Regeneration and transplantation of fin rays in the goldfish. *The Anatomical Record*, 648.

Borday, V., Tharon, C., Avaron, F., Brulfert, A., Casane, D., Laurenti, P., & Graudie, J. (2001). evx1 Transcription in bony fin rays segment boundaries leads to a reiterated pattern during zebrafish fin development and regeneration. *Developmental Dynamics*, *220*(2), 91–98. https://doi.org/10.1002/1097-0177(2000)9999:9999<::AID-DVDY1091>3.0.CO;2-J

Borisov, V., & Shkil, F. (2024). Effects and phenotypic consequences of transient thyrotoxicosis and hypothyroidism at different stages of zebrafish Danio rerio (Teleostei; Cyprinidae) skeleton development. *The Anatomical Record*. https://doi.org/10.1002/AR.25592

Braunstein, J. A., Robbins, A. E., Stewart, S., & Stankunas, K. (2021). Basal epidermis collective migration and local Sonic hedgehog signaling promote skeletal branching morphogenesis in zebrafish fins. *Developmental Biology*, *477*, 177–190. https://doi.org/10.1016/j.ydbio.2021.04.010

Buchholz, D. R., Hsia, S.-C. V., Fu, L., & Shi, Y.-B. (2003). A Dominant-Negative Thyroid Hormone Receptor Blocks Amphibian Metamorphosis by Retaining Corepressors at Target Genes. *MOLECULAR AND CELLULAR BIOLOGY*, *23*(19), 6750–6758. https://doi.org/10.1128/MCB.23.19.6750-6758.2003

Campinho, M. A. (2019). Teleost metamorphosis: The role of thyroid hormone. *Frontiers in Endocrinology*, *10*(JUN), 448915. https://doi.org/10.3389/FENDO.2019.00383/BIBTEX

Cardeira-Da-Silva, J., Bensimon-Brito, A., Tarasco, M., Brandão, A. S., Rosa, J. T., Borbinha, J., Almeida, P. J., Jacinto, A., Cancela, M. L., Gavaia, P. J., Stainier, D. Y. R., & Laizé, V. (2022). Fin ray branching is defined by TRAP+ osteolytic tubules in zebrafish. *Proceedings of the National Academy of Sciences of the United States of America*, *119*(48), e2209231119. https://doi.org/10.1073/PNAS.2209231119/SUPPL_FILE/PNAS.2209231119.SM02.AVI

Chablais, F., & Jaźwińska, A. (2010). IGF signaling between blastema and wound epidermis is required for fin regeneration. *Development*, *137*(6), 871–879. https://doi.org/10.1242/dev.043885

Chopra, K., Ishibashi, S., & Amaya, E. (2019). Zebrafish duox mutations provide a model for human congenital hypothyroidism. *Biology Open*, *8*(2). https://doi.org/10.1242/bio.037655

Chowdhury, K., Lin, S., & Lai, S. L. (2022). Comparative Study in Zebrafish and Medaka Unravels the Mechanisms of Tissue Regeneration. *Frontiers in Ecology and Evolution*, *10*, 783818. https://doi.org/10.3389/FEVO.2022.783818/BIBTEX

Christou, M., Iliopoulou, M., Paul, |, Witten, E., & Koumoundouros, | George. (2018). *Segmentation pattern of zebrafish caudal fin is affected by developmental temperature and defined by multiple fusions between segments*. https://doi.org/10.1002/jez.b.22825

Curado, S., Stainier, D. Y. R., & Anderson, R. M. (2008). Nitroreductase-mediated cell/tissue ablation in zebrafish: A spatially and temporally controlled ablation method with applications in developmental and regeneration studies. *Nature Protocols*, *3*(6), 948–954. https://doi.org/10.1038/nprot.2008.58

Daane, J. M., Blum, N., Lanni, J., Boldt, H., Iovine, M. K., Higdon, C. W., Johnson, S. L., Lovejoy, N. R., & Harris, M. P. (2021). Modulation of bioelectric cues in the evolution of flying fishes. *Current Biology*, *31*(22), 5052-5061.e8. https://doi.org/10.1016/J.CUB.2021.08.054

Daane, J. M., Lanni, J., Rothenberg, I., Seebohm, G., Higdon, C. W., Johnson, S. L., & Harris, M. P. (2018). Bioelectric-calcineurin signaling module regulates allometric growth and size of the zebrafish fin. *Scientific Reports 2018 8:1*, *8*(1), 1–9. https://doi.org/10.1038/s41598-018-28450-6

Dagenais, P., Blanchoud, S., Pury, D., Pfefferli, C., Aegerter-Wilmsen, T., Aegerter, C. M., & Jazwinska, A. (2021). Hydrodynamic stress and phenotypic plasticity of the zebrafish regenerating fin. *Journal of Experimental Biology*, *224*(15). https://doi.org/10.1242/JEB.242309/269186/AM/HYDRODYNAMIC-STRESS-AND-PHENOTYPIC-PLASTICITY-OF

Darras, V. M., Van Herck, S. L. J., Heijlen, M., & De Groef, B. (2011). Thyroid Hormone Receptors in Two Model Species for Vertebrate Embryonic Development: Chicken and Zebrafish. *Research Journal of Thyroid Research*, *2011*. https://doi.org/10.4061/2011/402320

de Both, N. J. (1968). Transplantation of axolotl heads. *Science (New York, N.Y.)*, *162*(3852), 460–461. https://doi.org/10.1126/SCIENCE.162.3852.460

De Robertis, E. M. (2009). Spemann's organizer and the self-regulation of embryonic fields. *Mechanisms of Development*, *126*(11–12), 925. https://doi.org/10.1016/J.MOD.2009.08.004

Desvignes, T., Robbins, A. E., Carey, A. Z., Bailon-Zambrano, R., Nichols, J. T., Postlethwait, J. H., & Stankunas, K. (2022). Coordinated patterning of zebrafish caudal fin symmetry by a central and two peripheral organizers. *Developmental Dynamics*, *251*(8), 1306–1321. https://doi.org/10.1002/DVDY.475

Duncan Bassett, J. H., & Williams, G. R. (2016). Role of thyroid hormones in skeletal development and bone maintenance. In *Endocrine Reviews* (Vol. 37, Issue 2, pp. 135–187). Endocrine Society. https://doi.org/10.1210/er.2015-1106

Duran, I., Csukasi, F., Taylor, S. P., Krakow, D., Becerra, J., Bombarely, A., & Marí-Beffa, M. (2015). Collagen duplicate genes of bone and cartilage participate during regeneration of zebrafish fin skeleton. *Gene Expression Patterns*, *19*(1–2), 60–69. https://doi.org/10.1016/j.gep.2015.07.004

Durán, I., Marí-Beffa, M., Santamaría, J. A., Becerra, J., & Santos-Ruiz, L. (2011). Actinotrichia collagens and their role in fin formation. *Developmental Biology*, *354*(1), 160–172. https://doi.org/10.1016/j.ydbio.2011.03.014

Echeverri, K., & Tanaka, E. M. (2005). Proximodistal patterning during limb regeneration. *Developmental Biology*, *279*(2), 391–401. https://doi.org/10.1016/J.YDBIO.2004.12.029

Ferretti, P., & Géraudie, J. (1995). Retinoic acid-induced cell death in the wound epidermis of regenerating zebrafish fins. *Developmental Dynamics*, *202*(3), 271–283. https://doi.org/10.1002/aja.1002020306

Furutani-Seiki, M., & Wittbrodt, J. (2004). Medaka and zebrafish, an evolutionary twin study. *Mechanisms of Development*, *121*(7–8), 629–637. https://doi.org/10.1016/j.mod.2004.05.010

Ghaddar, B., & Diotel, N. (2022). Zebrafish: A New Promise to Study the Impact of Metabolic Disorders on the Brain. *International Journal of Molecular Sciences 2022, Vol. 23, Page 5372*, *23*(10), 5372. https://doi.org/10.3390/IJMS23105372

Gicquel, C., & Le Bouc, Y. (2006). Hormonal regulation of fetal growth. *Hormone Research*, *65 Suppl 3*(SUPPL. 3), 28–33. https://doi.org/10.1159/000091503

Goldman, J. A., & Poss, K. D. (2020). Gene regulatory programmes of tissue regeneration. *Nature Reviews Genetics*, *21*. https://doi.org/10.1038/s41576-020-0239-7

Goldsmith, M. I., Fisher, S., Waterman, R., & Johnson, S. L. (2003). Saltatory control of isometric growth in the zebrafish caudal fin is disrupted in long fin and rapunzel mutants. *Developmental Biology*, *259*(2), 303–317. https://doi.org/10.1016/S0012-1606(03)00186-6

Gomez, C., & Pourquie, O. (2009). Developmental control of segment numbers in vertebrates. *Journal of Experimental Zoology Part B: Molecular and Developmental Evolution*, *312B*(6), 533–544. https://doi.org/10.1002/JEZ.B.21305

Grotek, B., Wehner, D., & Weidinger, G. (2013). Notch signaling coordinates cellular proliferation with differentiation during zebrafish fin regeneration. *Development*, *140*(7), 1412–1423. https://doi.org/10.1242/DEV.087452

Hamada, H., Watanabe, M., Lau, H. E., Nishida, T., Hasegawa, T., Parichy, D. M., & Kondo, S. (2014). Involvement of Delta/Notch signaling in zebrafish adult pigment stripe patterning. *Development*, *141*(2), 318–324. https://doi.org/10.1242/DEV.099804

Harper, M., Hu, Y., Donahue, J., Acosta, B., Braes, F. D., Nguyen, S., Zeng, J., Barbaro, J., Lee, H., Bui, H., & Mcmenamin, S. K. (2023). Thyroid hormone regulates proximodistal patterning in fin rays. *Proceedings of the National Academy of Sciences*, *120*(21), e2219770120. https://doi.org/10.1073/PNAS.2219770120

Harris, M. P. (2021). Bioelectric signaling as a unique regulator of development and regeneration. *Development (Cambridge)*, *148*(10). https://doi.org/10.1242/DEV.180794/264925

Harris, M. P., Daane, J. M., & Lanni, J. (2021). Through veiled mirrors: Fish fins giving insight into size regulation. *Wiley Interdisciplinary Reviews: Developmental Biology*, *10*(4). https://doi.org/10.1002/WDEV.381

Hasebe, T., Fujimoto, K., Kajita, M., Fu, L., Shi, Y. B., & Ishizuya-Oka, A. (2017). Thyroid Hormone-Induced Activation of Notch Signaling is Required for Adult Intestinal Stem Cell Development During Xenopus Laevis Metamorphosis. *Stem Cells (Dayton, Ohio)*, *35*(4), 1028. https://doi.org/10.1002/STEM.2544

Heijlen, M., Houbrechts, A. M., Bagci, E., Van Herck, S. L. J., Kersseboom, S., Esguerra, C. V., Blust, R., Visser, T. J., Knapen, D., & Darras, V. M. (2014). Knockdown of Type 3 Iodothyronine Deiodinase Severely Perturbs Both Embryonic and Early Larval Development in Zebrafish. *Endocrinology*, *155*(4), 1547–1559. https://doi.org/10.1210/EN.2013-1660

Hörlein, A. J., Näär, A. M., Heinzel, T., Torchia, J., Gloss, B., Kurokawa, R., Ryan, A., Kamei, Y., Söderström, M., Glass, C. K., & Rosenfeld, M. G. (1995). Ligand-independent repression by the thyroid hormone receptor mediated by a nuclear receptor co-repressor. *Nature 1995 377:6548*, *377*(6548), 397–404. https://doi.org/10.1038/377397a0

Houbrechts, A. M., Delarue, J., Gabriëls, I. J., Sourbron, J., & Darras, V. M. (2016). Permanent Deiodinase Type 2 Deficiency Strongly Perturbs Zebrafish Development, Growth, and Fertility. *Endocrinology*, *157*(9), 3668–3681. https://doi.org/10.1210/EN.2016-1077

Hu, Y., Mauri, A., Donahue, J., Singh, R., Acosta, B., & McMenamin, S. (2019). Thyroid hormone coordinates developmental trajectories but does not underlie developmental truncation in danionins. *Developmental Dynamics*, *248*(11), 1144–1154. https://doi.org/10.1002/DVDY.76

Huang, P., Xiong, F., Megason, S. G., & Schier, A. F. (2012). Attenuation of Notch and hedgehog signaling is required for fate specification in the spinal cord. *PLoS Genetics*, *8*(6). https://doi.org/10.1371/journal.pgen.1002762

Iovine, M. K., Higgins, E. P., Hindes, A., Coblitz, B., & Johnson, S. L. (2005). Mutations in connexin43 (GJA1) perturb bone growth in zebrafish fins. *Developmental Biology*, *278*(1), 208–219. https://doi.org/10.1016/j.ydbio.2004.11.005

Iovine, M. K., & Johnson, S. L. (2000). Genetic Analysis of Isometric Growth Control Mechanisms in the Zebrafish Caudal Fin. *Genetics*, *155*(3).

Kallman, K. D., & Gordon, M. (1957). Transplantation of find in Xiphophorin fishes. *Annals of the New York Academy of Sciences*, *71*(3), 307–318. https://doi.org/10.1111/j.1749-6632.1957.tb54603.x

Kawasaki, K. (2009). The SCPP gene repertoire in bony vertebrates and graded differences in mineralized tissues. *Development Genes and Evolution*, *219*(3), 147. https://doi.org/10.1007/S00427-009-0276-X

Keer, S., Cohen, K., May, C., Hu, Y., McMenamin, S., & Hernandez, L. P. (2019). Anatomical Assessment of the Adult Skeleton of Zebrafish Reared Under Different Thyroid Hormone Profiles. *Anatomical Record*, *302*(10), 1754–1769. https://doi.org/10.1002/ar.24139

Kinutani, M., Coltey, M., & Le Douarin, N. M. (1986). Postnatal development of a demyelinating disease in avian spinal cord chimeras. *Cell*, *45*(2), 307–314. https://doi.org/10.1016/0092-8674(86)90395-8

Kinutani, M., & Le Douarin, N. M. (1985). Avian spinal cord chimeras: I. Hatching ability and posthatching survival in homo- and heterospecific chimerase. *Developmental Biology*, *111*(1), 243–255. https://doi.org/10.1016/0012-1606(85)90449-X

Knopf, F., Hammond, C., Chekuru, A., Kurth, T., Hans, S., Weber, C. W., Mahatma, G., Fisher, S., Brand, M., Schulte-Merker, S., & Weidinger, G. (2011). Bone regenerates via dedifferentiation of osteoblasts in the zebrafish fin. *Developmental Cell*, *20*(5), 713–724. https://doi.org/10.1016/j.devcel.2011.04.014

Kong, J. H., Yang, L., Dessaud, E., Chuang, K., Moore, D. M., Rohatgi, R., Briscoe, J., & Novitch, B. G. (2015). Notch Activity Modulates the Responsiveness of Neural Progenitors to Sonic Hedgehog Signaling. *Developmental Cell*, *33*(4), 373. https://doi.org/10.1016/J.DEVCEL.2015.03.005

König, D., Page, L., Chassot, B., & Jaźwińska, A. (2018). Dynamics of actinotrichia regeneration in the adult zebrafish fin. *Developmental Biology*, *433*(2), 416–432. https://doi.org/10.1016/j.ydbio.2017.07.024

Kopan, R., & Ilagan, M. X. G. (2009). The Canonical Notch Signaling Pathway: Unfolding the Activation Mechanism. *Cell*, *137*(2), 216. https://doi.org/10.1016/J.CELL.2009.03.045

Lalonde, R. L., & Akimenko, M.-A. (2018). Effects of fin fold mesenchyme ablation on fin development in zebrafish. *PLOS ONE*, *13*(2), e0192500. https://doi.org/10.1371/journal.pone.0192500

Lalonde, R. L., Moses, D., Zhang, J., Cornell, N., Ekker, M., & Akimenko, M. A. (2016). Differential actinodin1 regulation in zebrafish and mouse appendages. *Developmental Biology*, *417*(1), 91–103. https://doi.org/10.1016/j.ydbio.2016.05.019

Lanni, J. S., Peal, D., Ekstrom, L., Chen, H., Stanclift, C., Bowen, M. E., Mercado, A., Gamba, G., Kahle, K. T., Harris, M. P., & Zubir, S. (2019). *Integrated Kþ channel and KþCl-cotransporter functions are required for the coordination of size and proportion during development*. https://doi.org/10.1016/j.ydbio.2019.08.016

Laudet, V. (2011). The Origins and Evolution of Vertebrate Metamorphosis. *Current Biology*, *21*(18), R726–R737. https://doi.org/10.1016/J.CUB.2011.07.030

Lee, Y., Grill, S., Sanchez, A., Murphy-Ryan, M., & Poss, K. D. (2005). Fgf signaling instructs position-dependent growth rate during zebrafish fin regeneration. *Development*, *132*(23), 5173–5183. https://doi.org/10.1242/DEV.02101

Lee, Y., Kim, D., & Lee, C.-J. (2020). Suppressive effects of valproic acid on caudal fin regeneration in adult zebrafish. *Animal Cells and Systems*, *24*(6), 349–358. https://doi.org/10.1080/19768354.2020.1860126

Lewis, V. M., Saunders, L. M., Larson, T. A., Bain, E. J., Sturiale, S. L., Gur, D., Chowdhury, S., Flynn, J. D., Allen, M. C., Deheyn, D. D., Lee, J. C., Simon, J. A., Lippincott-Schwartz, J., Raible, D. W., & Parichy, D. M. (2019). Fate plasticity and reprogramming in genetically distinct populations of Danio leucophores. *Proceedings of the National Academy of Sciences of the United States of America*, *116*(24), 11806–11811. https://doi.org/10.1073/PNAS.1901021116/SUPPL_FILE/PNAS.1901021116.SD02.XLS

Li, J., Sultan, Y., Sun, Y., Zhang, S., Liu, Y., & Li, X. (2021). Expression analysis of Hsp90α and cytokines in zebrafish caudal fin regeneration. *Developmental & Comparative Immunology*, *116*, 103922. https://doi.org/10.1016/J.DCI.2020.103922

Li, Q., Sachs, L., Shi, Y. B., & Wolffe, A. P. (1999). Modification of chromatin structure by the thyroid hormone receptor. In *Trends in Endocrinology and Metabolism* (Vol. 10, Issue 4, pp. 157–164). Elsevier Current Trends. https://doi.org/10.1016/S1043-2760(98)00141-6

Löhr, H., & Hammerschmidt, M. (2011). Zebrafish in endocrine systems: recent advances and implications for human disease. *Annual Review of Physiology*, *73*, 183–211. https://doi.org/10.1146/ANNUREV-PHYSIOL-012110-142320

Londono, R., Sun, A. X., Tuan, R. S., & Lozito, T. P. (2018). Tissue repair and epimorphic regeneration: an overviews. *Curr Pathobiol Rep*, *6*(1), 61–69. https://doi.org/10.1007/s40139-018-0161-2

Marí-Beffa, M., & Murciano, C. (2010). Dermoskeleton morphogenesis in zebrafish fins. *Developmental Dynamics*, *239*(11), 2779–2794. https://doi.org/10.1002/DVDY.22444

Mashanov, V., Akiona, J., Khoury, M., Ferrier, J., Reid, R., Machado, D. J., Zueva, O., & Janies, D. (2020). Active Notch signaling is required for arm regeneration in a brittle star. *PLOS ONE*, *15*(5), e0232981. https://doi.org/10.1371/JOURNAL.PONE.0232981

Mateus, R., Fuhrmann, J. F., & Dye, N. A. (2021). Growth across scales: Dynamic signaling impacts tissue size and shape. *Current Opinion in Cell Biology*, *73*, 50–57. https://doi.org/10.1016/J.CEB.2021.05.002

Matsuda, H. (2018). Zebrafish as a model for studying functional pancreatic β cells development and regeneration. *Development, Growth & Differentiation*, *60*(6), 393–399. https://doi.org/10.1111/dgd.12565

Matsuda, H., Mullapudi, S. T., Zhang, Y., Hesselson, D., & Stainier, D. Y. R. (2017). Thyroid Hormone Coordinates Pancreatic Islet Maturation During the Zebrafish Larval-to-Juvenile Transition to Maintain Glucose Homeostasis. *Diabetes*, *66*(10), 2623–2635. https://doi.org/10.2337/DB16-1476

Mccluskey, B. M., Postlethwait, J. H., & Yeager, M. (n.d.). *Phylogeny of Zebrafish, a "Model Species," within Danio, a "Model Genus."* https://doi.org/10.1093/molbev/msu325

McMenamin, S. K., Bain, E. J., McCann, A. E., Patterson, L. B., Eom, D. S., Waller, Z. P., Hamill, J. C., Kuhlman, J. A., Eisen, J. S., & Parichy, D. M. (2014). Thyroid hormone-dependent adult pigment cell lineage and pattern in zebrafish. *Science*, *345*(6202), 1358–1361. https://doi.org/10.1126/science.1256251

McMenamin, S. K., Carter, C., & Cooper, W. J. (2017). Thyroid Hormone Stimulates the Onset of Adult Feeding Kinematics in Zebrafish. *Zebrafish*, *14*(6), 517. https://doi.org/10.1089/ZEB.2017.1453

McMenamin, S. K., Minchin, J. E. N., Gordon, T. N., Rawls, J. F., & Parichy, D. M. (2013). Dwarfism and Increased Adiposity in the gh1 Mutant Zebrafish vizzini. *Endocrinology*, *154*(4), 1476. https://doi.org/10.1210/EN.2012-1734

McMenamin, S. K., & Parichy, D. M. (2013). *Metamorphosis in Teleosts*. https://doi.org/10.1016/B978-0-12-385979-2.00005-8

McMenamin, S., Shkil, F., & Koyama, T. (2022). Editorial: Hormones and Life History Strategies. *Frontiers in Ecology and Evolution*, *10*, 838555. https://doi.org/10.3389/FEVO.2022.838555/BIBTEX

Michaud, J., Simpson, K. M., Escher, R., Buchet-Poyau, K., Beissbarth, T., Carmichael, C., Ritchie, M. E., Schütz, F., Cannon, P., Liu, M., Shen, X., Ito, Y., Raskind, W. H., Horwitz, M. S., Osato, M., Turner, D. R., Speed, T. P., Kavallaris, M., Smyth, G. K., & Scott, H. S. (2008). *Integrative analysis of RUNX1 downstream pathways and target genes*. https://doi.org/10.1186/1471-2164-9-363

Miyamoto, K., Abe, G., & Tamura, K. (2024). The dwarf neon rainbowfish Melanotaenia praecox, a small spiny-rayed fish with potential as a new Acanthomorpha model fish: I. Fin ray ontogeny and postembryonic staging. *Developmental Dynamics*, *253*(9), 829–845. https://doi.org/10.1002/DVDY.699

Morte, B., Gil-Ibáñez, P., & Bernal, J. (2018). Regulation of Gene Expression by Thyroid Hormone in Primary Astrocytes: Factors Influencing the Genomic Response. *Endocrinology*, *159*(5), 2083–2092. https://doi.org/10.1210/EN.2017-03084

Mullur, R., Liu, Y. Y., & Brent, G. A. (2014). Thyroid hormone regulation of metabolism. *Physiological Reviews*, *94*(2), 355–382. https://doi.org/10.1152/PHYSREV.00030.2013/ASSET/IMAGES/LARGE/Z9J002142686 0003.JPEG

Münch, J., González-Rajal, A., & de la Pompa, J. L. (2013). Notch regulates blastema proliferation and prevents differentiation during adult zebrafish fin regeneration. *Development (Cambridge)*, *140*(7), 1402–1411. https://doi.org/10.1242/dev.087346

Murciano, C., Fernández, T. D., Durán, I., Maseda, D., Ruiz-Sánchez, J., Becerra, J., Akimenko, M. A., & Marí-Beffa, M. (2002). Ray–Interray Interactions during Fin Regeneration of Danio rerio. *Developmental Biology*, *252*(2), 214–224. https://doi.org/10.1006/DBIO.2002.0848

Murciano, C., Pérez-Claros, J., Smith, A., Avaron, F., Fernández, T. D., Durán, I., Ruiz-Sánchez, J., García, F., Becerra, J., Akimenko, M. A., & Marí-Beffa, M. (2007). Position dependence of hemiray morphogenesis during tail fin regeneration in Danio rerio. *Developmental Biology*, *312*(1), 272–283. https://doi.org/10.1016/j.ydbio.2007.09.026

Muzzio, A. M., Noyes, P. D., Stapleton, H. M., & Lema, S. C. (2014). Tissue distribution and thyroid hormone effects on mRNA abundance for membrane transporters Mct8, Mct10, and organic anion-transporting polypeptides (Oatps) in a teleost fish. *Comparative*

Biochemistry and Physiology Part A: Molecular & Integrative Physiology, *167*, 77–89. https://doi.org/10.1016/J.CBPA.2013.09.019

Nabrit, S. M. (1929). The Rôle of the Fin Rays in the Regeneration in the Tail-Fins of Fishes. (In Fundulus and Goldfish). In *Bulletin* (Vol. 56, Issue 4). https://about.jstor.org/terms

Nachtrab, G., Kikuchi, K., Tornini, V. A., & Poss, K. D. (2013). Transcriptional components of anteroposterior positional information during zebrafish fin regeneration. *Development*, *140*(18), 3754–3764. https://doi.org/10.1242/DEV.098798

Nakagawa, H., Kuroda, J., Aramaki, T., & Kondo, S. (2022). Mechanical role of actinotrichia in shaping the caudal fin of zebrafish. *Developmental Biology*, *481*, 52–63. https://doi.org/10.1016/J.YDBIO.2021.09.003

Nauroy, P., Guiraud, A., Chlasta, J., Malbouyres, M., Gillet, B., Hughes, S., Lambert, E., & Ruggiero, F. (2019). Gene profile of zebrafish fin regeneration offers clues to kinetics, organization and biomechanics of basement membrane. *Matrix Biology*, *75–76*, 82–101. https://doi.org/10.1016/J.MATBIO.2018.07.005

Nechiporek, A., & Keating, M. T. (2002). A proliferation gradient between proximal and msxb-expressing distal blastema directs zebrafish fin regeneration | Development. *Development*, 2607–2617. https://dev.biologists.org/content/129/11/2607

Neumann, C. J., & Nuesslein-Volhard, C. (2000). Patterning of the zebrafish retina by a wave of sonic Hedgehog activity. *Science*, *289*(5487), 2137–2139. https://doi.org/10.1126/science.289.5487.2137

Olsen, A. M., & Westneat, M. W. (2015). StereoMorph: an R package for the collection of 3D landmarks and curves using a stereo camera set-up. *Methods in Ecology and Evolution*, *6*(3), 351–356. https://doi.org/10.1111/2041-210X.12326

Orozco, A., & Valverde-R, C. (2005). Thyroid Hormone Deiodination in Fish. *Https://Home.Liebertpub.Com/Thy*, *15*(8), 799–813. https://doi.org/10.1089/THY.2005.15.799

Ortega Granillo, A., Zamora, D., Schnittker, R. R., Scott, A. R., Spluga, A., Russell, J., Brewster, C. E., Ross, E. J., Acheampong, D. A., Zhang, N., Ferro, K., Morrison, J. A., Rubinstein, B. Y., Perera, A. G., Wang, W., & Sánchez Alvarado, A. (2024). Positional information modulates transient regeneration-activated cell states during vertebrate appendage regeneration. *IScience*, *27*(9), 110737. https://doi.org/10.1016/J.ISCI.2024.110737

Parichy, D. M., Elizondo, M. R., Mills, M. G., Gordon, T. N., & Engeszer, R. E. (2009). Normal table of postembryonic zebrafish development: Staging by externally visible anatomy of the living fish. *Developmental Dynamics*, *238*(12), 2975–3015. https://doi.org/10.1002/DVDY.22113

Parsons, M. J., Pisharath, H., Yusuff, S., Moore, J. C., Siekmann, A. F., Lawson, N., & Leach, S. D. (2009). Notch-responsive cells initiate the secondary transition in larval zebrafish pancreas. *Mechanisms of Development*, *126*(10), 898–912. https://doi.org/10.1016/j.mod.2009.07.002

Perathoner, S., Daane, J. M., Henrion, U., Seebohm, G., & Higdon, C. W. (2014). Bioelectric Signaling Regulates Size in Zebrafish Fins. *PLoS Genet*, *10*(1), 1004080. https://doi.org/10.1371/journal.pgen.1004080

Porazzi, P., Calebiro, D., Benato, F., Tiso, N., & Persani, L. (2009). Thyroid gland development and function in the zebrafish model. *Molecular and Cellular Endocrinology*, *312*(1–2), 14–23. https://doi.org/10.1016/J.MCE.2009.05.011

Qu, J., Fang, Y., Tao, R., Zhao, J., Xu, T., Chen, R., Zhang, J., Meng, K., Yang, Q., Zhang, K., Yan, X., Sun, D., & Chen, X. (2024). Advancing thyroid disease research: The role and potential of zebrafish model. *Life Sciences*, *357*, 123099. https://doi.org/10.1016/J.LFS.2024.123099

Rabinowitz, J. S., Robitaille, A. M., Wang, Y., Ray, C. A., Thummel, R., Gu, H., Djukovic, D., Raftery, D., Berndt, J. D., & Moon, R. T. (2017). Transcriptomic, proteomic, and metabolomic landscape of positional memory in the caudal fin of zebrafish. *Proceedings of the National Academy of Sciences of the United States of America*, *114*(5), E717–E726. https://doi.org/10.1073/pnas.1620755114

Robinson, M. D., McCarthy, D. J., & Smyth, G. K. (2010). edgeR: a Bioconductor package for differential expression analysis of digital gene expression data. *Bioinformatics*, *26*(1), 139. https://doi.org/10.1093/BIOINFORMATICS/BTP616

Rojo-Laguna, J. I., Garcia-Cabot, S., & Saló, E. (2019). Tissue transplantation in planarians: A useful tool for molecular analysis of pattern formation. *Seminars in Cell & Developmental Biology*, *87*, 116–124. https://doi.org/10.1016/J.SEMCDB.2018.05.022

Rolland-Lagan, A. G., Paquette, M., Tweedle, V., & Akimenko, M. A. (2012). Morphogen-based simulation model of ray growth and joint patterning during fin development and regeneration. *Development*, *139*(6), 1188–1197. https://doi.org/10.1242/DEV.073452

Roux, N., Vianello, S., & Laudet, V. (2024). Physiology of metamorphosis. *Encyclopedia of Fish Physiology*, 229–244. https://doi.org/10.1016/B978-0-323-90801-6.00134-8

Salis, P., Roux, N., Huang, D., Marcionetti, A., Mouginot, P., Reynaud, M., Salles, O., Salamin, N., Pujol, B., Parichy, D. M., Planes, S., & Laudet, V. (2021). Thyroid hormones regulate the formation and environmental plasticity of white bars in clownfishes. *Proceedings of the National Academy of Sciences of the United States of America*, *118*(23), e2101634118. https://doi.org/10.1073/PNAS.2101634118/SUPPL_FILE/PNAS.2101634118.SAPP.PDF

Saunders, L. M., Mishra, A. K., Aman, A. J., Lewis, V. M., Toomey, M. B., Packer, J. S., Qiu, X., McFaline-Figueroa, J. L., Corbo, J. C., Trapnell, C., & Parichy, D. M. (2019). Thyroid hormone regulates distinct paths to maturation in pigment cell lineages. *ELife*, *8*. https://doi.org/10.7554/ELIFE.45181

Schulte, C. J., Allen, C., England, S. J., Juárez-Morales, J. L., & Lewis, K. E. (2011). Evx1 is required for joint formation in zebrafish fin dermoskeleton. *Developmental Dynamics*, *240*(5), 1240–1248. https://doi.org/10.1002/DVDY.22534

Sehring, I. M., & Weidinger, G. (2020). Recent advancements in understanding fin regeneration in zebrafish. *WIREs Developmental Biology*, *9*(1). https://doi.org/10.1002/wdev.367

Sehring, I., Mohammadi, H. F., Haffner-Luntzer, M., Ignatius, A., Huber-Lang, M., & Weidinger, G. (2022). Zebrafish fin regeneration involve generic and regeneration-specific osteoblast injury responses. *ELife*, *11*. https://doi.org/10.7554/ELIFE.77614

Shibata, E., Liu, Z., Kawasaki, T., Sakai, N., & Kawakami, A. (2018). Robust and local positional information within a fin ray directs fin length during zebrafish regeneration. *Development Growth and Differentiation*, *60*(6), 354–364. https://doi.org/10.1111/dgd.12558

Silic, M. R., Wu, Q., Kim, B. H., Golling, G., Chen, K. H., Freitas, R., Chubykin, A. A., Mittal, S. K., & Zhang, G. J. (2020). Potassium Channel-Associated Bioelectricity of the Dermomyotome Determines Fin Patterning in Zebrafish. *Genetics*, *215*(4), 1067–1084. https://doi.org/10.1534/GENETICS.120.303390

Silva, N., Louro, B., Trindade, M., Power, D. M., & Campinho, M. A. (2017). Transcriptomics reveal an integrative role for maternal thyroid hormones during zebrafish embryogenesis. *Scientific Reports 2017 7:1*, *7*(1), 1–11. https://doi.org/10.1038/s41598-017-16951-9

Sims, K., Eble, D. M., & Iovine, M. K. (2009). Connexin43 regulates joint location in zebrafish fins. *Developmental Biology*, *327*(2), 410–418. https://doi.org/10.1016/J.YDBIO.2008.12.027

Sinha, R., & Yen, P. M. (2000). Cellular Action of Thyroid Hormone. In *Endotext*. MDText.com, Inc. http://www.ncbi.nlm.nih.gov/pubmed/25905423

Sirakov, M., Boussouar, A. A., Kress, E., Frau, C., Lone, I. N., Nadjar, J., Angelov, D., & Plateroti, M. (2015). The thyroid hormone nuclear receptor TRα1 controls the Notch signaling pathway and cell fate in murine intestine. *Development (Cambridge)*, *142*(16), 2764–2774. https://doi.org/10.1242/DEV.121962/VIDEO-3

Smith, A., Zhang, J., Guay, D., Quint, E., Johnson, A., & Akimenko, M. A. (2008). Gene expression analysis on sections of zebrafish regenerating fins reveals limitations in the whole-mount in situ hybridization method. *Developmental Dynamics*, *237*(2), 417–425. https://doi.org/10.1002/DVDY.21417

Solini, G. E., Dong, C., & Saha, M. (2017). Embryonic transplantation experiments: Past, present, and future. *Trends in Developmental Biology*, *10*, 13–30.

Stewart, S., Le Bleu, H. K., Yette, G. A., Henner, A. L., Robbins, A. E., Braunstein, J. A., & Stankunas, K. (2021). longfin causes cis-ectopic expression of the kcnh2a ether-a-go-go K+ channel to autonomously prolong fin outgrowth. *Development (Cambridge)*, *148*(11). https://doi.org/10.1242/DEV.199384/260597/AM/LONGFIN-CAUSES-CIS-ECTOPIC-EXPRESSION-OF-THE

Stewart, T. A., Lemberg, J. B., Taft, N. K., Yoo, I., Daeschler, E. B., & Shubin, N. H. (2020). Fin ray patterns at the fin-to-limb transition. *Proceedings of the National Academy of*

Sciences of the United States of America, *117*(3), 1612–1620. https://doi.org/10.1073/PNAS.1915983117/SUPPL_FILE/PNAS.1915983117.SM03.MP4

Stocum, D. L. (1984). The urodele limb regeneration blastema: Determination and organization of the morphogenetic field. *Differentiation*, *27*(1–3), 13–28. https://doi.org/10.1111/J.1432-0436.1984.TB01403.X

Takayama, S., Hostick, U., Haendel, M., Eisen, J., & Darimont, B. (2008). An F-domain introduced by alternative splicing regulates activity of the zebrafish thyroid hormone receptor α. *General and Comparative Endocrinology*, *155*(1), 176–189. https://doi.org/10.1016/j.ygcen.2007.04.012

Tanaka, M. (2018). Alterations in anterior–posterior patterning and its accompanying changes along the proximal-distal axis during the fin-to-limb transition. *Genesis*, *56*(1), e23053. https://doi.org/10.1002/DVG.23053

Thisse, C., Degrave, A., Kryukov, G. V. G. V., Gladyshev, V. N., Obrecht-Pflumio, S., Krol, A., Thisse, B., & Lescure, A. (2003). Spatial and temporal expression patterns of selenoprotein genes during embryogenesis in zebrafish. *Gene Expression Patterns*, *3*(4), 525–532. https://doi.org/10.1016/S1567-133X(03)00054-1

Thisse, C., & Thisse, B. (2007). *High-resolution in situ hybridization to whole-mount zebrafish embryos*. https://doi.org/10.1038/nprot.2007.514

Thorimbert, V., König, D., Marro, J., Ruggiero, F., & Jazwinska, A. (2015). Bone morphogenetic protein signaling promotes morphogenesis of blood vessels, wound epidermis, and actinotrichia during fin regeneration in zebrafish. *The FASEB Journal*, *29*(10), 4299–4312. https://doi.org/10.1096/fj.15-272955

Tornini, V. A., Puliafito, A., Slota, L. A., Thompson, J. D., Nachtrab, G., Kaushik, A. L., Kapsimali, M., Primo, L., Di Talia, S., & Poss, K. D. (2016). Live Monitoring of Blastemal Cell Contributions during Appendage Regeneration. *Current Biology*, *26*(22), 2981–2991. https://doi.org/10.1016/j.cub.2016.08.072

Tu, S., & Johnson, S. L. (2011). Fate restriction in the growing and regenerating zebrafish fin. *Developmental Cell*, *20*(5), 725–732. https://doi.org/10.1016/j.devcel.2011.04.013

Tung, A., & Levin, M. (2020). Extra-genomic instructive influences in morphogenesis: A review of external signals that regulate growth and form. *Developmental Biology*, *461*(1), 1–12. https://doi.org/10.1016/J.YDBIO.2020.01.010

Uemoto, T., Abe, G., & Tamura, K. (2020). Regrowth of zebrafish caudal fin regeneration is determined by the amputated length. *Scientific Reports*, *10*(1), 649. https://doi.org/10.1038/s41598-020-57533-6

Van Der Spek, A. H., Fliers, E., & Boelen, A. (2017). *The classic pathways of thyroid hormone metabolism*. https://doi.org/10.1016/j.mce.2017.01.025

Van Eeden, F. J. M., Granato, M., Schach, U., Brand, M., Furutani-Seiki, M., Haffter, P., Hammerschmidt, M., Heisenberg, C. P., Jiang, Y. J., Kane, D. A., Kelsh, R. N., Mullins, M. C., Odenthal, J., Warga, R. M., & Nüsslein-Volhard, C. (1996). Genetic analysis of fin

formation in the zebrafish, Danio rerio. *Development*, *123*(1), 255–262. https://doi.org/10.1242/DEV.123.1.255

VanWinkle, P. E., Lee, E., Wynn, B., Nawara, T. J., Thomas, H., Parant, J., Alvarez, C., Serra, R., & Sztul, E. (2024). Disruption of the creb3l1 gene causes defects in caudal fin regeneration and patterning in zebrafish Danio rerio. *Developmental Dynamics*. https://doi.org/10.1002/DVDY.726

VanWinkle, P. E., Wynn, B., Lee, E., Nawara, T. J., Thomas, H., Parant, J. M., Alvarez, C., Serra, R., & Sztul, E. (2024). Lack of Nuclear Localization of the Creb3l1 Transcription Factor Causes Defects in Caudal Fin Bifurcation in Zebrafish Danio rerio. *Cells Tissues Organs*, 1–19. https://doi.org/10.1159/000540103

Vatine, G. D., Zada, D., Lerer-Goldshtein, T., Tovin, A., Malkinson, G., Yaniv, K., & Appelbaum, L. (2012). *Zebrafish as a Model for Monocarboxyl Transporter 8-Deficiency*. https://doi.org/10.1074/jbc.M112.413831

Walker, M. B., & Kimmel, C. B. (2007). A two-color acid-free cartilage and bone stain for zebrafish larvae. *Biotechnic & Histochemistry*, *82*(1), 23–28. https://doi.org/10.1080/10520290701333558

Walpita, C. N., Van der Geyten, S., Rurangwa, E., & Darras, V. M. (2007). The effect of 3,5,3′-triiodothyronine supplementation on zebrafish (Danio rerio) embryonic development and expression of iodothyronine deiodinases and thyroid hormone receptors. *General and Comparative Endocrinology*, *152*(2–3), 206–214. https://doi.org/10.1016/J.YGCEN.2007.02.020

Wang, X., Kopinke, D., Lin, J., McPherson, A. D., Duncan, R. N., Otsuna, H., Moro, E., Hoshijima, K., Grunwald, D. J., Argenton, F., Chien, C. Bin, Murtaugh, L. C., & Dorsky, R. I. (2012). Wnt Signaling Regulates Postembryonic Hypothalamic Progenitor Differentiation. *Developmental Cell*, *23*(3), 624–636. https://doi.org/10.1016/j.devcel.2012.07.012

Wang, Y. T., Tseng, T. L., Kuo, Y. C., Yu, J. K., Su, Y. H., Poss, K. D., & Chen, C. H. (2019). Genetic Reprogramming of Positional Memory in a Regenerating Appendage. *Current Biology*, *29*(24), 4193-4207.e4. https://doi.org/10.1016/j.cub.2019.10.038

Wehner, D., Cizelsky, W., Vasudevaro, M. D., Özhan, G., Haase, C., Kagermeier-Schenk, B., Röder, A., Dorsky, R. I., Moro, E., Argenton, F., Kühl, M., & Weidinger, G. (2014). Wnt/β-catenin signaling defines organizing centers that orchestrate growth and differentiation of the regenerating zebrafish caudal fin. *Cell Reports*, *6*(3), 467–481. https://doi.org/10.1016/j.celrep.2013.12.036

Wehner, D., & Weidinger, G. (2015). Signaling networks organizing regenerative growth of the zebrafish fin. In *Trends in Genetics* (Vol. 31, Issue 6, pp. 336–343). Elsevier Ltd. https://doi.org/10.1016/j.tig.2015.03.012

Wolpert, L. (1969). Positional information and the spatial pattern of cellular differentiation. *Journal of Theoretical Biology*, *25*(1), 1–47. https://doi.org/10.1016/S0022-5193(69)80016-0

Wolpert, L. (2011). Positional information and patterning revisited. *Journal of Theoretical Biology*, *269*(1), 359–365. https://doi.org/10.1016/J.JTBI.2010.10.034

Woltering, J. M., Irisarri, I., Ericsson, R., Joss, J. M. P., Sordino, P., & Meyer, A. (2020). Sarcopterygian fin ontogeny elucidates the origin of hands with digits. *Science Advances*, *6*(34). https://doi.org/10.1126/SCIADV.ABC3510/SUPPL_FILE/ABC3510_SM.PDF

Yashiro, K., Zhao, X., Uehara, M., Yamashita, K., Nishijima, M., Nishino, J., Saijoh, Y., Sakai, Y., & Hamada, H. (2004). Regulation of retinoic acid distribution is required for proximodistal patterning and outgrowth of the developing mouse limb. *Developmental Cell*, *6*(3), 411–422. https://doi.org/10.1016/S1534-5807(04)00062-0

Yi, C., Spitters, T. W. G. M., Al-Far, E. A. D. A., Wang, S., Xiong, T., Cai, S., Yan, X., Guan, K., Wagner, M., El-Armouche, A., & Antos, C. L. (2021). A calcineurin-mediated scaling mechanism that controls a K+-leak channel to regulate morphogen and growth factor transcription. *ELife*, *10*. https://doi.org/10.7554/ELIFE.60691

Yu, G., Wang, L. G., Han, Y., & He, Q. Y. (2012). clusterProfiler: an R Package for Comparing Biological Themes Among Gene Clusters. *OMICS : A Journal of Integrative Biology*, *16*(5), 284. https://doi.org/10.1089/OMI.2011.0118

Zada, D., Tovin, A., Lerer-Goldshtein, T., & Appelbaum, L. (2016). Pharmacological treatment and BBB-targeted genetic therapy for MCT8-dependent hypomyelination in zebrafish. *DMM Disease Models and Mechanisms*, *9*(11), 1339–1348. https://doi.org/10.1242/DMM.027227/257264/AM/PHARMACOLOGICAL-AND-BBB-TARGETED-GENETIC-THERAPIES

Zhang, J., Jeradi, S., Strähle, U., & Akimenko, M.-A. (2012). *Laser ablation of the sonic hedgehog-a-expressing cells during fin regeneration affects ray branching morphogenesis*. https://doi.org/10.1016/j.ydbio.2012.03.008

Zwahlen, J., Gairin, E., Vianello, S., Mercader, M., Roux, N., & Laudet, V. (2024). The ecological function of thyroid hormones. *Philosophical Transactions of the Royal Society B*, *379*(1898). https://doi.org/10.1098/RSTB.2022.0511